ERNEST ORLANDO LAWRENCE
BERKELEY NATIONAL LABORATORY

Development of Hydrologic Characterization Technology of Fault Zones

Kenzi Karasaki, Tiemi Onishi, and Yu-Shu Wu

Earth Sciences Division, Lawrence Berkeley National Laboratory

March 2008

NUMO-LBNL Collaborative Research Project Report

Executive Summary

This is the year-end report of the first year of the NUMO-LBNL collaborative project: Development of Hydrologic Characterization Technology of Fault Zones under NUMO-DOE/LBNL collaboration agreement, the task description of which can be found in the Appendix.

Literature survey is conducted to study past works that relate geology to hydrology of fault zones. This includes study in sediments, sedimentary and crystalline (igneous and metamorphic) rocks with examples from various parts of the world. We focus on studies of hydrology of fault zones in the field and the laboratory as well as through modeling performed in all types of faults (i.e. normal, thrust and reverse, and strike-slip). We find that there is very limited amount of work on the subject, particularly in the field using borehole testing. The common elements of a fault include a core, and damage zones. The core usually acts as a barrier to the flow across it, whereas the damage zone controls the flow either parallel to the strike or dip of a fault. In most of cases the damage zone is the one that is controlling the flow in the fault zone and the surroundings. The permeability of damage zone is in the range of two to three orders of magnitude higher than the protolith. The fault core can have permeability up to seven orders of magnitude lower than the damage zone. In general, most fault studies in the literature fit into combined-conduit barrier classification by Caine et al., 1996.

The main results are listed in three tables which summarize the main geological, structural and hydrological characteristics for each type of fault. At the end of the chapter, we suggest a characterization strategy for classifying faults based on available information (i.e. stress field, scaling relationship, fluid flow concentrated on one side of a fault) The fault types (normal, reverse, and strike-slip) by themselves do not appear to be a clear classifier of the hydrology of fault zones. However, there still remains a possibility that other additional geologic attributes and scaling relationships can be used to predict or bracket the range of hydrologic behavior of fault zones. We identify potential U.S. locations to conduct analogue studies and to extend the current effort on fault zone classification and development of characterization technology.

Next we examine in the literature the characterization technologies employed and the information used to identify the hydrologic properties of faults. The findings are listed by the location. AMT(Audio frequency Magneto Telluric) and seismic reflection techniques are often used to locate faults. In some cases AMT results are successfully used to infer the hydrologic properties. Geochemical signatures and temperature distributions are often used to identify flow domains and/or directions. ALSM(Airborne Laser Swath Mapping) or LIDAR (Light Detection and Ranging) method may prove to be a powerful tool for identifying lineaments in place of the traditional photogrammetry. Nonetheless not much work has been done to characterize the hydrologic properties of faults by directly testing them using pump tests. There are some uncertainties involved in analyzing pressure transients of pump tests: both low permeability and high permeability faults exhibit similar pressure responses.

A physically based conceptual and numerical model is presented for simulating fluid and heat flow and solute transport through fractured fault zones using a multiple-continuum medium approach. The suggested multiple-continuum concept is a natural extension of the classic double-porosity model, with the fracture continuum responsible for conducting global flow, while vuggy (if any) and matrix continua, locally connected and interacting with globally connecting fractures, provide storage space for fluid and solute. The proposed conceptual model can be implemented into a general multidimensional numerical reservoir simulator TOUGH2 using a control-volume, finite-difference approach, which can be used to simulate single-phase flow, solute transport, and heat transfer in 1-D, 2-D, and 3-D fractured faulted systems. Model application is demonstrated by modeling two well-flow problems at ambient geothermal and water flow conditions. Data from the Horonobe URL site are analyzed to demonstrate the proposed approach and to examine the flow direction and magnitude on both sides of a suspected fault.

Finally, we describe a strategy for effective characterization of fault zone hydrology. We make a step-by-step recommendation of the technologies to be employed and decisions to be made along the preliminary characterization process. The recommendations are written in Japanese to ensure quick and easy consumption by the NUMO personnel. We recommend conducting a long term pump test followed by a long term buildup test. We do not recommend isolating the borehole into too many intervals. We do recommend to ensure durability and redundancy for long term monitoring.

Table of Contents

List of Tables

List of Figures

1 Introduction

The Nuclear Waste Management Organization of Japan (NUMO) and the Department of Energy of the United States of America (DOE) established a cooperative agreement in the field of radioactive waste management on July 10, 2002. In May 2005, NUMO and the Regents of the University of California as the DOE Management and Operating Contractor for the Ernest Orlando Lawrence Berkeley National Laboratory (LBNL) entered into an agreement to collaborate, and for LBNL to conduct work under the auspices of the bilateral agreement.

In 2006, ANRE (Agency for Natural Resources and Energy) jointly with JAEA (Japan Atomic Energy Agency) identified outstanding technological issues and needs regarding the research and development for geologic disposal of HLW subsequent to the publication of the Second Progress Report by JNC (Japan Nuclear Cycle Development Institute) in 1999. Research organizations in Japan as well as NUMO have been conducting investigations on these issues and needs. In the area of groundwater hydrology, four R&D needs were identified and are currently being investigated: improvement of groundwater flow characterization technology, development of testing and characterization technology in coastal areas, development of testing equipment and technology, and field application of testing and characterization technology. NUMO has been incorporating the results of the outcome of these R&Ds as they become available and are deemed appropriate, and is in the process of systematizing the testing and characterization technology to form a solid technical foundation for selecting the sites for detailed investigation.

The first NUMO-LBNL collaborative project was entitled “Feature Detection, Characterization and Confirmation Methodology,” which was designed to further develop radioactive waste management technologies related to an investigation strategy and technology for detection, characterization, and confirmation of key geologic features at possible nuclear waste repository sites. The project was carried out from May 2005 through March 2007. Among other important findings, the study has identified the hydrologic properties of fault zones as one of the most important parameters that need to be evaluated during the preliminary investigation stage. Based on the lessons learned at

the Mizunami and Horonobe URLs, as well as at numerous mines, dams, and tunnels—and given the geologic environment of the Japanese Islands—faults are likely to exist almost ubiquitously, which need to be assessed both at the preliminary and the detailed investigation stage (the length scale of the faults of interest would range from several kilometers in the former down to several hundred meters in the latter). However, none of the four R&D activities mentioned above sufficiently addresses the development of systematized hydrologic characterization technology specifically tailored for fault zones. At present, it is necessary to use perhaps overly conservative values for the hydrologic parameters of fault zones for the design and performance assessment of a repository. Therefore, development of a more efficient and reliable fault-zone characterization technology is highly desirable. The geologic properties of faults and the relationships among their geometry, type, fault parameters, and internal structures are being investigated mostly overseas. Hydrologic investigation of faults of various sizes are also being conducted at foreign as well as at domestic characterization sites. However, the relationship between the geologic and hydrologic properties of faults is not yet studied sufficiently.

The objectives of the present study is to organize the information available from overseas to ultimately establish an efficient and systematized methodology for hydrologic investigation and characterization of faults at the scale of interest during the preliminary investigation stage, for more practical design and performance assessment. The present study will be conducted as a collaborative study between NUMO and USDOE/LBNL. It should be possible to apply/transfer the results of the study obtained at a site in the West Coast of the United States, whose tectonic environment is just as active as that in Japan, to the Japanese repository program when they will be needed. These actions would also be beneficial to the U.S. program.

In addition to this introduction, the report is comprised of four main chapters: In Chapter 2, we search and examine the literature that studies faults and their hydrologic properties. We investigate the relationship between geologic attributes and hydraulic properties of faults. We group and tabulate known geologic and hydraulic features of a given fault by fault types. Chapter 3 surveys literature on characterization technologies of fault zones and lists by the location including a couple of sites from Japan. In addition,

potential difficulties of correctly characterizing a fault by analyzing pressure transient data during pump tests conducted in a formation containing a fault are discussed. The chapter is intentionally written in Japanese to help NUMO personnel understand the contents readily and clearly. In Chapter 4, we discuss conceptualization and modeling approach of fault zone hydrology. We propose a numerical model that can represent various coupled physical processes that are expected to take place in the fault zone. We conclude with Chapter 5 that discusses the characterization strategy of fault zones. We make a step-by-step recommendation for effective characterization of fault zone hydrology during the preliminary investigation stage.

2 Geological Structure of Fault Zones and Hydrology

2.1 Introduction

Fault zone hydrology, a key issue for many different geological disciplines, has in recent years been the subject of increasing interdisciplinary effort. For example, faults have been studied as part of research regarding (1) ore deposits associated with geothermal migration (Hammond and Evans, 2003); (2) groundwater management (Moran and Hudson, 2000; Stamos et al., 2003; Nishikawa et al., 2004); (3) petroleum migration (Antonellini and Aydin, 1994, Dholakia et al., 1998; Sorkhabi et al, 2002a,b, Takahashi 2003a,b, Jourde et al, 2002); (4) geotechnical projects, such as tunneling and underground construction (Yanagisawa et al., 1995); (5) fault slip propagation (Sibson, 1981); and (6) nuclear waste disposal (Onishi and Shimizu, 2002; JNC, 2000; Davison and Kozak, 1988; Le Cain et al., 1998; Swedish Nuclear Fuel, 2005; Henriksen, 2008, Andersson et al., 1991).

Structurally, over regional or local tectonic history, faults and fractures are responsible for rock-mass weakness. Faults and fractures are also the main pathways for fluid, gas, and heat, greatly enhancing hydrogeological properties. With respect to fluid flow, a fault with distinct hydraulic properties may act as a conduit, a barrier, or both (Caine et al, 1996).

Permeability structures of fault zone have been reported in the literature, largely through investigations of natural faults (Evans et al., 1997; Caine and Forster, 1999; Caine et al., 1996; Onishi et al., 2002; Wibberly and Shimamoto, 2003), using outcrop and small core samples for permeability measurements. The main limitation to this method is that large faults and fractures are not taken into account, and therefore permeability values can be underestimated. Allowing for this limitation, these studies suggest that the permeability structure is related to fault evolution (i.e., geologic time, reactivations), stress field, juxtaposition of rock types, amount of displacement, depth (temperature and pressure), fluid-rock interaction, fracture interconnectivity, fault-rock heterogeneity, and the extent of fracture filling by mineral precipitation. These factors affect fault distribution, as well as the length and width of the fault zone.

This report summarizes the fault hydrology studies now available in the literature. We point out the importance of fault zone hydrology, discuss its complexity, and make recommendations for future work, including analogue studies in the USA and characterization strategies. In more detail, we present several tables that show each type of fault (i.e., normal, strike-slip, reverse/thrust) with structural and hydrologic descriptions for reference.

2.2 Fault Anatomy

Faults are generally defined as a planar or zonal structure, which accommodates shear displacement. Faults are sometimes considered as planes or surfaces (Hobbs et al., 1976), slip planes, or shear fractures (Aydin, 2000). Indeed, most faults are defined by two primary components: damage zone and fault core (Caine et al., 1996; Chester and Logan, 1986). In general, the deformation process operating in the damage zone produces a wide range of fracture networks, the presence of small faults, folds, veins, and deformation bands. Fracture density in the damage zone can be three to five times greater than in the host rock (Evans et al., 1997).

The fault core, where the deformation is concentrated, can be very heterogeneous. It consists of breccia, cataclasite, or gouge, in crystalline rock; and sheared layers of weak lithologies (such as clay smearing, grain scale mixing, grain reorientation and pore collapse, cataclasis with deformation bands) in lithified and poorly lithified sedimentary rock. The width of fault core can vary from a few millimeters to a few centimeters.

These principal fault zone components are encompassed by the protolith, or undeformed host rock. Boundaries between the damage zone and fault core are typically sharp, whereas the damage zone to protolith transition is usually gradational (Caine et al., 1996). The amount and distribution of each component depend upon the lithology and the geologic setting in which the fault has formed (Caine et al., 1996, Evan et al., 1997).

Caine et al. (1996) classified fault zone architecture and permeability structure according to the percentage of damage zone versus the percentage of fault core. This is a simplified conceptual model that includes structural and hydrological characteristics. As a result, Caine et al. have identified four end members: localized conduit, distributed

conduit, combined conduit-barrier and localized barrier. Their conceptual model shows a qualitative relationship between fault internal structure and fault permeability, based on outcrop observation and permeability data from laboratory measurements. However, faults are structurally and hydrologically heterogeneous. Therefore, their model does not address current fault-rock interaction, flow paths, or flow properties. As indicated by Caine et al. (1996), the simplified conceptual model represents only one stage in the temporal evolution of a fault. Larger faults, such as the Median Tectonic Line and Carbonaras Fault, are more complex and do not fall into this classification (Faulker et al., 2003; Wibberley and Shimamoto, 2003).

It is well known that the permeabilities of rock obtained from outcrop are two orders of magnitude higher than those of rock obtained from drill cores (Morrow and Lockner, 1994). The permeability of exhumed fault rock tends to display less pressure sensitivity owing to the presence of weathering products in fractures. Nonetheless, core plug scale tests aid in understanding the permeability structure of fault zone components, although permeability values should be used with caution in developing quantitative models of fluid flow. *In situ* permeability tests would probably yield higher permeability values, given the interconnectivity of fractures that are missed in core plug scale investigations. It is evident that insufficient downhole data from across the fault zone exists in the literature, as described in the following sections.

2.3 Structural characteristics of faults in various rock types

2.3.1 SEDIMENTS AND SEDIMENTARY ROCKS

In connection with oil exploration, investigators have studied the impact of faults in sedimentary rock over a wide range and degree of lithification in sedimentary basins (Antonellini and Aydin, 1994).

One of the main characteristics of faults in sedimentary rock is the formation of deformation bands, i.e., the fault damage zone consists of deformation bands. Idealized representations of fault architecture in sandstones often include a fault core composed of low-permeability fault rock, high-permeability slip surfaces, and a surrounding damage zone (Figure 2-1). In such scenarios, the fault rock extent and permeability are crucial for

determining the fault's perpendicular flow component. Slip surfaces, the most continuous structural element, often control fault-parallel flow and are commonly treated as two planar surfaces separated by a constant overall aperture.

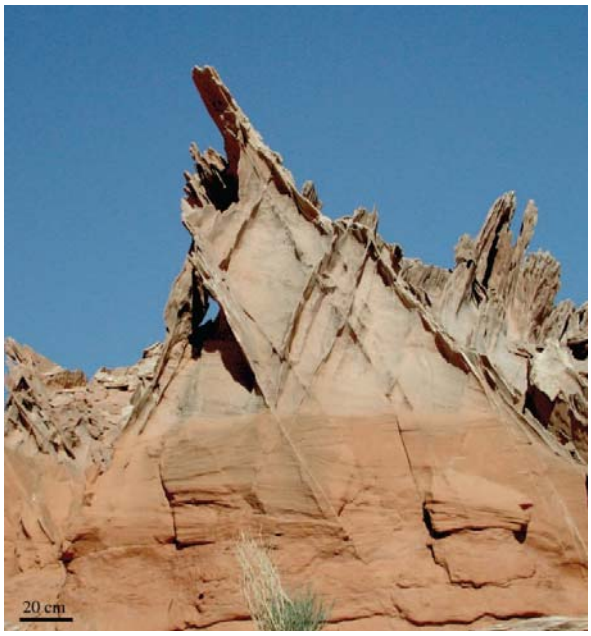

Figure 2-1. Deformation bands at Estrada Sandstone. Fossen and Bale, 2007

According to Fossen and Bale, 2007, deformation bands form in sediments with porosity higher than 16%. In sandstones, they occur as single structures, as clusters, and in fault damage zones. Deformation bands are millimeter-thick tabular zones of localized strain. They deviate from regular fractures by their lack of a single, continuous slip surface. For this reason, they do not share all of the properties of regular fractures (Fossen and Bale, 2007). In sediments rich in phyllosilicates, such as mica and clay, deformation bands will be formed by alignment of those minerals to form fabric parallel to the band (Knipe et al, 1997). Aydin and Johnson (1978) reported a different type of deformation band, a cataclastic band. In such bands, grains are crushed (cataclasis) and the grain size is consequently reduced.

Cementation and dissolution at grain-grain contact points can reduce porosity in any type of deformation band. Deformation bands may be preferentially cemented

because of their fresh grain surfaces formed during frictional grain sliding and comminution. Many factors influence the deformation mechanism and, hence, the type of deformation band that is formed, including mineralogy, grain size, grain shape, grain sorting, degree and type of cementation, porosity, and confining pressure (Fossen and Bale, 2007).

Shear smear is another term commonly associated with a fault core rich in clay minerals. It is observed when the fault displaces layers of sandstone and shale. Laboratory experiments by Takahashi (2003a), using interlayered sandstone and shale, suggested that during normal fault deformation, faults are sealed by shale smear impacting the mechanics and hydrologic properties of the fault zone. Field observations by Hynekamp et al. (1999) and Eichhub et al. (2005) described a narrow core zone flanked by a wider footwall and hanging-wall mixed material, suggesting that sediments transported during normal fault-shearing are thinned and tectonically mixed within the core zone. Transport distances are greater for clay and less for sand.

2.3.2 CRYSTALLINE AND VOLCANIC ROCKS

Crystalline rocks in this report refer to any type of rock that was originated by magmatic or metamorphic processes and where minerals are visible to the naked eye. The most commonly studied crystalline rocks are granite, granodiorite, gneiss, and schists. As for volcanic rocks, welded and nonwelded tuffs have been extensively studied within the Yucca Mountain Program (USA). Faults in crystalline rocks have been studied in connection with mineral and geothermal exploration, tunneling, and nuclear waste disposal programs (in such countries as Canada, Sweden, Finland, and Japan).

The observation of ore deposits filling veins in the proximity of fault zones indicates paleo-fluid migration during fault activity. Eichhubl and Boles (2000, 2001) evaluated mineral precipitation in veins to infer fluid volume and chemistry. Because the fractures and faults were sealed at the times of these studies, fractures and faults are in this case most likely to act as barriers to fluid flow.

All types of faults occur in crystalline rock, one example being Dixie Valley, Nevada, an active normal fault studied for geothermal exploration. Thrust faults with

large displacement are often observed in stable cratons in orogenic belts, such as at Lac Du Bonnet batolith in Canada, the Finnsjon and Forskmark sites in Sweden, and the East Fork, Wyoming and Elkhorn, Colorado faults in the USA. Such sites usually show a combination of ductile and brittle deformation, caused by formation depth, followed by subsequent uplift and fault reactivations in brittle regimes. At sites in Canada and Sweden, faults zones are defined as deformation zones, because faults are more complex and the deformation diffuse. The Nojima and Tsukiyoshi faults in Japan are examples of active and inactive reverse faults, respectively.

The majority of the hydrologically characterized strike-slip faults around the world are from regions located along plate boundaries. These include several strands of the San Andreas Fault, which juxtapose granodiorite with metarmorphic and sedimentary rocks such as at Punchbowl, San Gabriel, Gemini, and Bear Creek Camp faults. Investigations of the Median Tectonic Line in Japan and the Carbonara Fault in Spain are found in metamorphic rocks.

One characteristic of faults in crystalline rocks is the presence of variable amounts of *breccia*, *gouge*, and *cataclasite* (Figure 2-2). These terms are used for rocks formed from shearing under brittle conditions, at depths less than 10–15 km. Faulted rocks greater than 15 km depth occur under ductile conditions, where *milonites* are formed.

Another well-known characteristic of faults cutting across crystalline rock is the presence of micas and clay minerals in the fault core, resulting from large amounts of silicate minerals reacting with fluids and comminuted minerals as a result of shearing. Hence, a significant reduction in permeability is observed in studies conducted in such lithologies (Evans et al., 1997; Forster et al., 1994; Seront et al., 1998; Forster and Evans, 1991; Onishi et al., 2002; Wibberley and Shimamoto, 2003; Lockner et al., 2000; Mizoguchi and Shimamoto, 2001; Forster et al., 2003).

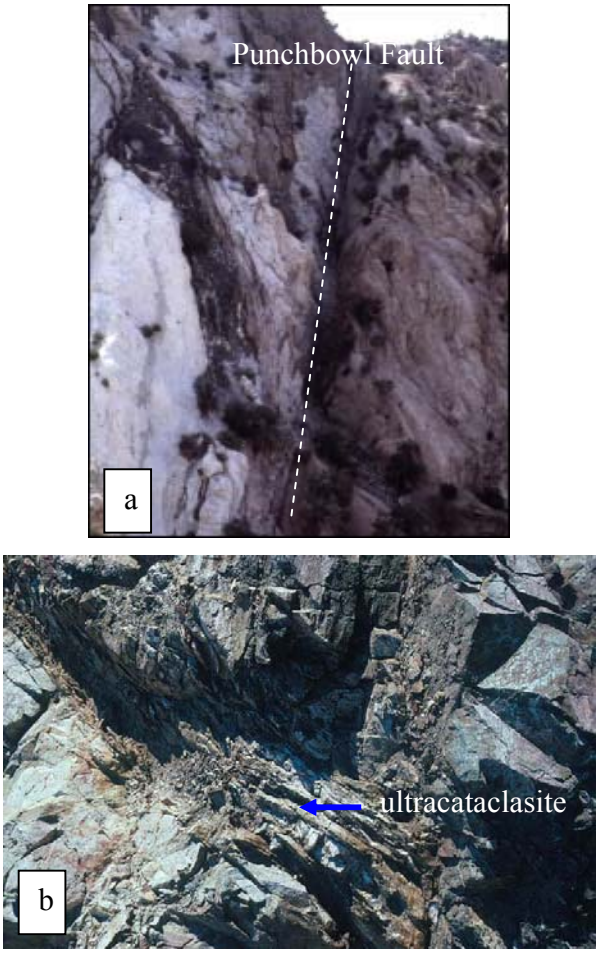

Figure 2-2 (a)- Strike-Slip Punchbowl Fault (inactive strand of the San Andreas Fault) juxtaposing sandstone and granite; (b) photo showing ultracataclasite (from field guide to Punchbowl Fault, Chester, 1999)

2.4 Survey of past and current hydrologic characterization activities of fault zones

According to the classification system devised by Anderson (i.e., "Andersonian classification"), there are three fundamental fault types: normal, thrust or reverse, and strike-slip. Each of these fault types can combine to form a more complex fault system.

In theory, considering the tectonic regime that generates these types of faults, we would expect the hydrologic regime to be controlled by the orientation of open fractures formed by tensional forces acting on the rock mass (Neubauer, 2005). In such a case,

reverse faults would be straightforward with respect to fluid flowing upwards, because most tensional fissures are subhorizontal and often not interconnected. By contrast, strike-slip faults have subvertically oriented fissures that would enhance fluid flow circulation. However, such models are not realistic, as we find when we compare several examples of fault hydraulic properties collected from the literature. This might be caused by spatial heterogeneity in the fault system, the location and depth of formation, the mechanical properties of different lithologies, variations in the stress field with depth, etc. Below, we describe the main characteristics gathered from our literature survey for each type of fault.

2.4.1 NORMAL FAULTS

Normal faults are associated with crustal extensions and mostly with basin formations. As described in Section 2.3.1, they are important structures for hydrocarbon reservoirs. Normal faults zones in sedimentary rock have been described in a number of recent studies—Devatzes et al. (2005); Antonellini and Aydin (1994, 1995); Antonellini et al. (1994); Eichhubl et al. (2005); Fossen and Bale (2007).

The hydraulic properties of deformation bands have been widely described, using numerous laboratory measurements and well log studies. Porosity loss and pore-throat collapse in deformation bands reduce permeability (Antonellini and Aydin, 1994; Antonellini et al., 1994; Fisher and Knipe, 1998; Matthäi et al., 1998). Permeability within deformation bands is about three orders of magnitude lower than in the host rock (Pittman, 1981; Antonellini and Aydin, 1994, 1995; Shipton et al., 2002; Taylor and Pollard, 2000), and porosity is less than 1% (Shipton and Cowie, 2003). Usually the

hydraulic conductivity of a fault core is reduced as a result of clay smearing, grain-scale mixing, and iron-oxide precipitation (Bense et al., 2003). Antonellini and Aydin (1994) reported that cataclastic deformation may reduce sandstone permeability by as much as 10^4 (to 10^{-16} to 10^{-19} m^2) within fine-grained deformation bands (Figure 2-3).

However, in eolian sandstone, such as described by Antonellin and Aydin (1994) and Shipton et al. (2002), the bulk permeability is higher than in the deformation bands by up to three orders of magnitude. These are observed in several examples shown in Table 2-2 including the Sand Hill Fault, the fault at Arches National Park, the Big Hole fault, and the fault at Vale of Fire State Park. In addition, joint openings or slips across established joints, which produces dilation caused by surface roughness along fracture walls (Brown, 1987), increases the permeability of joints in sandstone (Taylor et al., 1999).

In the Hazel-Atlas fault, Eichhub et al. (2005) found that deformation during the evolution of the fault involved a complex mixture of clay mineralogy reducing its permeability. The change in clay fabric—by distinct increase and aligning parallel to the fault plane—suggests that the fault acts as a barrier to fluid flow across itself.

Bhrun et al. (1994) compared three normal faults in similar granitic rock at various sites: Dixie Valley, Nevada; Wasatch, Utah; and Mineral Mountain, Utah. These sites were all intensely fractured and hydrothermally altered, and they also all had transition zones (i.e., damage zone) in the footwall composed of variably fractured and altered rock. The transition zones were spatially heterogeneous, with thicknesses ranging from 20 to 200 m. The slip zones ranged from <10 m in the Mineral Mountains to 20 m in parts of the Dixie Valley and Wasatch fault zones. Although the normal fault zones displayed similar gross zonations, characteristics of fracture networks varied with depth.

Permeability measurements by Seront et al. (1998) found permeability anisotropy from outcrop samples. Their study (in granodirite) suggested lower permeability in the core (cataclasite, implosion breccia, and breccia). They noted that permeability decreased with increasing confining pressure over a range of four orders of magnitude (from 10^{-16} m^2 to $10^{-20}m^2$). However, because of the high degree of alteration, great hysteresis during pressure cycles was observed when compared with relatively unaltered granites.

In another study, Caine and Forster (1999) simulated fault zone permeability in 3D based on fracture data from a series of normal faults in low-permeability rock. Because strike-slip and thrust faults contain similar architectural elements, the model results from Caine and Forster's study may be applicable for those faults. Their findings suggest fault permeability anisotropy is controlled by a fracture network's internal bulk anisotropy (e.g., related to aperture, fracture roughness, and anisotropy in the fracture topography), and the lithological contrast when juxtaposing different fault-zone components. The permeability anisotropy in three orthogonal flow directions suggested a lower permeability across the fault of up to five orders of magnitude when compared to the two directions parallel to the fault plane. Similar results were found by bulk permeability of Stillwater fault zone. The bulk permeability of the fault zone probably exceeded that of the protolith by at least five orders of magnitude, and likely exceeds the permeability of breccia pods in the fault core by at least seven orders of magnitude (Seront et al., 1998).

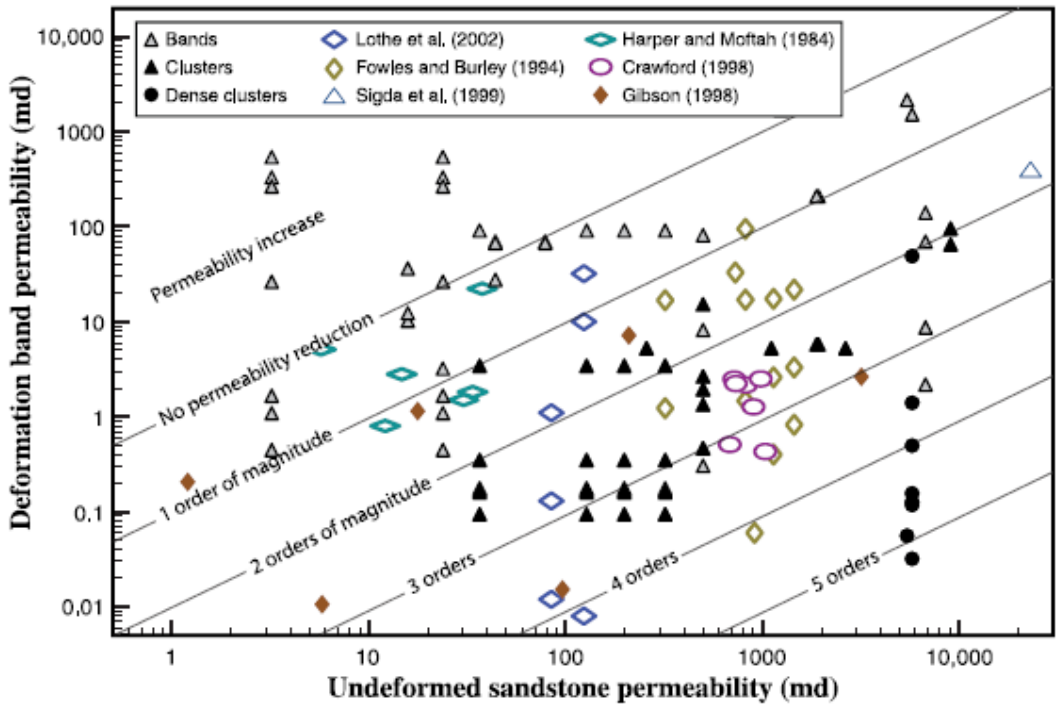

Figure 4. Permeability of host rock plotted against that of deformation bands as measured from plugs drilled perpendicular to the bands. Most of the bands are cataclastic deformation bands. Our data, mostly from southern Utah, are separated into single bands, clusters, and dense clusters of deformation bands. Previously published data are shown for comparison (not separated into single bands and clusters).

Figure 2-3

Figure 2-4 shows a schematic representation of deformation-band hydraulic characterization. As shown in Figure 2-4 deformation-band faults can be an important barrier to fluid flow in hydrocarbon reservoir rocks. Conversely, it has been suggested that an increase in permeability is created in the direction parallel to slip because of dilatancy and slip-surface generation (Antonellini and Aydin, 1994).

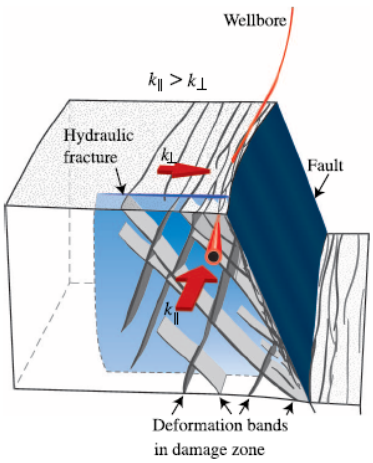

Figure 2-4 Deformation bands at Estrada Sandstone. Fossen and Bale, 2007

The Yucca Mountain Project, the investigation into a proposed nuclear-waste repository in Nevada, is one of the best examples of studies in volcanic rock, specifically hydraulic studies in welded and nonwelded tuffs. Yucca Mountain is dominated by a series of north-striking normal faults, with bedrock displaced several hundred meters (maximum ~600 m) along many of the faults, which occur within or along the flanks of Yucca Mountain (Fenster, 1999). Hydrologic data on fault zones in this area was limited. Air injection tests and trace tests were conducted along the Ghost Dance and Bow Ridge faults at this site to determine air permeability, porosity, and tracer transport (BSC, 2004b, Section 2.2.3). According to LeCain et al. (1998), porosity and permeability in the fault core was up to one order of magnitude higher than in the host rock. Faults could either be major conduits for flow or may be locally impermeable to lateral flow, resulting in perched water (Flint et al., 2001).

Fault-zone studies of ore deposits suggest some evidence that fluid migration is confined to one side of the fault (Logan and Decker, 1993; Hammond and Evans, 2003, Diment and Craig, 1999). Examples include mineralization exclusively in the hanging wall in Coastal Somerset, UK; gold mineralization in South Keno Fault, Nevada, and Tritina Fault, Yukon; and gold mineralization in the footwall North Keno Fault. This selective mineralization is possibly due to structural control and the nature of repeated deformation events that enhance fault dilantacy.

Fault Name	Location	Fault type	Protolith	Age	displacement	Structure/microstructure			Hydraulic Properties Porosity (%) / Permeability (md, m2)			general description	Reference
						protolith	damage zone	core	protolith	damage zone	core		
Stillwater	**Dixie Valley, NE USA**	normal/ active	granodiorite, crystalline	fault displaces Tertiary volcanic sequence	3-6km	altered granodiorite, intragranular porosity, low fracture density	mesoscopic deformation, fracture lengths 1-10m	a. cataclasite b. microbreccia c. implosion breccia	$1x10^{-16}$ m^2 at 15 Mpa and $1x10^{-18}$ m^2 at 90 MPa at direction perpendicular to the fault plane	$7x10^{-18}$ m^2 (at 90 MPa) to $9x10^{-19}$ m^2 (at 90MPa) and 1% porosity	cataclasite = $6x10^{-17}$ m^2 (at 15MPa) to $9x10^{-19}$ m^2 (at 90MPa) and 1% porosity implosion breccia = $1x10^{-17}$ m^2 to $2x10^{-18}$ m^2 at 15MPa and $9x10^{-20}$ to $3x10^{-20}$ m^2 at 90MPa. and ~1-3%	outcrop samples, laboratory permeability. In the protolith, possible 3:1 permeability anisotropy. Great resistance to fluid flow is in a direction perpendicular to the fault plane. High permeaiblity for protolith due high degree of alteration. Composite deformation zone or combined conduit-barrier	Caine and Forster, 1999 ; Seront,Wong, Caine, Forster, Bruhn and Fredrich, 1998
Keno Fault	**Nevada**	normal	cuts siltstone and silt limestone	reactived multiple times from Mesozoic to Tertiary	55-100m	dolomitic shale in footwall and calcitic shale in hangingwall	faults and inumerable fractures in hanging wall and footwall	North fault= single 10-20mm wide clay-rich gouge zone. South fault= 5-170mm wide calcite veins with slickensides	$6.2x10^{-17}m^2$ for unaltered shale and $6.4x10^{-18}$ m^2 for silicified shale	$4.9x10^{-13}m^2$	clay gouge permeability = 10^{-22} to $10^{-18}m^2$	sedimentary-hosted disseminated gold deposits. North Keno Fault is a single slip surface and South consists of numerous hydrocarbon bearing calcite veins on which slip has occurred. Fault zone architecture in the N = Au mineralization in footwall while in the S the mineralization is in hanginwall. Distributed conduit to fluid flow	K.J. Hammond, J.P. Evans, 2003
Sand Hill Fault	**New Mexico, USA**	normal	poorly lithified sandstone, silt and mud	Tertiary	~10 to ~600m	unfaulted	may contain small faults, fractures, fracture network and veins	a. No macroscopic fractures b. breccia and or cataclasite, or gouge c.foliated clay d. calcite cement	~10^{-17} m^2 (clay) and ~ 10^{-11} (sand)	a. mixed zones: 10^{-17} m^2(sand clay) - 10^{-11} m^2 (sand) b. cemented mixed zones: 10^{-19} m^2 c. deformation bands: 10^{-13} m^2	10^{-18} m^2(clay)	a. three strike-perpendicular outcrop samples of the fault b. portable air permeability and consolidometer tests (pressure of 10-18 Mpa) . The fault is barrier because of absence of macroscopic fractures	Rawlin, G, Goodwin, LB, Wilson, JL, 2001; Heynekamp, Goodwin, Mozley & Haneberg, 1999
no name	**Arches National Park, Utah, USA**	normal	sandstone	Fault displaces Mesozoic sedimentary rocks	30-40m	sandstone	grain size reduction and formation of deformation bands		630 to > 10000 md and porosity varies from 5-30%	0.005 md (wall rock)	3 md (deformation band) and porosity <1 to 10%	Outcrop samples. Localized barrier perpendicular to the deformation band	Antonellini and Aydin, 1994
Hazel-Atlas	**Black Diamond Mine, Antioch, CA, USA**	normal	intercalation of sandstone and shale, coal layers	Domengine Formation, Eocene	9 m	sandstone-shale sequence	transition zone=justaposition of sandstone from footwall against the shale from hangingw wall. Attenuated shales(deformation bands and granular flow)		shale porosity 18-24%(unjacted) and 18-21% jacketed; shale air permeability 0.019 - 3.8md (unjacted) and 0.01-0.4md (jacked)	unjacted porosity (not specified sand or shale) 22-30%	unjacted porosity (not specified sand or shale) 18 to 27%and 23, 30%(jackted); Air permeability 0.04-0.1md (unjacted) and 0.02-0,07md(jackted)	the fault zone is interpreted as result of distributed deformation during the evolution of the fault. It is based not only in the simple mixing of clay and non-clay minerals but accounting for the shale composition and stratigraphy, changes in shale entrainment mechanism with increasing fault slip, clay fabric development,and changes in shale composition caused by burial diagenetic reactions. The fault is barrier due clay mineral content of 47% along fault zone, increase in kaolinite (increase sealing capacity) and alignment of platy minerals in shale parallel to the fault zone.	Eichhubl, P., D'Onfro P.S., Aydin, A., Waters, J., and McCarty, D.K., 2005 (AAPG)
Corral Canyon	**Mineral Mountain, Utah**	low angle normal fault	granite	cuts Tertiary granite and Paleozoic limestone and quartzite		unaltered granite	shear fractures	hydrothermaly altered cataclasite	no data			fractures in the damage zone (transition zone) are hydrothermaly altered to serecite, chlorite, epidote and calacite.	Brhun et al, 1994
Wasatch	**Utah**	exhumed normal fault	granite	cuts Oligocene granite	>11km	granite	presence of transition zone of variable fracture and altered rocks with slip zones ranging 20 m	discontinus lenses of breccia, finely comminuted cataclasite, highly altered and partially recrystalized phyllonite, and veins of recrystalized pseudotachylyte occur locally with phyllonite and cataclasite	no data	estimated permeabillity for fracture network 2D model: 10-13 m^2 to 10-19 m^2	no data	fluid transport was estimated using th emodel of Oda et al, 1987. Permeability range at depth of 10km, effective confining pressure approximately 170MPa if fluid pressure is hydrostatic to approximately 20MPa if fluid pressure is 0.9 lithostatic	Brhun et al, 1994

Table 2-2 Normal Faults

Dixie Valley Fault	**Dixie Valley, NE, Mirror lakes**	normal	granodiorite	cuts & deforms a 25-29 Ma old multiphase granite and overlying Tertiary volcanic rocks	~ 6km (3km in the last 10Ma)	granite	cross fractures and pinnate and steep extension fractures	breccia and cataclasite	fracture permeability vary from a high of 10^{-13} m^2 in a pre-rupture stress state marked by high fluid pressure to a low of 10^{-17} m^2 in a post-rupture state with hydrostatic fluid pressure			Geothermal fault. Fault zone is marked by a band of hydrothermal alteration and fracturing. Fractures are partially filled with cataclastic and mineral altered hydrothermally. Highest fluid temperature 305°C. Conduit according to Caine et al, 1996	data repository, Caine 1996 original Bruhn et al, 1994
Moab Fault	**Moab, Utah**	normal	juxtaposes sandstone,shale and limestone (footwall) with sandstone (hangging wall)	Triassic	44km long and trow of ~2.5km	sandstone, shale, limestone	fractured and cataclasatically deformed sandstone and shales	clay rich gouge zone 1-2 m wide in sandstone; shale smear	no data	aeolian sandstone= ~$9x10^{-18}$ to ~$120x10^{-18}$ m^2 at Pc=10-40MPa	clay-rich rocks = ~$3x10^{-21}$ at Pc=40MPa	fault rocks in sandstone are associated with cataclasis of quartz and feldspar in either deformation bands or due to abrasion of joint surfaces reactivated by shear. Conduit according to Caine et al, 1996 and hybrid conduit barrier by Devtzes, et al., 2005	data repository, Caine 1996 original Caine 1996; Devatzes, 2005, Solum et al, 2005
Ghost Dance and Bow Ridge Fault	**Yucca Mountain**	normal	volcanic	Miocene	4m	densed welded tuffs	intensely fractured rocks	uncemented fault breccia	footwall= 10 darcies and 0.03 porosity; hanginwall = 4 darcies and 0.03 porosity	footwall= 10 darcies and 0.03 porosity; hanginwall = 4 darcies and 0.03 porosity	14 darcies and 0.13 porosity	cross-hole pneumatic test. the footwall, hanging wall and fault zone appear to be isotropic	LeCain et al, 1998
Big Hole Fault	**San Rafael Swell, Utah**	normal	sandstone	Early Cretaceous	up to 29m	sandstone and limestone	anastomosing deformation bands. Individual deformation bands form by cataclastic grain crushing	fine grained cataclasticaly deformed rocks (30cm thick) and fine fault gouge	100-1000md for Navajo Sandstone Probe Permeameter: 5-10 Md	Probe Permeameter: deformormation bands - 1-134md Whole-core: 180md (perpendicular to the core axis)	fine fault gouge= permeability of at least seven orders of magnitude less than that of the host rock (Antonellini and Aydin, 1994). Probe Permeameter: 1-44md Whole-core: 1-2 md (paralle to the core axix)	surface and subsurface drill core samples (depth up to 100m). Data from five drill core HQ 58mm core barel. Permeability measurement by probe permeameter at 3 cm intervals and whole-core permeability in sample at decimeter scale in laboratory in three directions a confining pressure of 2.8MPa.	Shipton et al, 2002

2.4.2 THRUST AND REVERSE FAULTS

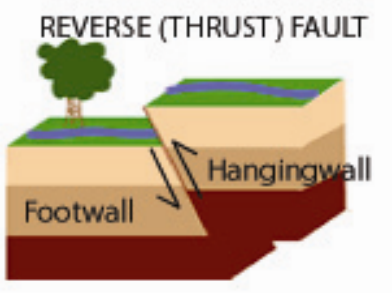

Thrusts faults are gently (~30 ^{o}) dipping faults in which the hanging wall has moved up relative to the footwall (Hatcher, Jr., 1995), while reverse faults are ith moderate-to-steep dip (more than 45^{o}). Both result from tectonic comp or shortening.

Thrust-fault hydraulic properties from field, laboratory, and modeli ies provide insights into permeability anisotropy within fault-zone components. A py in permeability was observed in a number of studies (Forster and Evans, 1991 et al., 1997; Locker et al., 2000; and Onishi et al., 2002), in which the low-pe ity fault was localized in the clay-rich gouge/cataclasite, while higher permea as found in faulted and fractured rocks in the damage zone. Permeability in the da ne was up to six orders of magnitude higher than in the fault core (Evans et al., as shown in Figure 2-5. In outcrop samples tested in three perpendicular orien by Evans et al. (1997), permeability anisotropy was clearly observed. In the studi ed by our report, which were conducted in exhumed fault zones in crystalline rock, it was noted that a gouge and/or cataclasite component act as a barrier to flow across the fault, whereas the damage zone enhanced flow within the plane of the fault. Similar results were obtained using core samples from the Tsukiyoshi fault in Japan. Onishi et al. (2002) report permeability as low as $10^{-19}m^2$ in the foliated cataclasite, with anisotropy in the damage zone ranging from 10^{-15} to $10^{-19}m^2$.

Table 2-2 Normal Faults (continued)

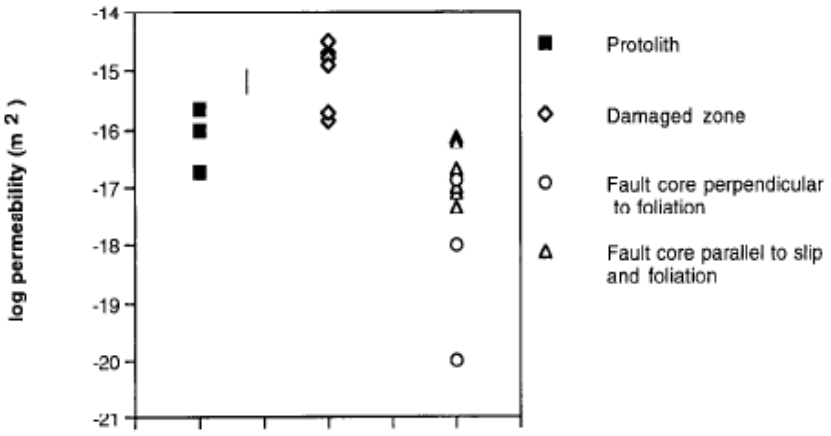

Figure 2-5 Shows the distribution of permeability across fault zone from Evans, Forster, Goddard, 1997

Two examples of permeabilities from slug and pumping tests in thrust and reverse faults, at the Elkhorn and Tsukiyoshi faults, suggest higher permeability values compared to laboratory measurements. In both cases, the permeabilities of the protolith and damage zone were found to be two to five orders of magnitude higher than laboratory values. See Table 2-4.

Table 2-4 Thrust/reverse faults

Fault Name	Location	Fault type	Protolith	Age	displacement	Structure/microstructure			Hydraulic Properties Permeability (md, m2) / Porosity (%)			General description	Reference
						protolith	damage zone	core	protolith	damage zone	core		
East Fork	**Wyoming, USA**	thrust Fault	granite-gneiss	fault juxtaposes granitic-gneiss of PreCambrian with Paleo-Mesoz sedimentary rocks	2 to 4km	unaltered granite and gneiss in both footwall and hanging wall	fractured and faulted damage zone w/ quartz veins. Fracture density in damage zone is 3 to 5x greater than protolith.	indurated and cataclasite zones (foliated cataclasite), Fault composition- clay rich gouge/cataclasite	a) 10^{-1} -10^{-3} md (Pc= 4MPa), b) 10^{-17} -10^{-18} m^2 c)1.4x10^{-16} and 2.3x10^{-16} m^2	a) 10^{-1} - 10^{-3}md (Pc= 4MPa), b) 10^{-16} -10^{-14} m^2 , c) 1.2x10^{-15} m^2 and 3.0x10^{-15} m^2	a) 10 to 10^{-3} md (Pc= 4MPa) b) <10^{-20} - 10^{-17} m^2 Parallel to fault and 10^{-18}-10^{-17} m^2 Perpendicular to fault 10^{-20} -10^{-17} m^2 c) 1x10^{-17} m^2(//1), 6.0x10^{-17} m^2 (//2) and perpendicular to the fault 2.0x10^{-17} m^2	a) fracture density and subsidiary faults increases toward the center of the fault zone. Deformation mechanisms is brittle and comminution of feldspars. Permeability test from outcrop samples (31 samples) b) 31 outcrop samples tested, cores 1 and 2 inches (3 perpendicular directions in relation to the fault plane), confining pressure 2-50MPa (applicable for upper 2km of the crust) c) outcrop core samples 2.5cm diameter (results from modeling not shown). Maximum permeability within the plane of the fault and minimun permeability perpendicular to the fault /conduit-barrier. It includes permeability results from modeling	a) Forster, Goddard and Evans, 1994 b)Evans, Foster & Goddard, 1997 c)Forster & Evans, 1991
Elkhorn Fault	**South Park,Co, USA**	low angle reverse fault	granite & arkose	Laramide age. fault juxtaposes Precambrian granite and sedimentary rocks	no data	granite and metamorphic rocks in the hanging wall and arkoses and conglomerates in the footwall	no data. Fault is not visible at surface. Most of data comes from geophysical studies	10 foot thick gouge	Slug test: **hydraulic conductivity** of crystalline rock range from 2.9 to 4.7 ft/day. **Hydraulic conductivity** of arkosic unit range from 0.194 to 0.368ft/day Slug test **permeability** for hanging wall (granite) = 1.0e^{-12} to 1.7e^{-12} m^2	Slug test: **hydraulic conductivity** of crystalline rock possible near the core range from 25 to 45ft/day. **Hydraulic conductivity** of arkosic unit ranges from 6.92 x10-4 to 1.31x10-3ft/day (later suggest well skin effects) Slug test: **Permeability** 8.8 e^{-12} to 1.6e^{-11} m^2 and pumping test = 2.2e^{-12} m^2	Slug test: permeability 6.8 e^{-14} to 1.3 e^{-13} m^2 and pumping test permeability 4.8 e^{-15} m^2	five piezometers installed across the fault for slug test. The exact location of well tests are not described. 42 slug tests performed by raising head and falling head tests in each well. Equipment used: electronic water level indicator, data logger, pressure transducer and PVC slugs of different volumes. According to Shemin Ge, the fault has higher angle than 45 degrees. Slug test from Marler, 2003 and pumping test from Ball et al, 2007. The paper suggest fault as a barrier. More analysis are been conducted.	Marler,J. & Ge,S., 2003; Ball, Ge and Caine, 2007 (AGU poster)
Tsukiyoshi Fault	**Mizunami, Gifu**	reactivated reverse	granite	Tertiary	~30m	unfractured granite	high fracture density, cataclasite seams	foliated cataclasite	H samples=10^{-15} m^2 (Pc=5) to $10^{-17}$$m^2$(Pc=180MPa); V samples= 10^{-16} m^2(Pc=0) to 10^{-17} m^2(Pc=180MPa)	H samples=10^{-15} m^2 (Pc=5) to $10^{-18}$$m^2$ (Pc=180MPa); V samples= 10^{-16} m^2(Pc=0) to 10^{-19} (Pc=180MPa)	V samples=10^{-14} m^2(Pc=5) to $10^{-19}$$m^2$ (Pc=180MPa)	permeability measurement using drill core samples at various depth using high-P apparatus. Permeability anisotropy observed along damage zone. According to Caine's classification the fault is a combined conduit-barrier	Onishi et al, 2002
Tsukiyoshi Fault	**Mizunami, Gifu**	reactivated reverse	granite	Tertiary	~30m	unfractured granite	high fracture density, cataclasite seams	no info	5.81x$10^{-12}$to 2.35x10^{-11} m^2	3.66x10^{-11} m^2	4.98x$10^{-9}$$m^2$	results from pumping test	MIU3 report
Tsukiyoshi Fault	**Mizunami, Gifu, Japan**	reactivated reverse	granite	Tertiary	~30m	unfractured granite	high fracture density, cataclasite seams	no info	1.16x10^{-11} to 5.35x$10^{-11}$$m^2$	4.7x$10^{-12}$to 3.15x10^{-11} m^2	1.46x10^{-11} to 1.40x10^{-10} m^2	results from slug test	MIU3 report
Nojima Fault	**Awajima, Kobe, Japan**	right-lateral strike-slip and reverse	kobe formation/ Cretaceous granodiorite	Active during the last 1.2Ma	490-540 m	granite	small faults, breccias, veins and alteration minerals; damage zone 50m thick. It is composed of non-foliated cataclasite and fault breccias; breccia zone (2m in width), fractured granite zone (~10m width). Gradational contact	gouge (0.1~0.15m in width) and cataclasite; about 30cm thickness by Fujimoto and 150cm thick by Lin et al.	less than $10^{-21}$$m^2$ at 50 Mpa (from Lockner et al 2000); 10^{-19} to 10^{-20} m^2 at Pc=100MPa (Mizoguchi and Shimamoto, 2001)	about $10^{-16}$$m^2$ at 50 Mpa (Lockner et al 2000); fractured granite= 10^{-14} to 10^{-16} at Pc=30MPa to 10^{-16} to 10^{-18} at 200MPa; fault breccia = 10^{-12} to 10^{-16} at Pc=30MPa to 10^{-14} to 10^{-17} at Pc=200MPa (Mizoguchi and Shimamoto, 2001)	0.1 to 1x $10^{-18}$$m^2$ at 50 MPa(from Lockner et al 2000); fault gouge= 10^{-14} to 10^{-19} at Pc=30MPa to 10^{-19} to 10^{-20} at Pc=200MPa(Mizoguchi and Shimamoto, 2001)	Lockner = fault rocks are composed of cataclastic rocks (foliated cataclasite, cataclasite, fault breccia, psedotachylyte and fault gouge); Mizoguchi and Shimamto measured permeability at room temperature using oscillating pore pressure method and nitrogen as pore fluid. Pore pressure held at 20MPa constant and Pc up to 90MPa or 200MPa. According to Lockner and Lin, the fault is a combined conduit-barrier; high permeability parallel to the fault (damage zone) and low permeability across the fault	Lockner et al, 2000, Mizoguchi et al, 2000; Lin et al,2007, Fujimoto et al, 2007;Hidemi et al, 2000
Chelungpu Fault	**Taiwan**	thrust fault	Pleistoce alluvium deposits	Holocene	11m horizontal and 7.5 m vertical	hanging wall - shallow marine strata of Pleistocene age footwall - fluvial strata	no data	2-3mm thick clayey fine fault gouge in the centerand 10mm thick foliated fault gouge and breccia	no data	no data	permeability of fault rocks range from 10^{-14} to 10^{-18} m^2	composed of three major fautl zones at detph 1111,1153 and 1222m depth.s. Permeability measured by gas permeability of core samples	Tanikawa, et al, 2005 AGU Fall meeting abstract; Sone et al, 2005 AGU Fall meeting abstract, Lin et al, 2001

Table 2-4 Thrust/reverse faults (Cont.)

Low angle fracture zone (Zone 2)	**LacDuBonnet Batholith, Canada**	thrust fault	granite	Pre Cambrian reactivated during Paleozoic	about 7.3m in Zone 2. Reverse dip-slip (up to 1m throws)	granite	small-scale fractures and associated alterations most in the hanging-wall and less in the footwall. Several conjugate shear and extensional fractures	cataclasite rich in clay and calcite; clay-goethite gouge	range from 10^{-17} m^2 to greater than 10^{-11} m^2		hydraulic testing consists of single-borehole stranddle tests and multiple-borehole hydraulic interference tests. Permeability values varied spatially by 6 orders of magnitude	National Research Council, 1996; Lopez&Smith, 1996; Davison and Kozak, 1988
Low angle fracture zone (Zone 2)	**Finnsjon site, Sweden**	thrust fault	granite	no data	no data	granite	increase fracturing and deformation	total thickness of Zone 2 is more than 100m	hydraulic conductivity withim Zone 2 range from 10-10ms^{-1} up to 10-3 ms^{-1}. Between two and five highly conductive subzones were identified in each borehole.		single hole injection test with different packer spacing, and hydraulic interference tests using multiple section observetaion boreholes were performed within Zone 2. Single-hole test shows that Zone 2 consists of long intervals of rock with low tc intermediate conductivity separeted by a few highly conductive narrow subzones.	Andersson et al, 1991
several deformation zones	**Forskmark Site Investigation, Sweden**	gentle dip shear zones	granite/granodiorite/applite (amphibolite-greenshist grades)	Pre-Cambrian (Proterozoic) fault reactivation during Ice Age (Holocene)	no data	granite, pegmatite/metamorphic rocks at amphibolite grade	combination of brittle and ductile deformation	high-strain zones (tectonic banding in ductile deoformation zones	Transmissivity values for gently dipping deformation zone: 0-200m= 10^{-3} to 10^{-5} m^2/s; 200-400m=10^{-4} m^2/s; 400-600m=$10^{-5}$$m^2/s$; 600-800m=$10^{-5}$ and $10^{-7}$$m^2/s$; 800-1000m=$10^{-8}$ and $10^{-9}$$m^2/s$. Transmissivity values for steep dipping deformation zone: 0-200m=10^{-3} to$10^{-5}$$m^2/s$; 200-400=$10^{-6}$ to $10^{-9}$$m^2/s$; 400-600m=$10^{-8}and10^{-9}$$m^2/s$; 600-800=$10^{-9}$$m^2/s$		Several low dip deformation zones defined by zones of high fracture related to ductile and brittle deformation. Hydraulic tests using single hole evaluation include logging during pumping using Posiva Flow Logging (PFL) and Double Packer injection using Pipe String System (PSS)	Swedish Nuclear Fuel, 2005
thrust fault	**Sobrella Village, North Portugal**	thrust	ultramafic rocks (hangingwall) and Cambrian slates and greywakes (footwall)	Hercyan orogeny	no data	serpentinites	no damage zone	mylonitized permeable, homogeneous and isotropic material	impermeable rock	Anomalous ground electrical conductivity is interpreted as fault having high permeability- fault zone aquifer. Transmissivities = $7x10^{-7}$ - $2x10^{-4}$$m^2/s$	pumping tests for wells penetrating aquifer in the hanging wall, includes observation and theoretical studies of drawdown evolution with pumping in fault zone. Host rock impermeable and permeable fault zone.	Antonio and Pacheco, 2002

2.4.3 STRIKE-SLIP FAULTS

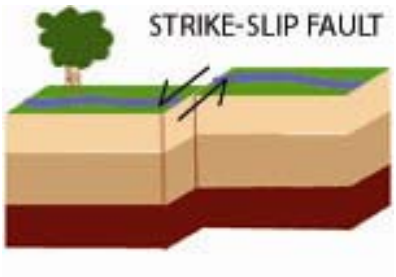

Strike slip faults are faults those in which the motion is parallel to the strike of the fault plane. They are characterized by steep dip and predominantly horizontal displacement. Most dips are more than 60º, and many approach vertical. In terms of tectonic regime, strike-slip faults have sub vertically oriented tensional fissures subparallel to the strike of the fault, as described previously (Neubauer, 2005). This orientation would allow the circulation of descending and ascending fluids parallel to the strike and dip of the fault plane.

In eolian sandstone, deformation bands reduced permeability by two to four orders of magnitude according to gas permeameter measurements (Freeman 1990) and two to four orders of magnitude lower than host rock according to gas injection minipermeameter measurements (Antonellini and Aydin, 1994). In addition, a 1.3-to-2.3 orders-of-magnitude reduction was observed in deformation bands (when compared to host rock) from field measurement of relic fluid gradients (Taylor and Pollard, 2000).

Most examples of strike-slip faults occur at plate boundaries. Examples include the San Andreas Fault and its strands in the USA; the Median Tectonic Line and Nojima Fault in Japan; the Carbonaras Fault in Spain; and the West Fissure Zone in Chile. The San Andreas Fault is one of the most well-known fault systems in the world. The fault is composed of numerous strands that run parallel to the main fault, some active and others inactive. Petrological, structural, and geophysical studies have been conducted at several areas along the San Andreas Fault; however, there remains a lack of hydrological information on fluid flow *across* the fault.

Faults in unconsolidated sediments are summarized in Table 2-3. Most hydraulic studies in unconsolidated sediments were found to be in alluviums, as part of groundwater management efforts for drinking water programs. For the purpose of water management, a number of wells have been drilled at shallow depth. Moran and Hudson (2000), Stamos et al. (2003), and Nishikawa et al. (2004) describe faults cutting through aquifers. Their hydrology was characterized by geochemical and isotopic signatures. In all cases, faults in unconsolidated sediment were found to reduce the hydraulic conductivity perpendicular to the fault.

Several strands of the San Andreas Fault showed changes in fault movement and dip direction due to reactivation and/or change on stress regime. Such changes in fault movement were observed in Japan by Onishi, (unpublished data from the Tsukiyoshi fault), from reverse to strike-slip, by analyzing slickensides on fault core; and by Hidemi et al. (2000) at the Nojima fault, a strike-slip fault that was recently reactivated as a reverse fault during the Kobe earthquake.

Table 2-5 Strike-slip faults

Fault Name	Location	Fault type	Protolith	Age	displacement	Structure/microstructure			Hydraulic Properties Permeability (md, m2) / Porosity (%)			General description	Reference
						protolith	damage zone	core	protolith	damage zone	core		
Punchbowl Fault	**CA (between San Gabriel Mt.and Mojave Desert), USA**	right lateral/inactive	sandsonte/ granodiorite	Fault juxtaposes crystalline rocks from basement with Paleocene sandstone	44 km	Pelona schists (quartz-albite-muscovite-actinolite schist)	40m damage zone(increase in veins, thin cataclasite bands, inter and itnragraunlar fractureing and altered host rock.	quartz-chlorite-albite-epidote ultracataclasite	no data			localized deformation zone or distributed conduit. (Fault weakening might be possible due to presence of micas in the protolith)	Chester and Logan, 1986, Schulz & Evans, 1998
San Grabiel Fault	**Pasadena, CA, USA**	right lateral	juxtaposes crystaline(granite,gneisse, amphibolite),/sedimentary rocks (conglomerate)	late Oligocene to middle Miocene	23km	Pelona schists (quartz-albite-muscovite-actinolite schist). unstrained protolith but between host rock and damage zone contain numerous cruss-cutting sets of healed, intragranular microfractures	orders of 100m thick. Near the core in the damage zone, the rock is pervasively brecciated and displays dense networks of intragranular and transgranular fractures, and microscopic cataclastic and ultracataclasitic zones	narrow layer (less than tens of cm) of ultracataclasite within a zone of soliated ctaclasite several meters thick . The rock is mineralogically altered, very fine granied cataclastic matrix, veins and porhyroclasts of veins fragments or relict protolith. The central ultracataclasite layers are composed almost entirely of particles less than several microns in diameter	no data			this study is based on petrological and mineralogical analysis of fault core. According to the author, exposure of cataclasite along the trace of San Gabriel Fault suggest areas of high uplift and erosion, while exposure of breccia represents the surface deformation. Fault thickness for both = 30-100m Conduit-barrier according to classification by Caine et al, 1996	data repository, Caine 1996 original Anderson et al, 1983, Anderson et al, 1983, Chester, Evans and Biegel, 1993
Helendele	**Mojave Desert**	strike-slip	floodplain aquifer on shallow depth and igneous and metamorphic rock for regional aquifer	Quaternary	no data	no data			Study based on water level, groundawter chemistry (dissolved -solids, arsenic concentration), stable isotope of oxygen and hydrogen, tritium, Carbon-14,			well data study indicate differences in groundwater chemistry, isotope from regional aquifers separated by the fault. barrier in the deeper regional aquifer but not in the overlying floodplain aquifer	Stamos, C.L, et al 2003 http://pubs.usgs.gov/wri/wri034069/wrir034069.book.pdf
Hayward Faut	**Hayward, California**	right lateral strike-slip	alluvium deposits	Quaternary	no data	no data			Study based well- data on tritum-helium isotope for groundwater management of Santa Clara County. Low permeability layers in the Below Hayward Fault sub-basin results in stratified groundwater with mean ages of 5, 20 and 30 years for the shallow, middle and deep aquifers respectively. Above Hayward Fault groundwater flow is unimpeded, and wells produce a large volume of young groundwater with a mean age of 5 years			Hayward Fault hydraullically divides the groundwater basin into "Above Hayward Fault" (AHF) and "Below Hayward Fault" (BHF) sub-basins on the east and west side of the basin. Fault is a barrier based on isotoope studies -tritium	Moran, J., and Hudson, G.B.
Mission Creek	**California**	right lateral strike slip	alluvium	Holocene	no data	no data			no data			Numericla modeling of hydraulic conductitivity of unconsolidated aquifer for groundwater management; apparent hydraulic gradient of 10% across the fault. Distinct change in temperatur and water chemistry. Model uses historic data of inflow-outflow of groundwater between two basins separated by the fault: Desert Hot Spring Subasin and Mission Creek Subasin Fault as barrier to groundwater flow	Mayer, et al, 2007
Bear Creek Camp	**Mount Abbot USGS quadrangle, CA**	coplanar left lateral	granodiorite	Cretaceous	10cm up to 100m	display of paralel faults	no data	cataclasite	no data			compound strike-slip faults. Barrier	data repository, Caine 1996 original Martel, 1990

Table 2-5 Strike-slip faults(Cont.)

Gemini Fault zone	**Mount Abbot USGS quadrangle, CA**	coplanar left lateral 10km long	granodiorite	Cretaceous	max 700m	undeformed/unfaulted	inexistent	chlorite breccias, minerals (serecite) formed along the fault zone formed close to the crystalization age of pluton	no data			fault zone formed and grew along preexisting parallel joints	Pachell, Evans, 2002 and Martel, 1990
Jalama beach fault	**Santa Barbara, CA**	lelft-lateral strike-slip	organic-rich, hemipelagic sequ of diatomaceous and phosphatic shale and organogenic dolostone	Miocene Monterey Formation	<100m	hemipelagic sequence; siliceous dolostone and dolomitic opal CT porcelinite and minor amounts of clay shale and chert	no data	breccia; cements (carbonate and quartz)along the fault zone	matrix permeability typically <1md	no data		Outcrop observation; microdrill samples. Fluid transport is estimated on measurement of strontium isotopes(87Sr/86Sr) of carbonate (dolomite) veins and fault cement. The presence of specific concentration indicates the stratigraphic location and thus the transport distance . Study suggest fluid flow focused along the fault. Presence of ppt carbonate and quartz along fault zone. Currently a barrier?	Eichhubl, P and Boles, JR,2000
Arroyo Burro	**Santa Barbara, CA, USA**	lelft-lateral strike-slip	dolomitic porcelinite and siliceous mudstone and subordinate dolostone	Miocene Monterey Formation	<100m	dolomitic porcelinite, silicious mudstone	no data	large amount of dolomite cement	no data			Outcrop observation. Fluid transport is estimated on measurement of strontium isotopes(87Sr/86Sr) of carbonate (calcite) veins and fault cement . The presence of large volume of cement in fault zone indicate large fluid flow along fault zones. Study suggest fluid flow focused along the fault. Presence of ppt carbonate and quartz along fault zone. Currently a barrier?	Eichhubl, P and Boles, JR,2001
no name	**Vale of Fire State Park, NE, USA**	strike-slip	Eolian Sandstone	Aztec Formation	6,14 and 150 m	sandstone	sheared joints	deformation bands	mean= 200md	0.1 md	0.1md (3 orders of magnitude smaller than host rock)	Result shows 2 to 5 orders of magnitude high flow parallel to the fault plan than to direction perpendicular depending on the fault slip lenght suggensting that deformation bands and shared joints act as barrier to flow	Jourde, H, et al, 2002 (AAPG)
Mission Creek	**California**	right lateral strike slip	alluvium	Holocene	no data				no data	no data	no data	Numericla modeling of hydraulic conductitivity of unconsolidated aquifer for groundwater management; apparent hydraulic gradient of 10% across the fault. Distinct change in temperatur and water chemistry. Model uses historic data of inflow-outflow of groundwater between two basins separated by the fault: Desert Hot Spring Subasin and Mission Creek Subasin. Barrier to groundwater flow	Mayer, et al, 2007
Carbonaras Fault	**Iberian Peninsula - Spain- part of Trans-Alboran shear zone**	lelft-lateral strike-slip	basement: andalusite-garnet bearing graphitic mica schists, phyllites, dolomites and gypsum	Early Tertiary - Miocene	40Km	mica schists(high grade metamorphic rocks - siliminite to migmatitic grade)	multiple strands of high strain zone - deformation zones ~5m thick. Damage zone in the order of 100 m thick	1 km widht. Mostly mica-schists derived. Composed of phylossicate -rich fault gouge. Cataclastic flow on localized deformation with some dolomite deposits	well foliated rocks with possible with very low permeability (no measurement). The gouge has a permeability anisotropy to up to three orders of magnitude with the lowest permeability in a direction normal to the fault of ~10^{-21} m^2 and fault parallel 10^{-18} m^2.			Fault has heterogeneous distribution of deformation with extreme localized high strain planes. Locally fault zone reach over 4km. Deformation in phylossilicate rich material leads to strian hardening behaivor. Fault zone is very complex, mixture of various types of rocks, combination of localized and distributed deformation. This fault does not fit into the classification proposed by Caine et al, 1996. It will act as combined conduit-barrier system although the damage zone will act as a flow conduit, the fractured lens of protolith in the core and dolomite pods with fractures can act as localized conduit	Faulkner, Lewis and Rutter, 2003

Table 2-5 Strike-slip faults(Cont.)

Median Tectonic Line	**Tsukide, W Mie Prefecture, Japan**	left lateral strike-slip and right lateral reactivation Tertiary	juxtaposes Ryoke belt mylonites (N) with Sambagawa schist (S)	Cretaceous	200 to 1000km	no data	**Ryoke Belt** = thickness varies from 0 to 300m. The fault rock zone varies from mylonite, fractured mylonite, cataclasite **Sambagawa Belt** (thickness varies from 0-15m)= the fault rock varies from clay-rich gouge, foliated gouges, schists	50-100mm wide slickenside-bound zone of extreme fine black gouge .Mostly foliated cataclasite up to 4m wide at Ryoke and black foliated gouge at Sambagawa	**Ryoke Belt** 10^{-14} to 10^{-16} m^2 at Pc 30MPa to 10^{-19} m^2 at Pc 200MPa **Sambagawa Belt** = schists = 10^{-14} m^2 at Pc 30MPa to 10^{-20} m^2 at Pc 200MPa	**Ryoke Belt** = fractured milonites and cataclasites = 10^{-14} m^2 to 10^{-17} at 30MPa to 10^{-17} m^2 at 100MPa and 10^{-18} m^2 at 200MPa. **Sambagawa Belt**= foliated and crenulated gouges 10^{-13} m^2 to 10^{-17} m^2 at 30MPa to 10^{-16} to 10^{-18} m^2 at Pc 200MPa.	**Ryoke Belt** =foliated cataclasite = 10^{-17} m^2 at 30MPa to 10^{-20} m^2 at Pc=200MPa. **Sambagawa Belt** = slip gouge = 10^{-17} to 10^{-19} m^2 at Pc 30MPa to 10^{-21} m^2 at Pc 200MPa	permeability measurement of oucrop samples using high-P apparatus. Samples cored parallel to foliation and lineation . the fault is too complex to be classified. In the Sambagawa belt (schists as protolith) the permeability depends upon microstructure and degree of cementation	Wimberley & Shimamoto, 2003
Neodani Fault	**Kimbara, Gifu, Japan**	left lateral strike-slip with reverse component	Mino sedimentary rocks (cherts, silicious mudstone, sandstone and basalt in dark gray mudstone matrix	Jurassic	up to 70 m	unfractured	15-30m breccia and cataclasite	200 mm of gouge	$7.46x10^{-21}$ m^2	breccia = $2.47x10^{-17}$ to $8.68x10^{-18}$ m^2 Fine-grained breccia = 10^{-20} m^2 severely fractured breccia = $1.38x10^{-14}$ to $1.45x10^{-15}$ m^2	black gouge = $2.36x10^{-19}$ and $8.32x10^{-21}$ m^2; green gouge= $4.38x10^{-18}$ and $2.18x10^{-20}$ m^2	permeability measurement of oucrop samples using high-P apparatus. Samples cored parallel to foliation for breccias and perpendicular to the foliation for gouges. Permeability data for effective pressure of 150MPa	Tsutsumi et al., 2004
Nojima Fault	**Awajima, Kobe, Japan**	right-lateral strike-slip and reverse	kobe formation/K granodiorite	during the last 1.2Ma	490-540 m	granite	small faults, breccias, veins and alteration minerals, damage zone 50m thick. It is composed of non-foliated cataclasite and fault breccias; breccia zone (2m in width), fractured granite zone (~10m width). Gradational contact	gouge (0.1~0.15m in width) and cataclasite, about 30cm thickness by Fujimoto and 150cm thick by Lin et al.	less than 10^{-21} m^2 at 50 Mpa (from Lockner et al 2000); 10^{-19} to 10^{-20} m^2 at Pc=100MPa (Mizoguchi and Shimamoto, 2001)	about 10^{-16} m^2 at 50 Mpa (from Lockner et al 2000), fractured granite= 10^{-14} to 10^{-16} at Pc=30MPa to 10^{-16} to 10^{-18} at 200MPa; fault breccia = 10^{-12} to 10^{-16} at Pc=30MPa to 10^{-14} to 10^{-17} at Pc=200MPa (Mizoguchi and Shimamoto, 2001)	0.1 to 1x 10^{-18} m^2 at 50 MPa(from Lockner et al 2000); fault gouge= 10^{-14} to 10^{-19} at Pc=30MPa to 10^{-19} to 10^{-20} at Pc=200MPa(Mizoguchi and Shimamoto, 2001)	Lockner et al = fault rocks are composed of cataclastic rocks (foliated cataclasite, cataclasite, fault breccia, psedotachylyte and fault gouge); Mizoguchi and Shimamto measured permeability at room temperature using oscillating pore pressure method and nitrogen as pore fluid. Pore pressure held at 20MPa constant and Pc up to 90MPa or 200MPa. Fault as combined conduit-barrier (Lockner and Lin); high permeability parallel to the fault (damage zone) and low permeability across the fault	Lockner et al, 2000, Mizoguchi et al., 2000; Lin et al,2007, Fujimoto et al, 2007;Hidemi et al, 2000

Table 2-5 Strike-slip faults(Cont.)

Mozumi-Sukenobu	**Gifu**	right-lateral strike-slip part of the Atotsugawa Fault System (previosly a thrust fault - Yokoyama Thrust juxtaposes gneisse on hanginwall and sand/shale on footwall)	cuts Jurassic Teori Gr. (imature pebble conglomerate, sitstones, sandstone	Quaternary	125-500m	sandstone and shale beds	open and filled fractures	siltstone, breccias, clay rich shear zone, black organic-rich shear , zonecataclasis and clay rich foliated zones		Hydraulic conductivity range from 10^{-6} to 10^{-7} cm/s	Lab Permeability range 10^{-13}-10^{-19} m^2 Hydraulic conductivity from clay-rich is in order of 10^{-8} to 10^{-9} cm/s	lab permeability & porosity measured by drillcore samples and water residence time chlorofluorocarbon. conduit-barrier Fault zonecomprises a complex structure with thin subvertical slivers (cm to m wide) of high-to-low permeability fault rocks. In situ hydraulic tests were carried out in four cored boreholes. Water discharge is observed along not filled conjugate Riedel shear and controled by lithology (shale layers)	Forster et al, 2003, Nohara, et al, 2006
West Fissure Zone	Chile	right lateral strike-slip fault reactivated as left-lateral strike-slip	forearc sediments(juxtaposes Late Cretaceous-Paleocene coarse-grained sandstone and conglomerates from Cretaceous tuffs)	Late Eocene/ Early Oligocene	101 km	sandstone and conglomerate Fracture density = 3.1 km-1	fracture density = 3.8km-1	fracture density higher than 5.8 fracture/km Fault width = 4km	no data	no data	narrow (100m) and shallow conducting anomaly visible down to 50 m. Apparent resistivity below 20 Wm	Regional fault studies using aerophotos, Audiomagnetotelluric (ATM) survey. Damage zone and core width = 4000m . Host Rock and Damage Zone boundary is marked by a signficant change in orientation of principal strain axis. Low resistivity can cause by clay-rich gouge zone	Jenssen et all, 2002
Limon Verde fault zone	Chile	splay of West Fissure zone	LVZ separates early Paleozoic metamorphic rocks from younger igenous rocks	Late Eocene/ Early Oligocene	35 km	main granite-diorite and minor gabbro and metamorphic rocks Fracture density = 3.1 km-1	fracture density = 3.8km-1	fracture density higher than 5.8 fracture/km Fault width= 7km	no data	no data	narros (200m) and shallow conducting anomaly visible down to 200 m. Apparent resistivity below 50 Wm	Regional fault studies using aerophotos, Audiomagnetotelluric (ATM) survey. Damage zone and core width = 7000m (interation of branche off West Fissure Zone and Limon Verde Fault)	Jenssen et all, 2003

2.5 Scaling relationship between fault components

Over the past two decades, studies in fault zones have also included the estimation of fault components and scaling relations. By using the distribution of faults, it was possible to estimate a linear interrelationship between (a) displacement and length, (b) fault width and length, and (c) fault width and displacement.

In the literature, it is observed that the amount of displacement (d) on a fault from natural faults is proportional to the mapped trace length (L), based on the fault scaling relationship $d=cL^n$, where $2 \geq n \geq 1$ and c is a variable that depends on rock properties and n a controversial exponent, related to the least-squares best-fit linear relationship (Cowie and Scholz, 1992).

Data relevant to the scaling relationship has been evaluated in all types of faults (i.e., normal, thrust, strike-slip), in a variety of tectonic environments, and for a range of length scales (Cowie and Scholz, 1992a and reference therein; Schultz and Fossen, 2002; Janssen et al., 2002). As a result of data plotting, Figure 2-6 and Figure 2-7 show log-log plots (derived from data plotting) of maximum displacement and length data for a wide range of tectonic environments. For example, faults tens of kilometers long typically have displacements on the order of hundred of meters, while faults of a few meters in length have offset on the order of only a few centimeters.

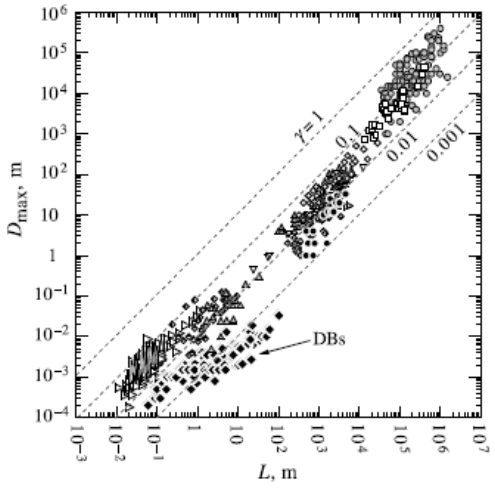

Figure 2-6 Compilation of displacement-length data in 2D. DB=deformation bands (Schultz and Fossen and reference therein, 2002).

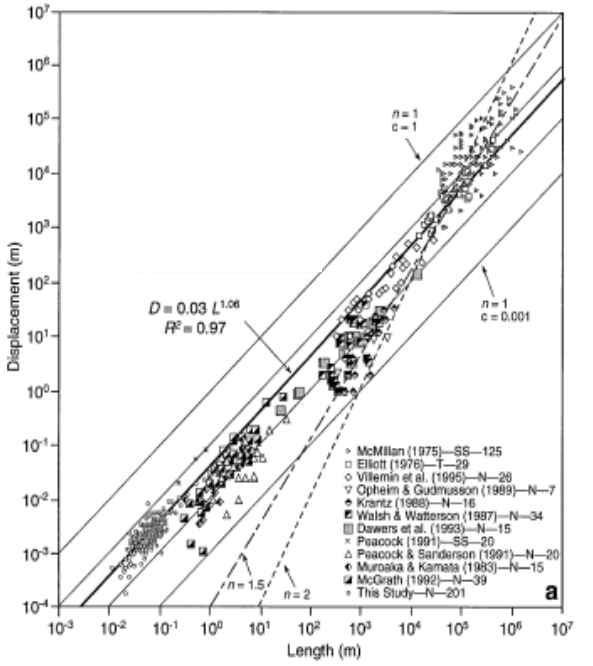

Figure 5. a: Log-log plot of displacement vs. length for various published fault populations as well as Solite data set. Abbreviations: N, normal faults; T, thrust faults; SS, strike-slip faults. Family of linear curves (n = 1) with various c values bound data; best-fit curve for all data is shown as heavy solid line. Also shown for reference are curves for n = 1.5 and n = 2. b: Size distribution of trace lengths of all faults from two-dimensional sampling of bedding surface on quarried boulder. Arrows delimit data points used to determine power-law exponent (1.4) for power-law distribution.

Figure 2-7 Log-log displacement–length from Schilische et al. (1996).

Another scaling relationship is related to fault length and fault-zone width. Janssen et al. (2002 and reference therein) predict that longer faults should have wider fault widths. Based on the cohesion-zone fault growth model of Cowie and Scholz (1992b), Scholz et al. (1993), postulated that the ratio between the width of the fault (W_f) and the length of the fault (L) is approximately 0.25/0.2. Vermilye (1996) and Vermilye and Scholz (1998) estimated a ratio of 10^{-2} for several meter scale faults. The ratio of fault width (w) to fault length calculated by Janssen et al. (2002) falls within an order of 10^{-2} (Figure 2-8). Jenssen et al. (2002) used estimates of fault lengths and widths from aerial photography, which fit quite well when compared with measured ratios from other natural faults (Figure 2-8).

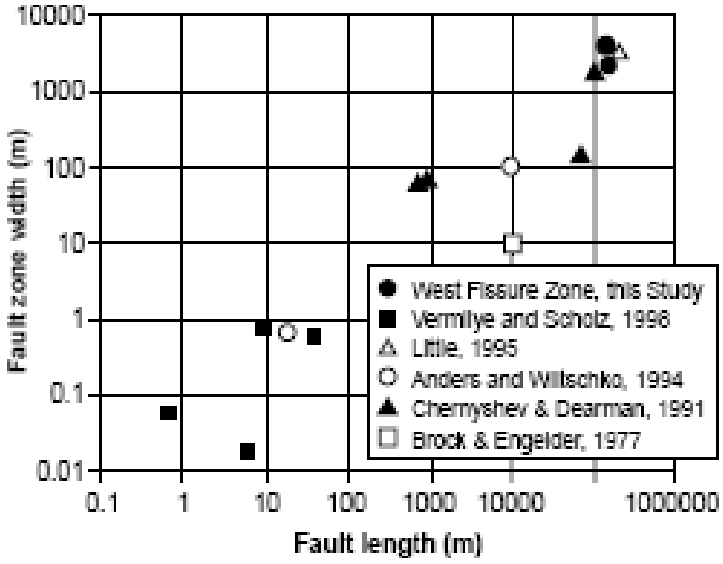

Figure 2-8 Plot of process zone (fault thickness) width versus fault length for this study and additional published data (Brock and Engelder, 1977, Cheraysbev and Dearman, 1991, Little, 1995 (Jenssen et al., 2002)

In addition, as shown in Figure 2-9, Otsuki (1978) (in JNC, 2000), within major strike-slip faults all over the world, found a linear relationship between cumulative displacement along the fault and the width of the shear zone. In this case, the shear zone of a fault with a cumulative displacement of tens of kilometers is estimated to be 200 m in width.

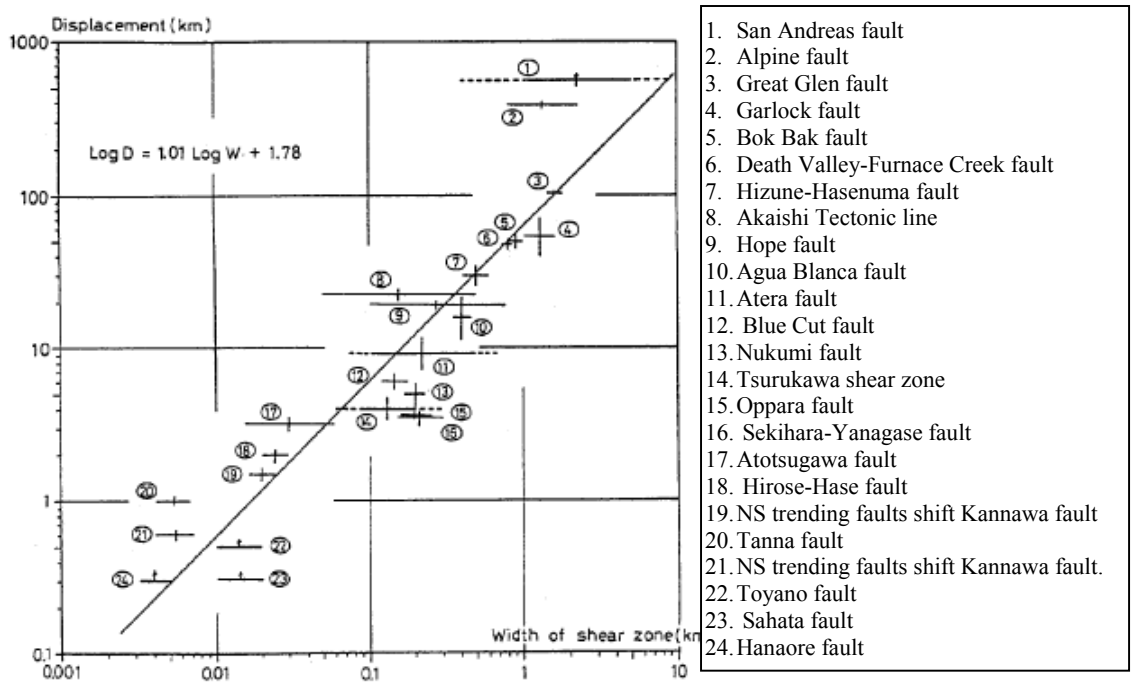

Figure 2-9 The relationship between width of shear zone and displacement for strike-slip faults

Although there is still controversy over whether all faults show a linear relationship between displacement, length, and fault width, it is generally agreed that such a linear relationship holds for larger faults, i.e. lengths of tens of kilometers. Schultz and Fossen (2002) noted that the scaling relationship does not fit quite so well for deformation bands on a meter scale, as observed in Figure 2.6.

2.6 Features to consider for hydraulic characterization of fault zones:

As reported in the literature, faults are complex structures. To effectively characterize fault-zone hydrology, we must take many factors into consideration. One important observation is that faults need to be evaluated in three dimensions, and possibly four. In this case, time (the fourth dimension) is an important variable that can affect the structural and hydrological behavior of faults. Below, we list the key factors when characterizing faults:

- Lithological variation (stratigraphy for sedimentary rocks and compositional variations for crystalline rocks)

- Lithological composition (mineralogy, texture, morphologic features of cements, percentage of clay minerals)
- Fault geographic distribution
- Fault internal geometry
- Fault structural evolution in space and time
- Fault history (age, formation depth, i.e. ductile or brittle regime and fault reactivations)
- Fluid-fault interaction (mineral precipitation, alteration)
- Fluid chemistry
- Fault length and displacement
- Changes on stress field (past and present)
- Change in climate conditions (precipitation, tectonic rebound due to ice melting)
- Deformation mechanism affecting the physical properties of rock, such as porosity and permeability
- Fluid and pore pressure, aperture, fault weakening or hardening related to episodic process of the seismic cycle
- Fracture network and connectivity in the damage zone
- Temperature and pressure, deformation rate
- Cyclic fault displacement and fluid migration: fluid migration and mineralization possibly alternates with periods of slip and rupture

2.7 Analogue studies in the USA

The main purpose of conducting analogue studies in the USA is to perform field studies at proposed site (s), to examine if the geologic properties and features of faults can be used to predict the fault-zone hydrological properties.

2.7.1 SUGGESTED TARGET STUDY AREAS IN THE USA

In this section, we list three potential U.S. sites, two in California and one in Colorado. The two sites in California are in Mesozoic to Cenozoic sedimentary rocks featuring strike-slip and normal faults, whereas in Colorado, a thrust juxtaposes sedimentary and granitic rocks.

2.7.1.1 CALIFORNIA STATE

The benefits of conducting analogue studies in California are as follows: (a) geological similarities with Japanese geology, i.e., rock types; (b) similar tectonics (i.e., convergent plate margins and active plate margins for the past 230 Ma); and (c) compressional and transpressional regimes.

Based on geology and tectonics, California is well suited for analogue studies on fault hydrology. The advantage of conducting field testing in California is the easy access to field location, data availability, cost, maintaining good public relations, and strengthening the US-Japan collaboration.

Site A—Lawrence Berkeley National Laboratory

The main characteristics that make this site appealing for analogue study are the location inside the LBNL property, which is cut by several well-known strike slip faults. The site also has the advantage of hundreds of drill-core data containing hydrological information. Figure 2-10 shows the location of the site and the distribution of the main fault zones.

Figure 2-10 Location of LBNL site (from Google maps)

The bedrock at LBNL consists primarily of Cretaceous marine mudstone, shales, and sandstones of the Great Valley Group, Miocene sedimentary nonmarine sandstone, mudstone, and conglomerates of the Orinda Formation, and volcanic rocks of the Moraga Formation. These units form a faulted homocline. The Cretaceous sequence forms the structurally lower portion of the homocline, which is overlain by the Orinda Formation and Moraga Formation, respectively (LBNL, 2000). Figure 2-11 illustrates the geology of the LBNL site, and Figure 2-12 cross section of the site.

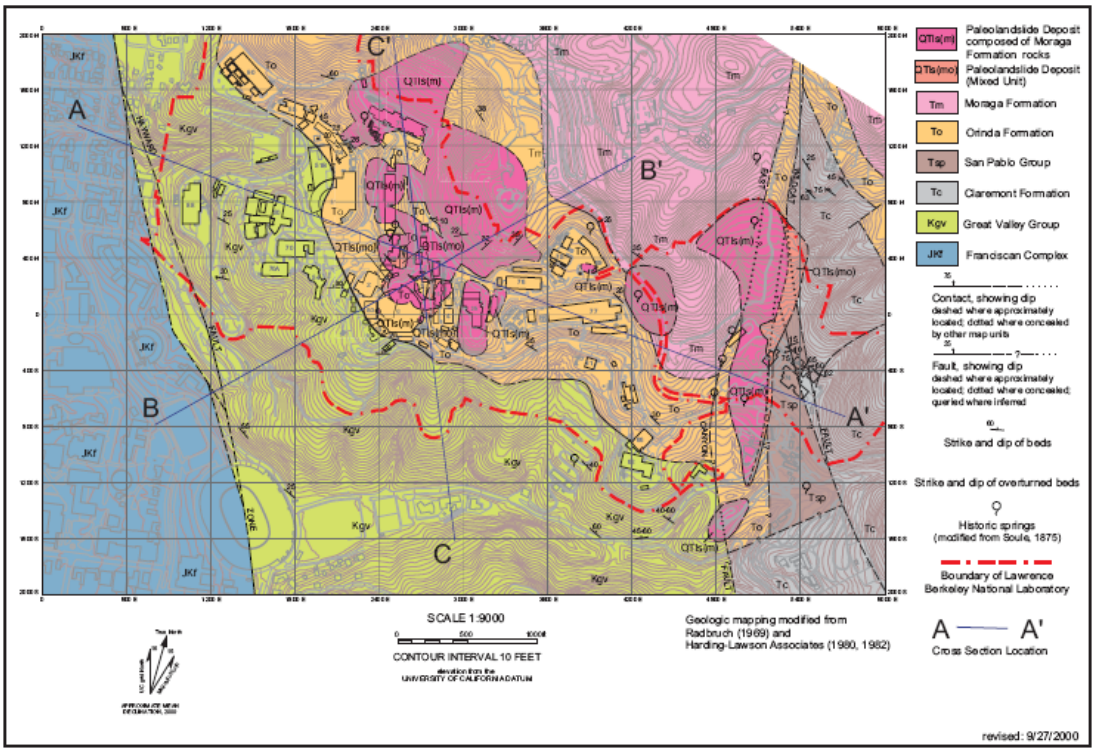

Figure 2-11 Distribution of geological formation at LBNL site

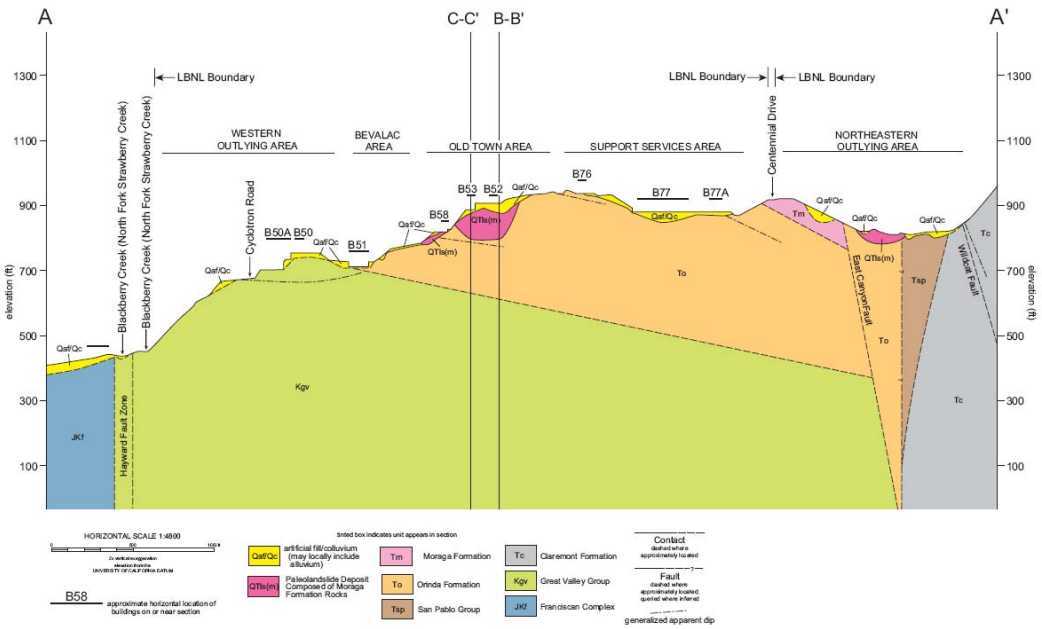

Figure 2-12 Geological cross section shown in Figure 2-11

During a day field trip at the LBNL site (led by geologist Preston Jordan, who has mapped in detail part of the lab site), several sites with faults were visited, including the Wild Cat and East Canyon Faults. Although they are not exposed, documentation and pictures of the fault zone are available from road and building construction and nearby well data.

Wild Cat and East Canyon Faults are minor, secondary splay faults associated with the Hayward Fault. The Hayward, a major branch of the San Andreas Fault system, is a zone of highly deformed rocks that trend N30 degrees west from an area southeast of San Jose to the San Pablo Bay. It exhibits creep along at least 68 km of its 100 km length, and its width ranges from 2 to 10 km.

Wild Cat and East Canyon Faults cut late Cenozoic strata, striking subparallel to the Hayward Fault. The Wild Cat Fault passes along the eastern margin of LBNL. Regionally, the fault is difficult to map throughout its length and appears to be discontinuous, although it clearly truncates and offsets strata at many locations. At LBNL, it juxtaposes the San Pablo Group (fossiliferous marine sandstone) and Claremont

Formation (marine siliceous rocks), and the strata adjacent to the fault have been severely disrupted by steep, east-to-northeast dipping subsidiary faults. The fault is inactive in this area, and studies suggest that it displaced the Moraga Formation by approximately 6 km northwest.

The trace of the East Canyon fault is based on historic spring locations, air photo analysis, and mapping. Apparent offset of the Orinda Formation (nonmarine sediments such as mudstone sand to fine-medium grained sandstones and conglomerates) and slickensided surfaces consistent with the orientation of the East Canyon Fault were observed in trenches along the fault trace.

As illustrated in Figure 2-13, three main locations were selected for possible analogue studies, based on geological and hydrological characteristics.

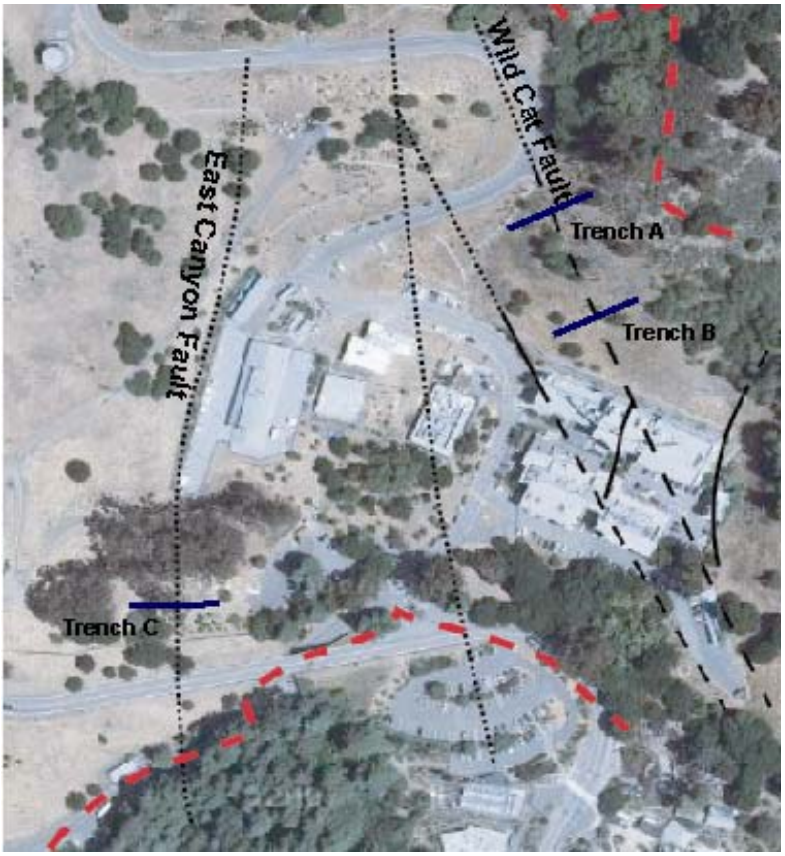

Figure 2-13 Proposed locations of trenches

Site B – Black Diamond Mine

The Black Diamond Mine is located 36 miles (23 km) east of Lawrence-Berkeley National Laboratory and 45 miles (28 km) from downtown San Francisco (Figure 2-14). It is part of the Regional Park of California State.

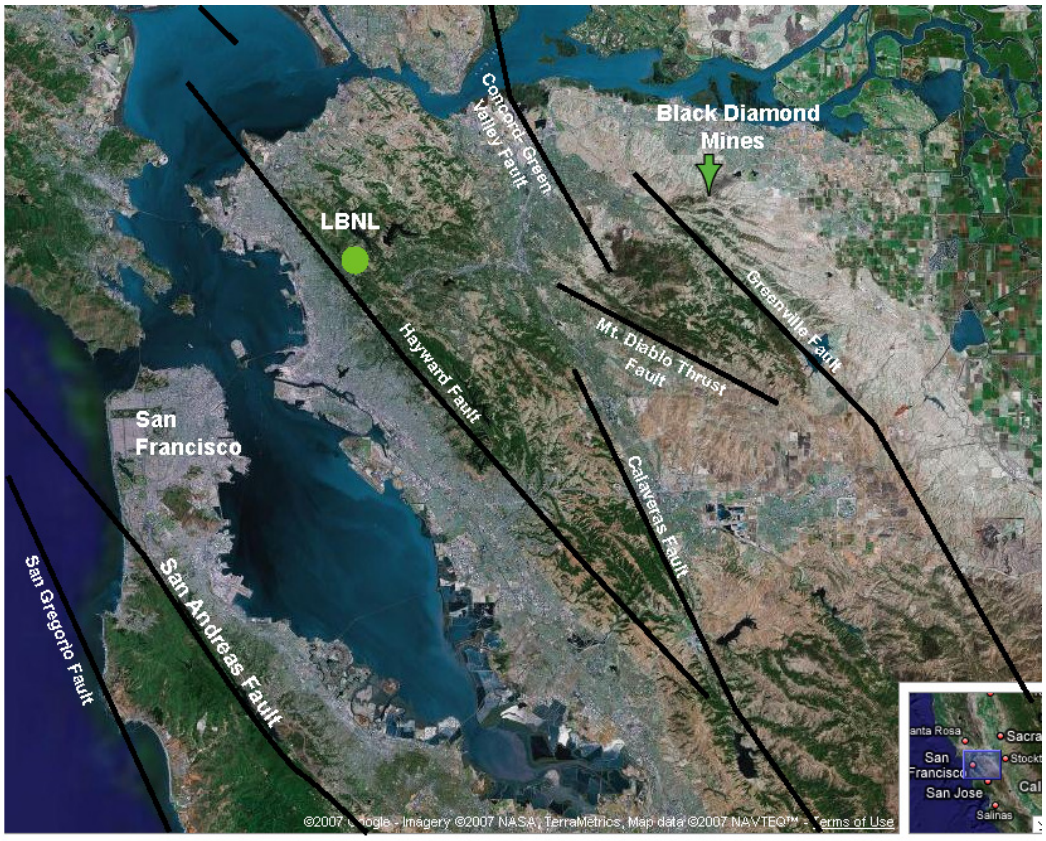

Figure 2-14 Location of Black Diamond Mine and distribution of main faults

Geologically, it is composed of Tertiary alternation of shallow marine sediments, a mixture of shoreface sandstone, offshore marine shales, and distal muddy turbidite deposits. The main formation observed at Black Diamond is the middle Eocene Domengine formation. A day visit with NUMO in October 2007 included a stop at the Hazel-Atlas normal fault described by Eichhubl et al. (2005). The site was primarily mined for coal beds intercalated with well-sorted sandstone, which was also mined for

glass industry. The mine is no longer active, and most of the shafts are open for visiting and scientific investigation.

The intercalation of white sandstone and shale, the presence of a fault, the support of scientific investigations in the mine, the access and proximity to LNBL—all make it one of the possible candidates for analogue study.

The Hazel-Atlas fault by Sullivan et al. (2003), shown in Figure 2-15, offsets a sandstone-shale sequence that is part of the 230–260-m (754–853 ft) thick Domengine Formation. The Hazel-Atlas fault displaces the sandstone-shale sequence by a dip separation of 9 m of normal fault. Shale smear is observed along the fault plane, where it deforms and attenuates to a few centimeters (Eichhubl et al., 2005).

Figure 2-15 Picture showing the Hazel-Atlas fault in the Black Diamond Mine, Antioch, CA

2.7.1.2 COLORADO STATE (POSSIBLE COLLABORATION)

Elkhorn Fault, South Park, Colorado (Figure 2-16)

A research project led by University of Colorado is focused on the Elkhorn fault, to investigate the hydrological properties of an exhumed thrust fault. Funded by the

National Science Foundation, this project assesses the impact of fault on regional groundwater flow. The Elkhorn fault juxtaposes Pre-Cambrian granitic rock in the hanging wall with sedimentary rocks in the footwall. Ongoing characterization studies in the Elkhorn fault are being conducted by the University of Colorado and USGS scientists. Preliminary estimations of fault-zone permeability were presented at the AGU Fall meeting 2007 (Figure 2-17). In this study, geological, hydrological, geophysical, and numeral modeling is being used to characterize the hydrology of the fault zone. A possibility of collaboration is been suggested. The results from this paper presented at AGU and previous studies are shown in Table 2-4.

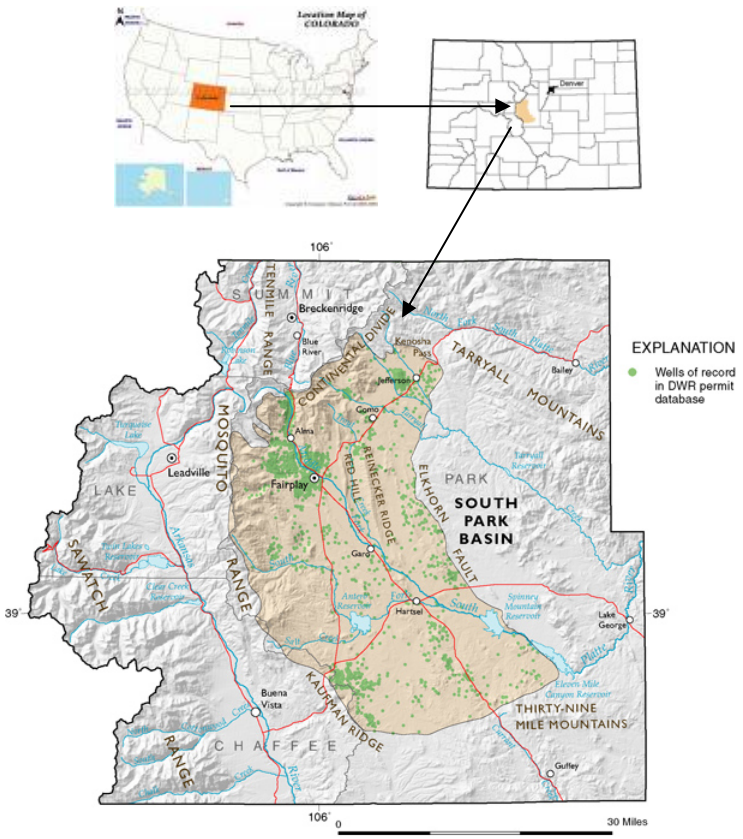

Figure 2-16 Location of Elkhorn Fault, Colorado

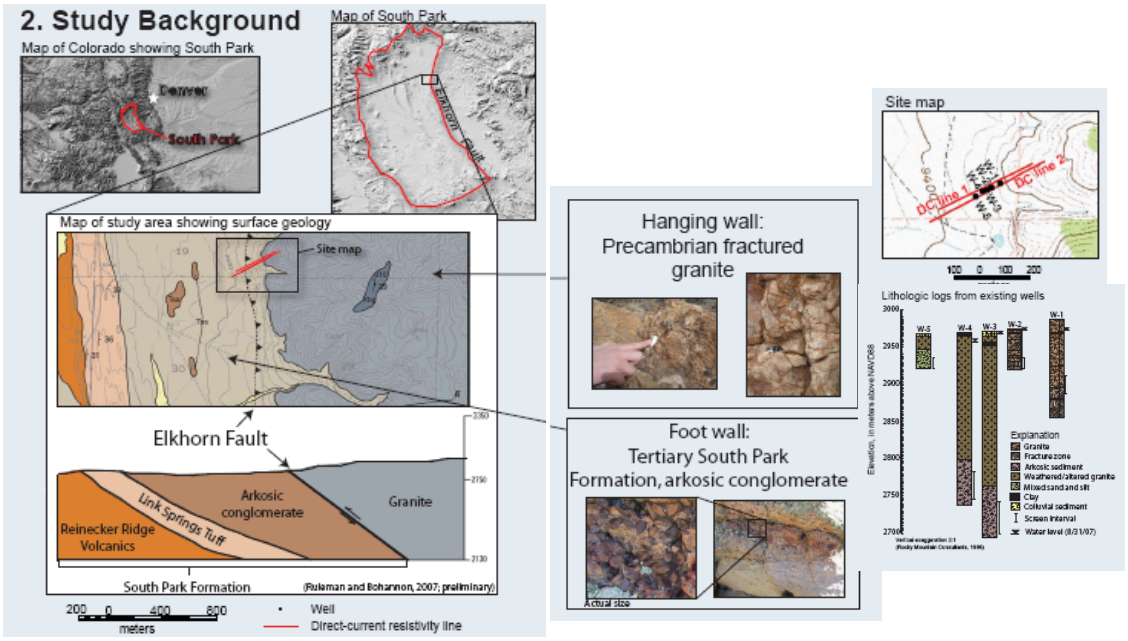

Figure 2-17 Geology and location of wells across the Elkhorn Fault (by http://www.agu.org/meetings/fm07/fm07-sessions/fm07_H23A.html)

2.8 Summary

1) Table 2-2 Normal FaultsTable 2-4,Table 2-5 list the main results from our literature survey regarding fault structural and hydraulic properties, separated by type of fault. Table 2-2 Normal Faults lists the main characteristics of normal faults, Table 2-2 the main characteristics of thrust and reverse faults, and Table 2-3 the main characteristics of strike-slip faults.

2) The overall conclusions of our fault study are that no matter what type of fault (i.e., normal, thrust, or strike-slip) or lithology (i.e., lithified sedimentary, crystalline, or welded volcanic rock), whether during inactive or interseismic deformation; the fault core will act as a barrier to fluid flow normal to the fault, while open fractures in the damage zone would act as a conduit (either parallel to the strike and dip) of a fault. However, the fault core would act as a short-lived, syn-deformational fluid-flow conduit during coseismic deformation, when there is an increase in pore pressure and changes in the elastic properties of rock.

3) Except for elolian sandstone, which might have higher matrix porosity and permeability than the deformation bands and fault core, most hydrological studies in fault zones within low-permeability rock suggest a semi-impermeable fault core, a highly permeable and conductive damage zone, and a low-porosity and low-permeability protolith. The permeability in the damage zone is found to be about two to three orders of magnitude higher than in the protolith, and the fault-core permeability is up to seven orders of magnitude lower than that of the damage zone. Such results implicitly suggest that faults are anisotropic.

4) Hydraulic properties in crystalline rock have been measured in laboratory, field, and modeling studies. Using different methodologies, we found that a pattern emerged when comparing permeability values from laboratory measurements. In general, the permeability of a protolith or host rock ranges from 10^{-14} to 10^{-16} m^2 at 4 to 30 MPa confining pressure. At much higher confining pressure, the permeability reaches a minimum, i.e. 10^{-21} m^2. In damage zones, the permeability varies according to fracture density, ranging from 10^{-12} to 10^{-19} m^2 over a wide range of confining pressures. In the fault core, the permeability ranges from 10^{-16} to 10^{-20} m^2, with confining pressures up to 200 MPa.

5) Hydraulic properties obtained from exhumed rock samples tend to display less pressure sensitivity, due to the presence of weathering products. Furthermore, tests on samples from any fault zone represent only one stage in the temporal evolution of the fault.

6) The permeability of rock obtained from outcrop is up to two orders of magnitude higher than that obtained from drill cores. Therefore, permeability values should be used with caution for developing quantitative models of fluid flow.

7) Permeability from slug and pumping tests at thrust and reverse faults suggest higher permeability values when compared to laboratory measurements. In both cases, the permeabilites of the protolith and damage zone were found to be two to five orders of magnitude higher than laboratory values.

8) Insufficient downhole data across fault zone exist in the literature for low-permeability rock. Borehole-scale studies of fault properties and fault structure are necessary to quantify *in situ* permeability structure of faults.

9) Although outcrop and core samples are often used to infer the permeability structure of fault zones, it is clear that the spatial heterogeneity is a 3 D problem.

10) The majority of faults used to compile this report fall into the combined conduit-barrier category of the Caine at al. (1996) classification. However, the Carbonaras and Median Tectonic Line are more complex and do not fit within Caine's classification.

11) Scaling relationships between fault length and displacement, fault-core width and displacement, and fault length and width exist, and should be taken in consideration during regional site investigations. Doing so would provide estimates for each fault component and possibly the extent of geological and hydrological investigation**.**

12) The possibility exists that fractures are localized and focused on one side of the fault, either in the hanging-wall or footwall. There is a few references related to ore deposits suggesting focused mineralization on one side of the fault zone. This would be a useful tool with which to classify fault-zone hydrology based on fracture intensity and fluid flow.

2.9 Characterization Strategy

In this section, we describe some of the characterization strategies for classifying fault-zone architecture used to minimize characterization efforts related to geological and hydrogeological systems. Also, in analyzing the geology of the Japanese archipelago, where faults are found ubiquitously, one of the main questions working with fault zones in Japan is whether the fault is a long-lived inactive fault.

In the case of an inactive fault, several kinds of efforts could be useful:

(1) Analyses of rock types around the fault zone and the age of last reactivation could help to estimate the extent of fluid-rock interaction (such as mineral precipitation and alteration);

(2) Knowledge of the current stress field could provide insights into crustal deformation/structural regimes.

(3) It is clear that in all types of rocks, faults are composed of two main components: damage zone and fault core. Therefore, this classification is also valid to site(s) in Japan.

(4) Scaling relationships can be used for fault characterization. Although there is still a lack of consensus among scientists, there is enough evidence that assert that linear relationships exist among fault length, displacement, damage zone, and width of fault core.

(5) Investigators should test the hypothesis that some fluid flow is confined to one side of fault zone, either on the hanging-wall or footwall. In this case, examples of mineralized ore deposits would be valuable in providing evidence that certain types of faults have such preferential flow characteristics.

(6) It is clear that there is a lack of *in situ* hydraulic investigation across/within faults to understand their overall hydrologic effects to the surrounding flow field. The majority of drill holes are focused on oil and ore exploration that treat faults as boundary conditions, and groundwater management that concentrates on shallow-depths studies.

(7) Based on our literature survey so far, the fault types (normal, reverse, and strike-slip) by themselves do not appear to be a clear classifier of the hydrology of fault zones. However, there still remains a possibility that other geologic attributes and scaling relationships can be used to predict or bracket the range of the hydrologic behavior of fault zones.

2.10 References

Anderson, J.L., Osborne, R.H., and Palmer, D.F., 1983, Cataclastic rocks of the San Gabriel fault- an expression of deformation at deeper crustal levels in the San Andreas Fault zone. Tectonophysics, 98, 209-251.

Andersson, J.E., Ekman, L., Nordqvist, R., and Winber, A., 1991, Hydraulic testing and modeling of a low fracture zone at Finnsjon, Sweden. Journal of Hydrology, 126, 45-77 .

Antonellini, M. and A. Aydin, 1994, Effect of faulting on fluid flow in porous sandstones: petrophysical properties, American Association of Petroleum Geologists Bulletin, v. 78, p. 355-377.

Antonellini, M. A., A. Aydin and D. D. Pollard, 1994, Microstructure of deformation bands in porous sandstones at Arches National Park, Grand County, Utah, Journal of Structural Geology, v. 16, no. 7, p. 941-959.

Antonio, F. and Pacheco, L., 2002, Response to pumping of wells in sloping fault zone aquifers. Journal of Hydrology, 259, 116-135.

Aydin, A., and Johnson, A.M., 1978, Development of Faults as Zones of Deformation Bands and as Slip Surfaces in Sandstone, Pure & Applied Geophysics, v. 116, p. 931-942.

Aydin, A., 2000, Fractures, faults, and hydrocarbon entrapment, migration and fl ow: Marine and Petroleum Geology, v. 17, p. 797–814, doi: 10.1016/S0264-8172(00)00020-9.

Ball, L.B., Ge, S., and Caine, J.S., 2007, Preliminary estimates of fault-zone permeability through integrated geophysical and hydrological data, Elkhorn Fault, South Park, Colorado, AGU Fall Meeting, H23A-1019.

Bense, V.F., van den Berg, E.H., and Van Balen, R.T., 2003, Deformation mechanisms and hydraulic properties of fault zones in unconsolidated sediments, the Netherdlands. Hydrogeology Journal, 11, 319-332, DOI 10.1007/s10040-003-0262-8.

Brown, S.R., 1987, Fluid flow through rock joints: Effects of surface roughness: Journal of Geophysical Research, 99, 9373–9390.

Bruhn, R. L. and W. A. Yonkee, 1988, Fracture networks: Implications for fault zone permeability and mechanics, EOS, v. 69, p. 484.

Bruhn, R.L., Parry, W.T., Yonkee, W.A. and Thompson, T., 1994, Fracturing and Hydrothermal Alteration in Normal Fault Zones, Pageoph, 142, 3 /4.

Caine, J.S. and Forster, C.B., 1999, Fault zone architecture and fluid flow: insights from field data and numerical modeling, in Faults and Subsurface Fluid Flow in the Shallow Crust, Geophysical Monograph Series 113, AGU, 101-128.

Caine, J. S., Evans, J. P., and Forster, C. B., 1996, Fault zone architecture and permeability structure, Geology, 18, 1025-1028.

Chester, F. J. and Logan J. M., 1986, Implications for mechanical properties of brittle faults from observations of the Punchbowl fault zone, California, Pure and Applied Geophysics, v. 124, p. 80-106.

Chester, F. M., 1999, Field Guide to the Punchbolw Fault Zone at Devil's Punchbowl Los Angeles County Park, California.

Chester, F.M., Evans, J.P., and Biegel, R.L.,1993, Internal structure and weakening mechanisms of the San Andreas Fault, J. Geophys. Res., 98, 771-786.

Campbell, K., Wolfsberg, A., Fabryka-Martin, J., and Sweetkind, D., 2002, Chlorine-36 data at Yucca Mountain: statistical tests of conceptual models for unsaturated-zone flow, Journal of Contaminant Hydrology, 1862, 1-19.

Cowie, P. A. and Scholtz, C. H., 1992, Physical explanation for the displacement-length relationship of faults using a post-yield fracture mechanics model. Journal of Structural Geology 14, 1133-l 148.

Davatzes, N. C., Eichhubl, P., and Aydin, A., 2005, Structural evolution of fault zones in sandstone by multiple deformation mechanisms: Moab fault, southeast Utah. Geological Society of America Bulletin, vol. 117, no. 1/2, p. 135-148.

Davison, C.C. and Kozak E.T., 1988, Hydrogeological Characteristics of Major Fracture Zones in a Granite Batholith of the Canadian Shield. In: Proceedings Fourth Canadian/American Conference on Hydrogeology, Banff, Alberta. Edited by B. Hitchon and S. Bachu.

Diment, R. and Craig, S., 1999, Brewery Creek gold deposit, central Yukon. *In:* Yukon Exploration and Geology 1998, C.F. Roots and D.S. Emond (eds.), Exploration and Geological Services Division, Yukon, Indian and Northern Affairs Canada, p. 225-230.

Dholakia, S.K., Aydin, A., Pollard, D.D., and Zoback, M.D., 1998, Fault-controlled hydrocarbon pathways in the Monterey Formation, California: American Association of Petroleum Geologists Bulletin, 82, 1551–1574.

Eichhubl, P. and Boles, J.R., 2000, Focused fluid flow along faults in the Monterey Formation, coastal California. GSA Bulletin, 112 (11), 1667-1679.

Eichhubl, P., Taylor, W. L., Pollard, D. D. and Aydin, A., 2004, Paleo-fluid flow and deformation in the Aztec Sandstone at the Valley of Fire, Nevada-Evidence for the coupling of hydrogeologic, diagenetic, and tectonic processes. Geological Society of America Bulletin, 116 (9), 1120-1136.

Eichhubl, P., D'Onfro, P., Aydin, A., Waters, J., and McCarty, D. K., 2005, Structure, petrophysics, and diagenesis of shale entrained along a normal fault at Black Diamond Mines, California--Implications for fault seal. AAPG Bulletin, 89 (9), 1113-1137.

Evans, J.P. and F.M. Chester, 1995, Fluid-rock interaction in faults of the San Andreas system: Inferences from San Gabriel fault rock geochemistry and microstructures, Journal of Geophysical Research, 100 (B7), 13007-13020.

Evans, J. P., Yonkee, W. A., Parry, W. T., and Bruhn, R. L., 1997, Fault-related rocks of the Wasatch normal fault, in: Brigham Young University Studies in Geology, Geological Society of America Fieldtrip Guidebook, 42, 279–297.

Evans, J.P., Forster, C.B., and Goddard, J.V.,1997, Permeability of fault-related rocks and implications for hydraulic structure of fault zones, Journal of Structural Geology, 19 (11), 1393-1404.

Evans, J. P., 1990, Textures and deformation mechanisms and the role of fluids in cataclastically deformed granitic rocks, in: Knipe, R. J., and Rutter, E., eds., Deformation Mechanisms, Rheology, and Tectonics, Geological Society of London Special Publication .54, 29-39.

Faulkner, D.R, Lewis, A.C., Rutter, E.H., 2003, On the internal structure and mechanics of large strike-slip fault zones: field, observations of the Carboneras fault in southeastern Spain, Tectonophysics, 367, 235– 251.

Fisher, Q. J., and Knipe R. J., 1998, Fault sealing processes in siliciclastic sediments, in G. Jones, Q. Fisher, and R. J. Knipe, eds., Faulting, fault sealing and fluid flow in hydrocarbon reservoirs: Geological Society (London) Special Publication 148, p. 117-134.

Flint, A.L., Flint, L.E., Bodvarsson, G.S., Kwicklis, E.M., and Fabryka-Martin, J., 2001, Evolution of the conceptual model of unsaturated zone hydrology at Yucca Mountain, Nevada. Journal of Hydrology, 247, 1-30.

Forster, C.B., Goddard, J.V., and J.P. Evans, 1994, Permeability structure of a thrust fault. Proceedings of Workshop LXIII, "The Mechanical Involvement of Fluids in Faulting", June 6-10, 1993. U.S.G.S. Open-File Report 94-228.

Forster, C. B. and Evans J. P., 1991, Hydrogeology of thrust faults and crystalline thrust sheets: results of combined field and modeling studies, Geophysical Research Letters, 18, 979-982.

Forster, C. B., Evans, J. P., Tanaka, H., Jeffreys, R., and Nohara, T., 2003, Hydrologic properties and structure of the Mozumi Fault, central Japan. Geophysical Research Letters, 30, 6, 8010, doi:10.1029/2002GL014904.

Fossen, H., and Bale, A., 2007, Deformation bands and their influence on fluid flow. AAPG Bulletin, 91,12, 1681-1700.

Freeman, D. H., 1990, Permeability effects of deformation bands in porous sandstones: Master's thesis, University of Oklahoma, Norman, Oklahoma, p. 90.

Goddard, J.V., and Evans, J.P., 1995, Fluid-rock interactions in faults of crystalline thrust sheets, northwestern Wyoming, USA: Inferences from Geochemistry of Fault-related Rocks: Journal of Structural Geology, 17, 533-549.

Goddard, J.V. and Evans, J.P.,1995, Chemical changes and fluid-rock interaction in faults of crystalline thrust sheets, northwestern Wyoming, U.S.A., Journal of Structural Geology, 17, 533-547.

Hammond, K.J., and Evans, J.P., 2003, Geochemistry, mineralization, structure, and permeability of a normal fault zone, Casino mine, Alligator Ridge District, north central Nevada. Journal of Structural Geology, 25, 717-736.

Henriksen, H., 2008, Late Quaternary regional geodynamics and hydraulic properties of the crystalline rocks of Fennoscandia, Journal of Geodynamics 45, 49–62.

Hatcher, Jr., R.D., 1995, Structural geology. Principles, Concepts, and Problems. Second Edition. Prentice Hall, 525p.

Heynekamp, M.R., Goodwin, L.B., Mozley, P.S., and Haneberg, W.C., 1999, Controls on fault zone architecture in poorly lithified sediments, Rio Grande Rift, New Mexico: implications for fault-zone permeability and fluid flow, in Faults and Subsurface Fluid Flow in the Shallow Crust, Geophysical Monograph Series 113, AGU, 27-50.

Hickman, S., R. Sibson, and R. Bruhn, 1995, Introduction to special section: Mechanical involvement of fluids in faulting, Journal of Geophysical Research, 100 (B7), 12831-12840.

Hobbs, B.E., Means, W.D. and Williams, P.F., 1976, An outline of structural geology, New York: Willey, 571p.

Janssen, C., Hoffman-Rothe, A., Tauber, S. and Wilke, H., 2002, Internal structure of the Precordilleran fault system (Chile)—Insights from structural and geophysical observations. Journal of Structural Geology, 24, 123-143.

Japan Nuclear Cycle Development Institute (JNC), 2000, H12 Project to Establish Technical Basis for HLW Disposal in Japan: Supporting Report 1, pp.154.

Jourde, H., Flodin, E., Aydin, A., Durlofsky, L., and Wen, X., 2002, Computing permeability of fault zones in eolian sandstone from outcrop measurements: American Association of Petroleum Geologists Bulletin, v. 86, p. 1187–1200.

Knipe, R. J., 1992, Faulting processes and fault seal, in R. M. Larsen, eds., Structural and Tectonic Modeling and its Application to Petroleum Geolgoy, Stavanger, NPF, p. 325-342.

Knipe, R. J., 1993, The influence of fault zone processes and diagenesis on fluid flow, in A. D. Horbury and A. G. Robinson, eds., Diagenesis and Basin Development, American Association of Petroleum Geologists, Studies in Geology #36, p. 135-148.

Knipe, R. J., Q. J. Fisher, M. R. Clennell, A. B. Farmer, A. Harrison, B. Kidd, E.McAllister, J. R. Porter, and E. A.White, 1997, Fault seal analysis: Successful methodologies, application and future directions, in P. Møller-Pedersen and A. G. Koestler, eds., Hydrocarbon seals: Importance for exploration and production: Norwegian Petroleum Society (NPF) Special Publication 7, p. 15– 40.

Knipe, R.J., Jones, G., Fisher, Q.J., 1998, Faulting, fault sealing and fl uid fl ow in hydrocarbon reservoirs: An introduction, *in* Knipe, R.J., Jones, G., Fisher, Q.J., eds., Faulting, Fault Sealing and Fluid Flow in Hydrocarbon Reservoirs: Geological Society [London] Special Publication 147, p. vii–xxi.

Lawrence Berkeley National Laboratory (LBNL), 2000, RCRA Facility Investigation Report for the Environmental Restoration Program

LeCain, Gary D., Severson, Gary R., 1998, Results of air-injection and tracer testing of the Ghost Dance Fault, Yucca Mountain, Nevada. 8th International Conference on High-Level Radioactive Waste Management, Las Vegas, NV (US), 05/11/1998--05/14/1998; PBD: 11 May 1998.

Lin, A., Ouchi, T., Chen, A., and Maruyama, T., 2001, Co-seismic displacements, folding and shortening structures along the Chelungpu surface rupture zone occurred during the 1999 Chi-Chi (Taiwan) earthquake Tectonophysics, 330, 3-4,225-24.

Lockner, D., H. Naka, H. Tanaka, H. Ito, and R. Ikeda, 2000, Permeability and strength of core samples from the Nojima fault of the 1995 Kobe earthquake, in *Proceedings of the Internaional Workshop on the Nojima Fault Core and Borehole Data Analysis*, Tsukuba, Japan, 22– 23, November 1999, H. Ito, K. Fujimoto, H. Tanaka, and D. Lockner (Editors), *U.S. Geol. Surv. Open-File Rept. 00-129*, 147–152.

Lopez, D.L, and Smith, L., 1996, Fluid flow in fault zones: Influence of hydraulic anisotropy and heterogeneity on the fluid flow and heat transfer regime, Water Resources Research, 32, 10, 3227-3235.

Marler, J. and Ge, S., 2003, The permeability of the Elkhorn Fault zone, South Park, Colorado. Groundwater, 41, 3, 321-332.

Martel, S.J., 1990, Formation of compound strike-slip fault zones, Mount Abbot quadrangle, California. Journal of Structural Geology, 12, 7, 869-882.

Martel, S.J., Pollard, D.D., and Segall, P., 1988, Development of simple fault zones in granitic rock, Mount Abbot quadrangle, Sierra Nevada: Journal of Geophysical Research, v. 94, p. 1451–1465.

Matthäi, S.K., Aydin, A., Pollard, D.D., and Roberts, S., 1998, Numerical simulation of deviations from radial drawdown in a faulted sandstone reservoir with joints and zones of deformation bands, *in* Jones, G.A.K., Fisher, Q.J., and Knipe, R.J., eds., Faulting, fault sealing and fl uid fl ow in hydrocarbon reservoirs: Geological Society [London] Special Publication 147, p. 157–191.

Mayer, A., May, W., Lkukkarila, C. and Diehl, J., 2007, Estimation of fault-zone conductance by calibration of a regional groundwater flow model: Desert Hot Springs, California, Journal of Hydrology, 15, 1093-1106.

McCaig, A. M., 1988, Deep fluid circulation in fault zones, Geology, 16, 867-870.

McCaig, A. M., 1989, Fluid flow through fault zones, Nature, 340, 600 .

Mizoguchi, K., Hirose, T., and Shimamoto, T., 2000, Internal and permeability structures of Nojima fault zone: data correlation from surface and core samples. Journal data.

Mizoguchi K., Hirose, T., Shimamoto, T. and Fukuyama, E., 2008, Internal structure and permeability of the Nojima fault, southwest Japan. Journal of Structural Geology, 30, 513-524.

Morrow, C. A., and Lockner, D.A., 1994, Permeability differences between surface-derived and deep drillhole core samples, Geophys. Res. Lett., 21, 2151–2154.

Mozley, P.S. and Goodwin, L.B., 1995, Patterns of cementation along a Cenozoic normal fault: A record of paleoflow orientations, Geology, v. 23, p. 539-542.

Moran, J.E., and Hudson, G. B., 2000, Using groundwater age and other isotopic signatures to delineate groundwater flow and stratification, Lawrence Livermore National Laboratory, U.S.A.

Myers, R., 1999, Mechanism and permeability of brittle faults in sandstone, Ph.D. dissertation, Stanford University, Stanford, California, 176 p.

National Research Council, 1996, Rock Fractures and Fluid Flow. Contemporary Understanding and Applications. National Academy of Sciences, Washington. 551p.

Neubauer, F., 2005, Fault zone properties and fault classification: the role of fault history. Geophysical Research Abstracts, 7, 02393.

Nishikawa, T., Izbicki, J.A., Hevesi, J.A., Stamos, C.L., and Martin, P., 2004, Evaluation of geohydrology framework, recharge estimates, and ground-water flow of the Joshua Tree area, San Bernardino County, California, USGS, Scientific Investigation Report 2004-5267, pp.113.

Nohara, T., Tanaka, H., Watanabe, K., Furukawa, N. And Takami, A., 2006, *In situ* hydraulic test in the active fault survey tunnel, Kamioka mine, excavated through the active Mozumi- Sukenobu fault zone and their hydrological significance. Island Arc, 15, 537-545.

Onishi, C.T., Shimizu, I., Mizoguchi, K, Uehara, S. and Shimamoto, T., 2002, Influence of fault on the anisotropy of pore structure and permeability in granite, Tono Area, Central Japan. American Geophysical Union Meeting, AGU Fall Meeting, San Francisco, U.S.A. Tectonophysics Session T21A-1074.

Pachell, M.A. and Evans, J.P., 2002, Growth, linkage, and termination processes of a 10-km-long strike-slip fault in jointed granite: the Gemini fault zone, Sierra Nevada, California. Journal of Structural Geology, 24, 1903-1924.

Pittman, E. D., 1981, Effects of fault-related granulation on porosity and permeability of quartz sandstones, Simpson Group (Ordovician), Oklahoma: AAPG Bulletin, v. 65, p. 2381– 2387.

Rawling, G., Goodwin, L., and Wilson, J., 2001, Internal architecture, permeability structure, and hydrologic significance of contrasting fault zone types, Geology, 29 (1), 43-46.

Schulz, S.E., and Evans, J.P., 1998, Spatial variability in microscopic deformation and composition of the Punchbowl fault, southern California: implications for mechanisms, fluid-rock interaction, and fault morphology, Tectonophysics, 295, 223-244.

Schulz, S.E., and Evans, J.P., 2000, Mesoscopic structure of the Punchbowl fault, southern California and the geologic and geophysical structure of active strike-slip faults: Journal of Structural Geology, 22, 913–930, doi: 10.1016/S0191-8141(00)00019-5.

Scholz, C.H. and Cowie, P.A., 1990, Determination of total strain from faulting using slip measurement. Nature, 346, 837-389.

Seront, B.,Wong, T.-F., Caine, J.S., Forster, C.B., Bruhn, R.L., 1998, Laboratory characterization of hydromechanical properties of a seismogenic normal fault system. J. Struct. Geol. 20, 865–881.

Sigda, J., Goodwin, L., Mozley, P., and Wilson, J., 1999, Permeability Alteration in Small-Displacement Faults in Poorly Lithified Sediments: Rio Grande Rift, Central New Mexico, in Haneberg, W., Mozley, P., Moore, J., and Goodwin, L., eds., Faults and Subsurface Fluid Flow in the Shallow Crust, American Geophysical Union Monograph, 113, 51-68.

Swedish Nuclear Fuel and Waste Management Co., 2005, Preliminary site description Forsmark Area – version 1.2, ISSN 1402-3091, SKB Rapport R-05-18, pp 745.

Sibson, R. H., 1973, Interactions between temperature and fluid pressure during earthquake faulting - A mechanism for partial or total stress relief, Nature, 243, 66-68.

Sibson, R. H., Moore, J., and Rankin, A.H., 1975, Seismic pumping—A hydrothermal fluid transport mechanism, Journal Geol. Soc. London, 131, 653-659.

Sibson, R. H., 1981, Fluid flow accompanying faulting: field evidence and models, in D. W. Simpson and P. G. Richards, eds., Earthquake Prediction: an International Review. American Geophysical Union Maurice Ewing Series 4, p. 593-603.

Sibson, R. H., 1987, Earthquake rupturing as a hydrothermal mineralizing agent, Geology, 15, 701-704.

Sibson, R. H., 1990, Conditions of fault-valve behavior, in R. J. Knipe and E. H. Rutter, eds., Deformation Mechanisms, Rheology and Tectonics. Geological Society Special Publication 54, p. 15-28.

Shipton, Z. K., Evans J. P., Robeson K., Forster C. B., and Snelgrove S., 2002, Structural heterogeneity and permeability in faulted aeolian sandstone: Implications for subsurface modeling of faults: AAPG Bulletin, 86, 863– 883.

Shipton, Z. K., and P. Cowie, 2003, A conceptual model for the origin of fault damage zone structures in high-porosity sandstone: Journal of Structural Geology, 25, 333–344.

Solum, J.G., van der Pluijim, B.A., and Peacor, D.R., 2005, Neocrystallization, fabrics and age of clay minerals from an exposure of the Moab Fault, Utah, Journal of Structural Geology, 27, 1563–1576.

Sorkhabi, R., Hasegawa, S., Inwanaga, S., and Fujimoto, M., 2002a, Sealing assessment of normal faults in clastic reservoir – The role of fault geometry and shale smear parameter -, Journal of Japanese Association for Petroleum Technology, 67, 6, 576-589.

Sorkhabi, R.; Hasegawa, S., Suzuki, K., Takahashi, M., Fujimoto, M., Sakuyama, N., and Iwanaga, S., 2002b, Modeling of shale smear parameters, fault seal potential, and fault rock permeability, AAPG Annual Meeting, Huston, Texas.

Stamos, C. L., Cox, B.F., Izbicki, J.A., and Mendez, G.O., 2003, Water Quality near the Helendale Fault in the Mojave River Basin, San Bernardino County, California, USGS, Water-Resources Investigations Report 03-4069. http://pubs.usgs.gov/wri/wri034069/wrir034069.book.pdf

Sone, H. and Shimamoto T., 2005, Transport and Frictional Properties of a Serpentinite Fault Zone Along Gokasho-Arashima Tectonic Line. Abstract, AOGS 2nd Annual Meetin, Singapore.

Sullivan, R., and J. Waters, 1980, History of Mount Diablo coalfield, Contra Costa County, California: California Geology, 33, 51–59.

Sullivan, R., J. Waters, and M. D. Sullivan, eds., 1994, Field guide to the geology of Black Diamond Mines Regional Preserve: Northern California Geological Society, 46 p.

Sullivan, M. D., R. Sullivan, and J. Waters, 2003, Reservoir characterization and sequence stratigraphy of the Domengine Formation, Black Diamond Mines Regional Preserve, Northern California. Domengine field trip guidebook: Pacific Section SEPM, 52 p.

Swedish Nuclear Fuel and Waste Management Co., 2005, Preliminary site description Forsmark area – version 1.2**,** SKB Rapport R-05-18, p. 745.

Schilische, R.W., Young, S. S., Ackermann, R.V. and Gupta, A., 1996, Geometry and scaling relations of a population of very small rift-relatad normal faults. Geology, 24, 683-686.

Takahashi, M., 2003a, Continuity and transport properties of shale smear in sedimentary basin, Journal of Geography 112 (5), 926-938. *In Japanese with English abstract.*

Takahashi, M, 2003b, Permeability change during experimental fault smearing, Journal of Geophysical Research, 108 (B5), 2234, doi:10.1029/ 2002JB001984 .

Tanaka, H., T. Matsuda, K. Omura, R. Ikeda, K. Kobayashi, K. Shimada, T. Arai, T. Tomita, and S. Hirano, 2001a, Complete fault rock distribution analysis along the Hirabayashi NIED core penetrating the Nojima fault at 1140 m depth, Awaji Island, Southweset Japan, Report of the National Research Institute for Earth Science and Disaster Prevention, No.61, 195– 221.

Tanaka, H., S. Hinoki, K. Kosaka, A. Lin, K. Takemura, A. Murata, and T. Miyata, 2001b, Deformation mechanisms and fluid behavior in a shallow, brittle fault zone during coseismic and interseismic periods: Results from drill core penetrating the Nojima Fault, Japan, Isl. Arc, 10, 381– 391.

Tanaka, H., K. Fujimoto, T. Ohtani, and H. Ito, 2001c, Structural and chemical characterization of shear zones in the freshly activated Nojima Fault Awaji Island, southwest Japan, J. Geophys. Res., 106(B4), 8789– 8810.

Tanaka, H.., Omura, K., Matsuda, T., Ikeda, R., Kobayashi, K., Murakami, M., and Shimada, K., 2007, Architectural evolution of the Nojima fault and identification of the activated slip layer by Kobe earthquake, Journal of Geophysical Research, 112, B07304, doi:10.1029/2005JB003977.

Tanaka, H., T. Ito, T. Nohara, and M. Ando, 2007, Descriptions of meso- and microscopic structures of fault zone rocks obtained from penetrating tunnel across the Mozumi-Sukenobu Fault, central Japan, in Geodynamics of Atotsugawa Fault System.

Tanikawa, W., Shimamoto, T., Lin, C-W., and Wey, W-K, 2005, Development of internal and permeability structures of thrusts in the western foothills of Taiwan, AGU Fall Meeting.

Taylor W, Pollard D, Aydin A., 1999, Fluid flow in discrete joint sets: field observations and numerical simulations. J Geophys Res., 104, 28983–29006.

Taylor, W.L., and D.D. Pollard, 2000, Estimation of *in situ* permeability of deformation in porous sandstone, Valley of Fire, Nevada: Water Resources Research, v. 36, p. 2595– 2606.

Tsutsumi, A., Nishino S., Mizoguchi K., Hirose T., Uehara S., Sato K., Tanikawa W., Shimamoto, T., 2004, Principal fault zone width and permeability of the active Neodani fault, Nobi fault system, Southwest Japan. Tectonophysics, 379, 93–108.

Vermilye, J.M., 1996, The growth of natural fracture systems: A fracture mechanics approach. PhD Thesis, Columbia University.

Vermilye, J.M., and Scholz, C.H., 1998, The process zone: A microstructural view of fault growth: Journal of Geophysical Research, 103 (B6), 12,223–12,237, doi: 10.1029/98JB00957.

Yanagizawa, K., Imai, I., Furuya, K, and Nishigaki. M., 1995, The effects of a shaft excavation experiment on the hydrology of the Tono research field, Japan. Journal of Hydrology, 171, 165-190.

Walderhaug, O., 1996, Kinetic modeling of quartz cementation and porosity loss in deeply buried sandstone reservoirs: AAPG Bulletin, 80, 731–745.

Wibberley, C.A.J., Shimamoto, T., 2003, Internal structure and permeability of major strike-slip fault zones: the Median Tectonic Line in Mie Prefecture, Southwest Japan. J. Struct. Geol., 25, 59–78.

3 断層の調査技術の実例、解析及びモデル化

本章では近年の各国各所での断層の現地調査の事例、原位置調査技術の実例、特に水理性状に関する調査、そのデータを使ったモデル化や解析結果をまとめた。加えて異なった水理性状を持った断層が存在する場合の揚水試験の数値シミュレーションを行い、圧力変化の分布や経時変化を調べ、水理試験の解析の知見を得た。

3.1 諸外国での事例

3.1.1 アス、ブラジル

ブラジル北東部に存在するアス貯水池において、貯水量の増減による微小地震の観測データを元に断層周辺のダメージゾーンの透水係数の空間的分布についての解析が行われた。アクダムは 1983 年に先カンブリア時代の楯状地に建設された 34m の高さの土塁ダムである。貯水池の水面の上下と微小地震の発生回数に相関性がある事が以前から知られており、これは低い透水性のマトリックスに囲まれた高い透水性の断層内の間隙水圧の拡散を通じて起こると考えられる。3 軸の高精度なデジタル地震計のネットワークを使って個々の断層内の微小地震の震源の複雑な分布と移動のパターンを解析する事によって、断層の水理パラメータの不均質性が存在する事が示された（do Nascimento et al., 2005）。

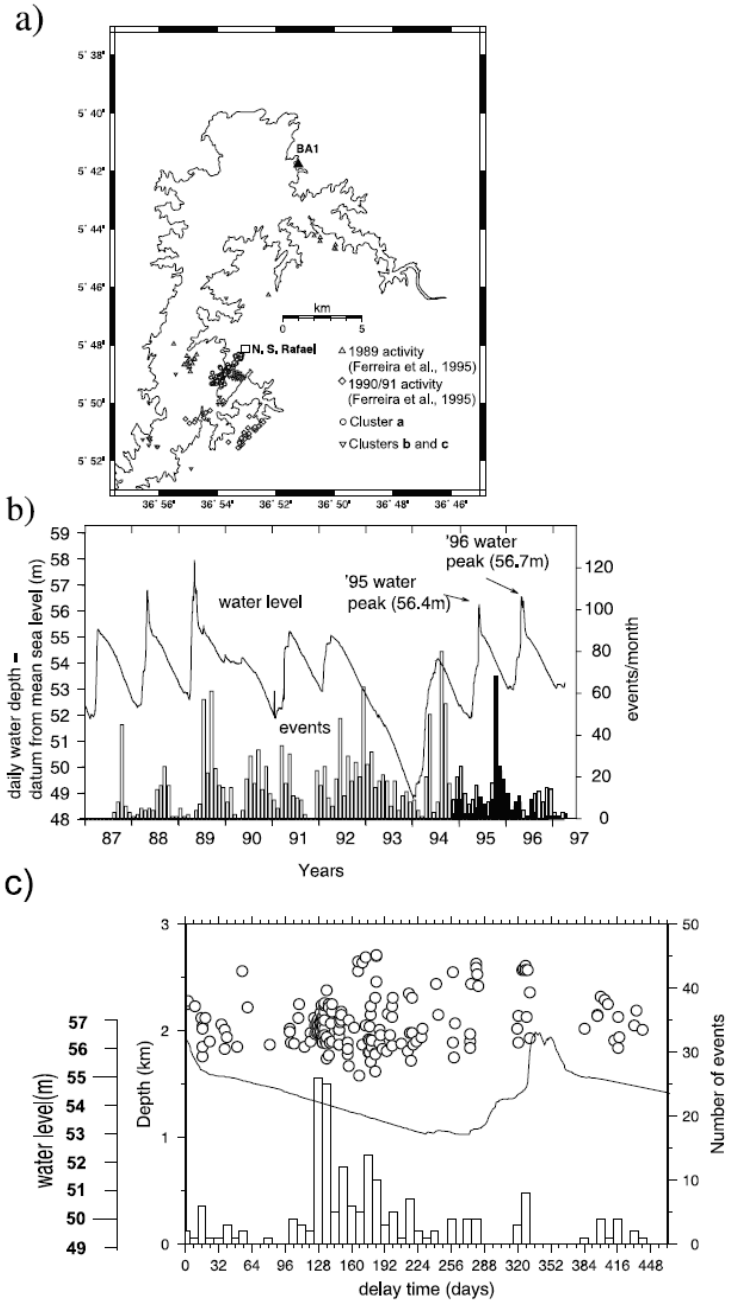

Figure 3-1 a)ブラジルアス貯水池　b) 微小地震と水深の関連性
c)水位変動と地震の遅れ（ do Nascimento et al., 2005）

3.1.2　アンデス南東域、ボリビア

ボリビアのサブアンデスゾーンの逆断層ゾーンのマクロとミクロ構造、及びセメント分布の解析を行ったところ、2.5km 以深ではシリカが 80–90°C を超える温度により、圧力による溶解-析出でセメンテーションが起こり石英が充填して閉じているが、浅部で

は断層はオープンであり外来性の炭酸を含む地層水の側方流動の水みちとなっている可能性がある。大きなスケールでは断層を横切る方向に低い透水性を示し、両側で異なった過程の水が見られる(Labaume et al, 2000)。

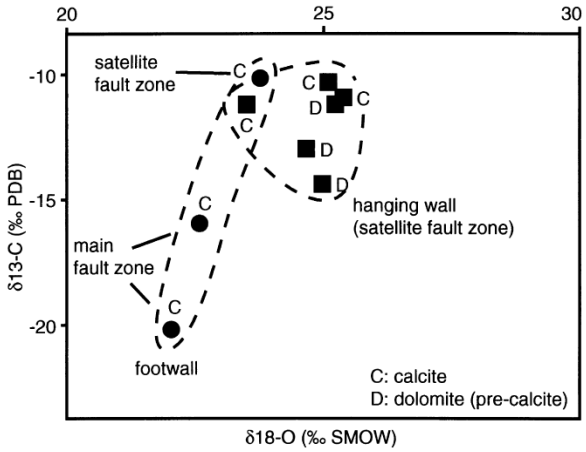

Figure 3-2　断層の部位によって異なる炭素と酸素の同位体の分布(Labaume et al, 2000)

3.1.3　レッドシーヒルズ、エジプト

Sultan ら (2008)によれば、エジプトのレッドシーヒルズの断層水理の解析は以下に記す数多くの手法（地質、物理探査、リモートセンシング等）を組み合わせて効率良く行われた。(1)　地質図 (1:500,000 スケール) (2) ランドサットの TM（Thermatic Mapper）バンド 1 ~7 のリフレクタンスイメージ（解像度 28.5m）、（3）ランドサット TM バンド 2（青）、4（緑）、7（赤）のフォールスカラーモザイク、（4）ランドサット TM のリフレクタンスバンド比モザイク(5/4 × 3/4, 5/1, 5/7)、（5）ASTER（Advanced Spaceborne Thermal Emission and Reflection Radiometer）のレベル 1 A 生データ画像から作成された数値標高モデル（DEMs, 解像度 60m）、（6）TOPAZ (Topographic Parameterization)手法を使った DEM からの水系網と流域界マップ、（7）TRMM （Tropical Rainfall Measuring Mission）の 1999-2001 年の累積降雨量データ、（8）以下の最低 1 つを含む孔井デー

タ：位置、名称、井戸のタイプ、最大水位低下量、溶質成分、TDS、酸素と水素の同位体比、及び地下水位。40 以上の地下水サンプル、EMWRI（Egyptian Ministry of Water Resources and Irrigation）が集めた 20 年に及ぶ 180 本以上の井戸データ、(9) TM バンド 3 と 4 のリフレクタンスから作成した植生データ：NDVI （Normalized Difference Vegetation Index）。これらのデータを総合した解析から、横ずれ断層は多くの場合、水を蓄えたり水みちになっている事が判明した。

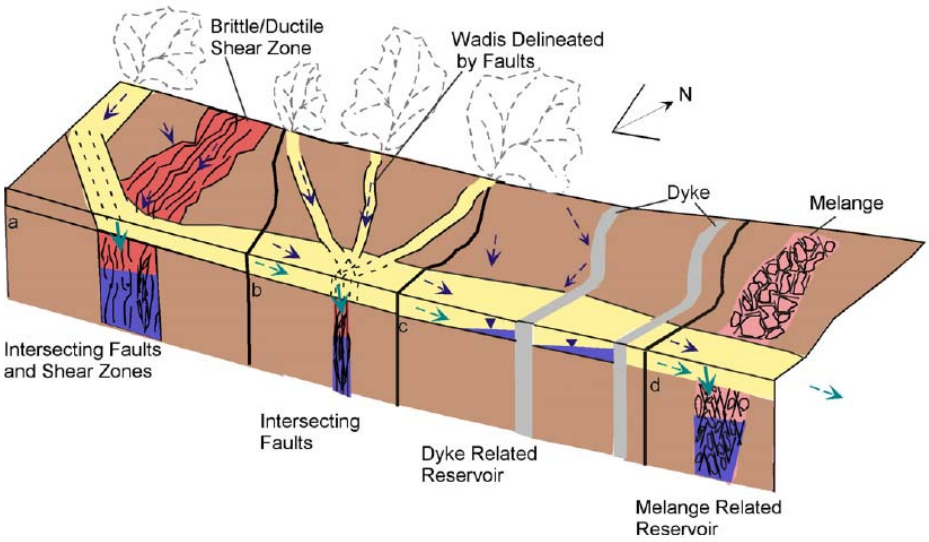

Figure 3-3　　Red Sea Hills、Egypt の横ずれ断層と帯水層(Sultan et al., 2008)

3.1.4　北サマーセット、イギリス

イギリスの北サマーセット地方のジュラ紀の堆積岩に存在する小規模から中規模の大きさの断層系のマッピングが Leckenby ら(2005)によって行われた。これらの断層は横ずれのオーバーステップと正断層である。マッピングは異なった断層スタイル中の地下水の流れの偏りや分布を予測計算する目的で行われた。方解石脈の厚さから過去の水の流れの分布が推定された。フラクチャー密度、開口幅、コンダクタンスの 3 つのパラメータについて調査が行われた。その結果、フラクチャー密度と透水係数には相関性が殆どなく、フラクチャー密度は水理の不均質性を反映してないことがわかった。反対に開口幅とコンダクタンスは水の流れの偏りを反映すると結論された。断層タイプによって違

った特性があり不均質性のパターンが予測可能であった。正断層系では、リレーランプではなく、断層沿いに最大の水の流れの局所化がおこり、収縮横ずれ断層では断層内に、膨張横ずれ断層ではオーバーステップに強い局所化が起こっている。しかし、何れのケースもオーバーステップのダメージの度合いが不均質性のパターンを左右している。

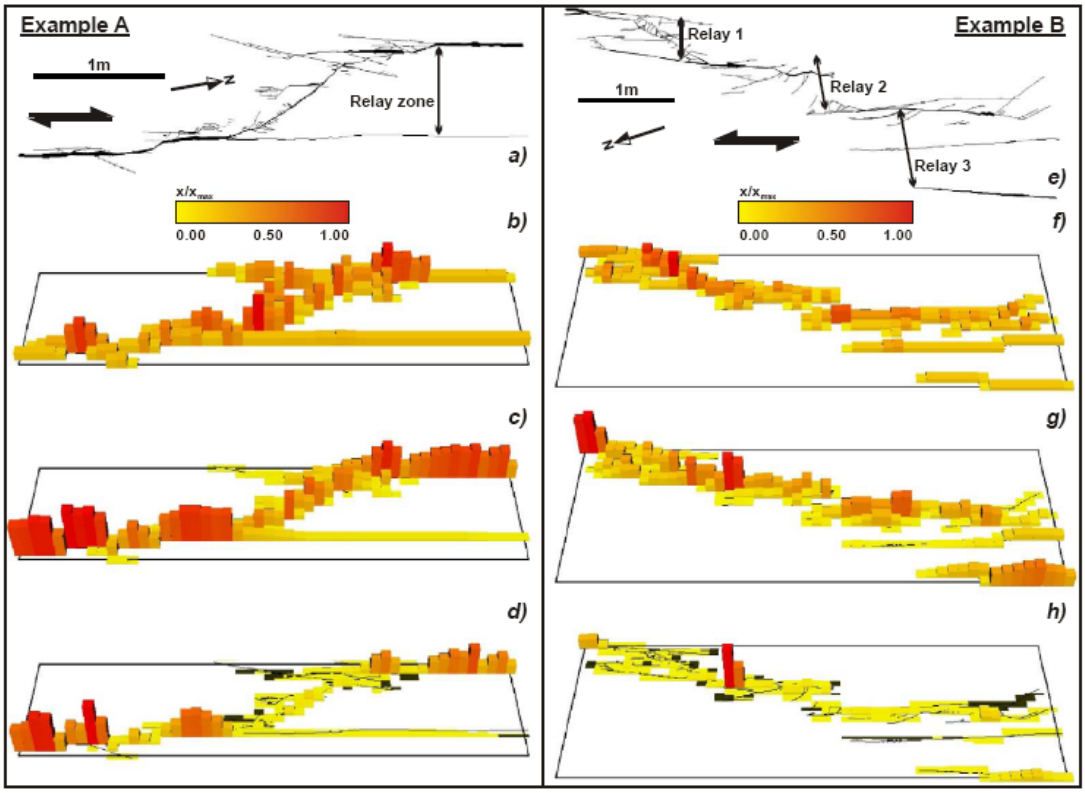

Figure 3-4　横ずれ断層沿いの不均質性の偏り b),f):割れ目頻度、c),g)開口幅、d),h) コンダクタンス分布。Leckenby et al, (2005)

3.1.5 オランダ

Bense と Kooi(2004)は空間的に密に(<10m)、季節毎に数回計測された浅部の温度分布データを使って垂直方向の地下水流動の水平分布を推定した。現場はオランダ南東部の未固結の珪質砕屑堆積岩を切る Peel Boundary 断層ゾーンである。Peel Boundary 断層はこの地域で各所で水平方向の流れに対して不透水性を示す重要な断層である。2℃以上

の温度異常が近在しており、季節ごとに逆の異常を呈する。Bense と Kooi は水と熱の流れの数値モデルを使って地下の温度の時間的、空間的な変動が地表の季節の温度変化と地下水の流れの分布との相互作用に起因していることを示した。温度の水平分布に加えて、井戸の深度方向の分布を制約として使って大きなスケールの地下水の流れの仕組みを推定した。地下の温度パターンをシミュレーションするには長期にわたる地表の温度変化も考慮することが必要であった。彼らの研究は近年の気候変化の影響を組み入れた点で新しい。

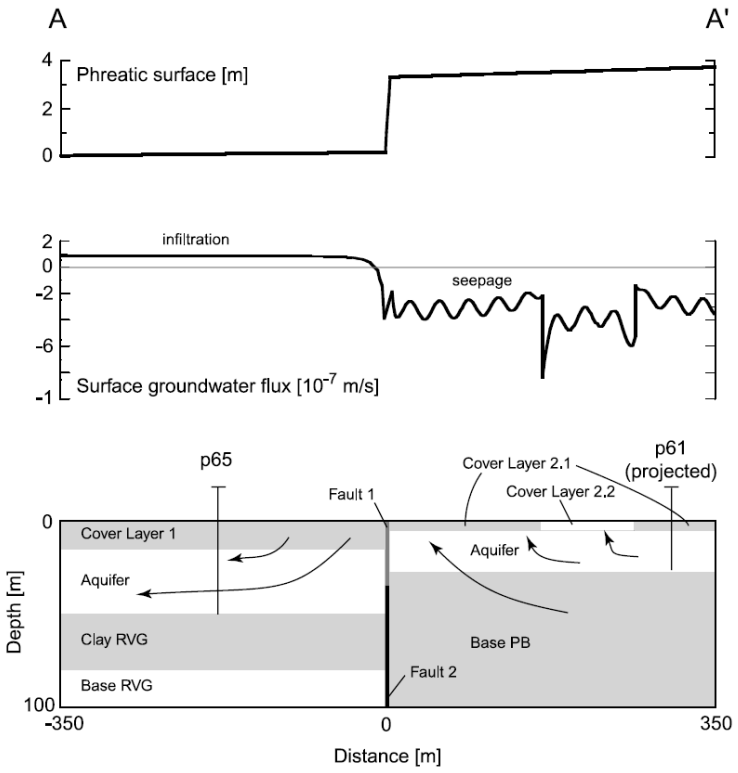

Figure 3-5　　Peel Boundary断層ゾーンの水頭分布、涵養量と湧水量分布（Bense とKooi, 2004)

Bense と van Balen(2003)は Roer Valley Rift System (RVRS)の断層が地下水流動に及ぼす影響を露頭スケールから広域スケールのデータを使って解明した。RVRS の断層は水平方向の流れに対して強い不透水性を示す一方、同じ位置で垂直方向の流れの水みちが卓越する。断層が横切る堆積岩の地下水流動をモデル化する際にはこの強い非等方性を考慮する必要があると説いた。Geleen 断層ゾーンの露頭では粒子の流れと粘土スミアに

ついて細かく調査することによって変形メカニズムが解明できたとしている。断層中のミクロスケールの水理性状の分布を定性、定量的に推定した。加えてコアプラグの計測からダメージゾーンが優先的な水みちを形成する可能性が示された。より大きなスケールでは Peel Boundary 断層は Uden 村の断層の近傍では断層の垂直方向の水みちが卓越して地下水が上昇して湧出していることが確認される。断層の存在とその水理性状の分布が如何に広域スケールでの地下水流動パターンに大きな影響を与えているかの例として、ドイツの リグナイト鉱山の近辺の水頭分布の調査の事例を示している。

3.1.6 ベルギー

Bense と van Balen (2004)によれば、ベルギーの Lower Rhine Embayment の未固結堆積層では断層が地下水流に大きな影響を及ぼしている。この地域の地下水頭マップ.を解析すると、多数に存在する個々の断層は地下水の流れに対してして難透水性であるが、断層のリレー構造が帯水層どうしを水理的に繋げる役割をしている。Lower Rhine Embayment にある最大規模の露天掘り鉱山の近くの Rurrand 断層の周りの地下水流動パターンは断層リレーゾーンを廻る流動の代表的な例であり、多くの記述が残されている。Bense らは Shale Gouge Ratio (SGR)を使って Cleay Smearing の影響を定量的に計算し、断層リレーの水理も数値モデルを使って解析した。その結果、帯水盆において、断層の封水程度を推定する際に断層リレーの影響を無視できないことがわかった。同時に水理挙動予測モデルにおいて、SGR は断層の水理性状の推定に有望な手段であることを示した。

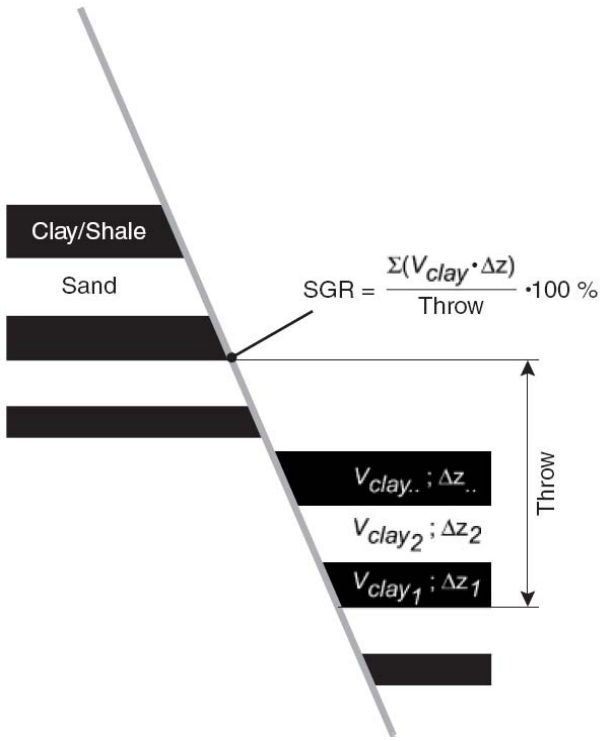

Figure 3-6　砂と粘土の互層を切る断層沿いの Shale Gouge Ratio (Bense and van Balen, 2004)

3.1.7 ブリタニー、フランス

Borgne ら(2006)は孔間フローメーター試験を使ってフランス、ブリタニーの沿岸付近の正断層に付随した割れ目の卓越した結晶岩性 Plœmeur 帯水層内の水みちの連続性に関する特性評価を行った。その結果、高い透水性が少なくとも 150m 以上サイト全体で連結している事が判明した。大きなスケールではボアホールスケールの不均質性は消滅し、高い透水係数側に収束する事が示された。地下の流れの場の構成、即ち高透水ゾーンの連続性に起因していると考えられる。

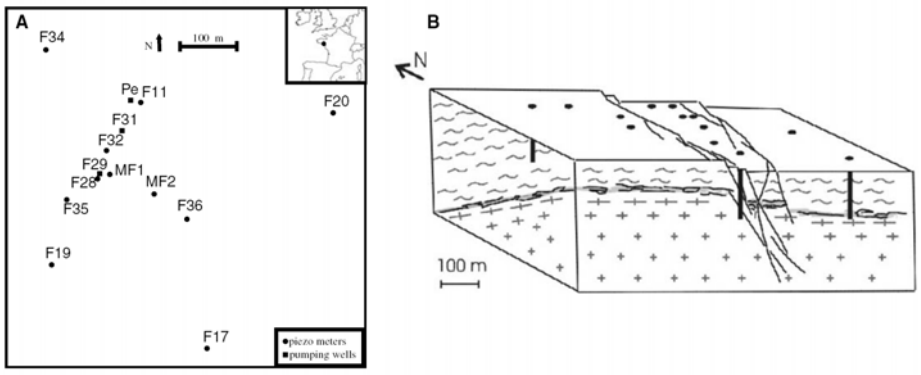

Figure 3-7　　Plœmeur帯水層を切る正断層と高透水ゾーン(Borgne et al, 2006)

3.1.8 プロバンス、南東フランス

地震災害予知の目的で活断層の特定とオフセット量や再発度などの地震変形パラメーターを限定する為に浅部の物理探査手法を用いた調査が頻繁に行われるようになった。Nguyen ら(2007)はフランス南東部のプロバンス地方で電気トモグラフィーを使ってゆっくり動く逆断層の場所の特定と複雑な地質環境下での電気トモグラフィーの断層探知に関する有用性の検証を行った。これは詳細な地質と地形の調査を組み合わせることによって初めて可能であった。褶曲した泥灰岩と石灰岩の互層した地層では電気探査イメージはスケールによっては電気伝導度のマクロな非等方性に大きく左右される。特に解像度が層厚より大きい場合は逆解析によって構造を解明することが困難である。順解析モデル中の地質構造のデータを計測データと逆解析結果を比較しながら試行錯誤的にアッ

プデートしている。浅部では解像度が非等方性のスケールより同じか小さい為、電気探査トモグラムによって比較的簡単に地下構造の解明が可能であった。

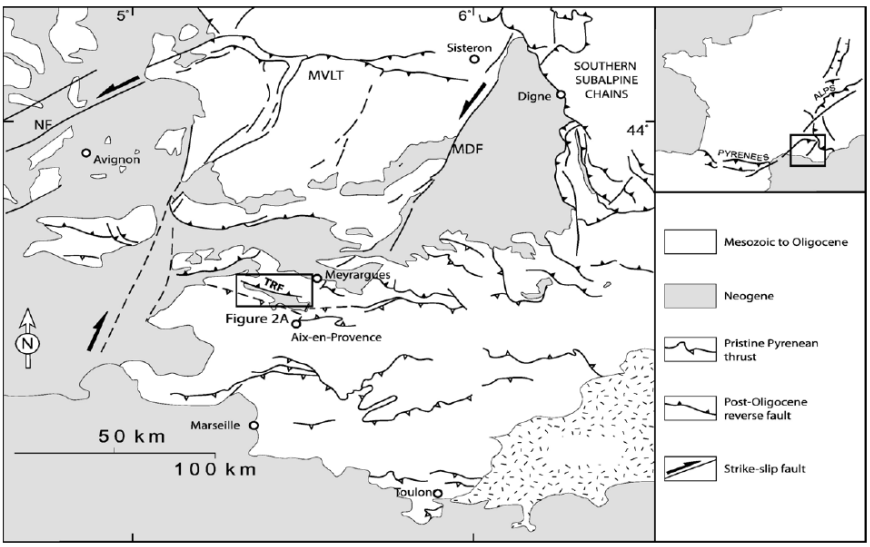

Figure 3-8　　Nguyenら(2007)が電気トモグラフィーを行った南フランスの断層

3.1.9　コリントス湾、ギリシャ

Micarelli らはギリシャのコリントス湾に存在する活断層のフラクチャーネットワークと断層水理について研究を行った。この正断層の両側で、少なくとも限られた時間と箇所で圧力の違いがあり、断層を横切る方向に遮水性があると考えられる。断層の上盤と下盤の両側の炭酸塩セメントを解析した結果、断層の発達の全段階に渡って局所的に遮水的であったと判断される。しかしながら、一方、井戸から得られた水のサンプルや圧力から推察すると、高地から海岸にに断層ゾーンを横切って天水が涵養していると考えられる。現地の定量的調査とコアの実験から広域スケールから断層のフラクチャーネットワークまで特定が可能であった。さらに、薄片の解析によって断層を形成する岩の種類まで特定した。これらのデータから断層の透水性を評価した。簡単な 3 次元の流動モデルを使い、断層の透水性構造、堆積物、地下水流動、断層の垂直方向のずれ、天水の涵養などをモデル化している。その結果、断層はセグメントごとに遮水性があるが、リレーの部分がに透水性があり、Peloponnese の高地から海岸までの広域流動を可能にしていると結論した。

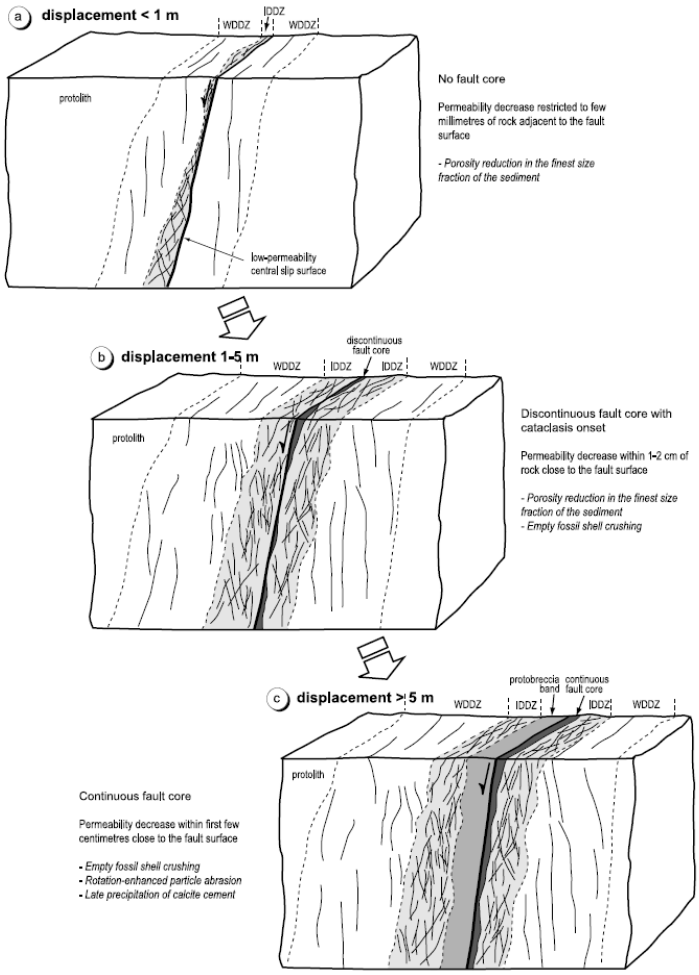

Figure 3-9　　Micarelli ら(2006) の提唱する正断層の発達過程と水理性状

3.1.10 コリントス、ギリシャ

Doan ら(2007)はギリシャのコリントス山脈にある Aigio 活断層を貫く 1000mの深さのボーリング孔の温度分布を測定した。熱流量は 53 mW/m^2 であり、造山活動が与える影響は殆ど無いと結論された。断層の近傍の温度は純粋に熱伝導のみの効果を考慮したモデルより高い。孔内圧力の長期にわたる測定結果から、これは断層の上側の地下水の流れに起因するとは考えにくい。さらに、Aigio 断層は小さな正断層で近年に動いていないことから、断層が滑った際の熱が原因であるとは考えにくい。これらのことから、今度異常は断層の下盤のカルスト地層内の熱対流が原因であると推察された。数値モデル

による計算でも測定値に近い高い温度値となった。これは地熱地帯以外の地域で断層付近の対流によって温度異常が起こされている珍しいケースと言える。

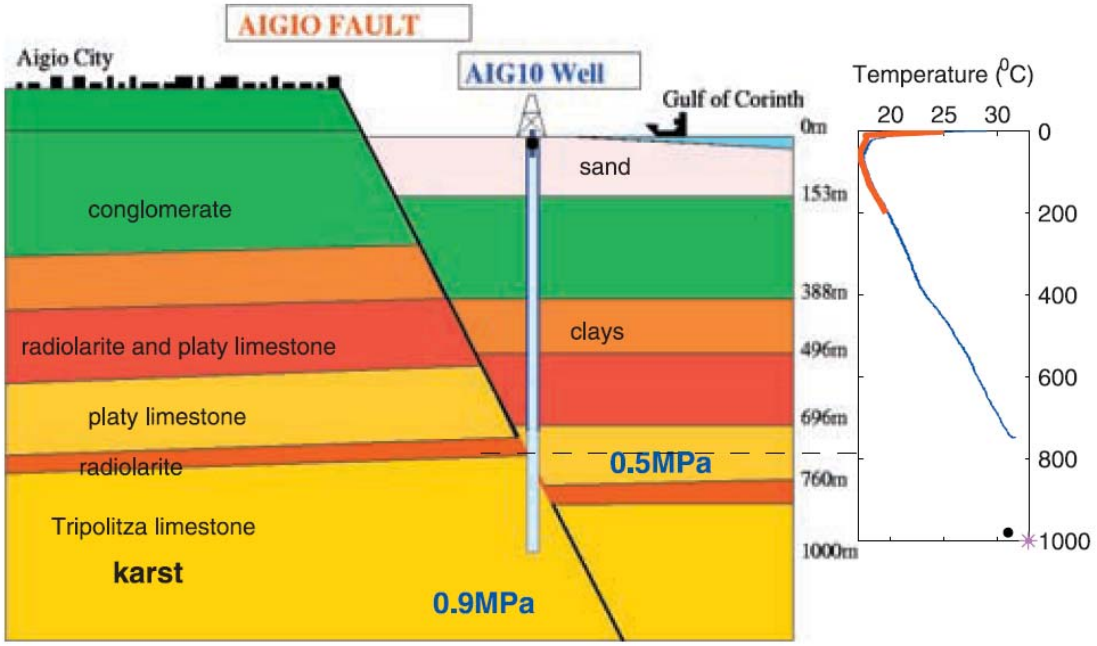

Figure 3-10　　Aigio 断層の断面図と断層を貫くボアホール沿いの温度分布(Doan ら、2007)

3.1.11 SOBREDA, 北ポルトガル

Antonio と Pacheco(2002)は傾斜の緩い逆断層で多数の短期可変揚水量試験を行った。この断層は衝上断層が多く存在する北ポルトガルの Sobreda 地域に位置し、蛇紋岩を横切っている。断層ゾーンは地質マッピング航空写真、および、電磁気探査によって存在と形状が特定された。ボアホール試験の解析の結果、断層の透水係数は 7×10^{-7}～$2\times10^{-4}m^2/s$、貯留係数は 2×10^{-5}～6.1×10^{-4}　と推測された。

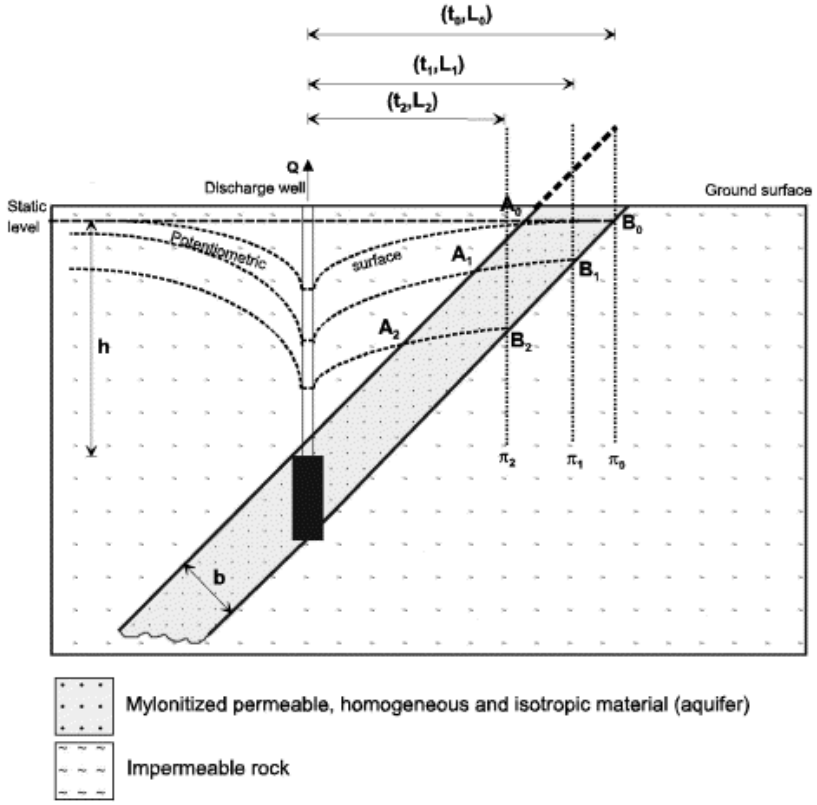

Figure 3-11　　ゆるい傾斜の逆断層の可変揚水量試験（AntonioとPacheco, 2002)

3.1.12 タグスバレー、ポルトガル

Carvalho らはポルトガルタグスバレー下部に位置する多くの伏在断層を特定する為には間接的な手法に頼らざるを得ないとしている。彼らは高精度の反射波を使った地震探査手法を使って近年の堆積物によって隠されたテクトニック構造の浅部の断層の特定に成功した。もっともこれらの断層は石油会社による深部の反射法による震探と地表の地質調査から存在が推定されていた。WNW−ESE-方向の断層帯(Porto Alto fault)と NNE−SSW-方向の逆断層帯(Vila Franca de Xira−Lisbon fault).である。高精度の反射法と 垂直電気探査法（Vertical electric sounding, VES）、さらに屈折波を反射法データから解析する方法を組み合わせることによって断層の特定が可能になった。

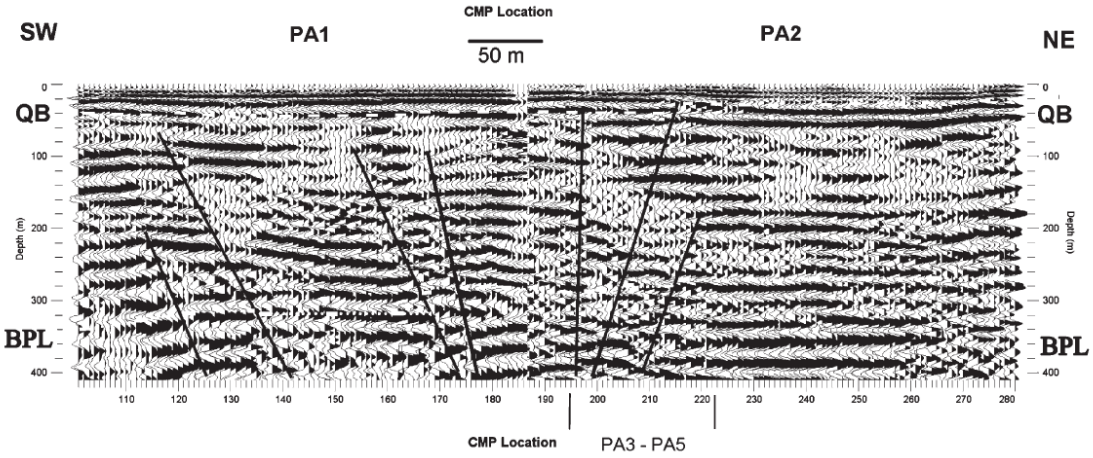

Figure 3-12　高精度の反射波を使った地震探査によって特定された断層群(Carvalho et al., 2006)

3.1.13 LAC DU BONNET, CANADA

カナディアンシールドでは断層とフラクチャーが主要な地質構造であり、花崗岩中の水の流れをコントロールしている(AECL, 1994a, 1994b)。Lac du Bonnet の URL（Underground Rock Laboratory）では、貫入岩中の応力場から断層やフラクチャーの透水性を推測し、地下構造物の長期的な安定性の予測に利用した。以下、カナダの Lac du Bonnet の URL の概要調査段階で断層の検知や性状の特定に有効であった物理探査手法をリストする。

- 航空電磁気測量
- VLF-EM
- 航空磁気測量
- 重力探査
- サイドスキャンレーダー
- 地表電気探査
- 反射法地震探査

3.1.14 ポンジョンギ、韓国

地下水組成の解析から断層の水理性状が推定された 1 つの実例として、韓国南東部のパンジョンギ地区での事例が挙げられる。当該地域では 10%の飲料用井戸（422 本）の

水が環境基準（1.5mg/l）を超えるフッ素を含有量している原因を調査する目的で自然同位体等の地化学データを使った研究が行われた。その結果、基準を超える地下水を産する井戸の大多数が断層沿いに存在することが判明した。安定同位体を使った解析により地下水の相対的な年代特定が可能となり、フッ素含有量の高い地下水は深部で循環している古地下水が断層沿いに上昇していると結論付けられた。しかしながら、断層に付随した亀裂が発達している断層ゾーンではフッ素濃度の高い地下水は殆ど観測されていない。これは同位体解析によれば逆に若い涵養水が断層沿いに深部に入り込んでいると推測される。

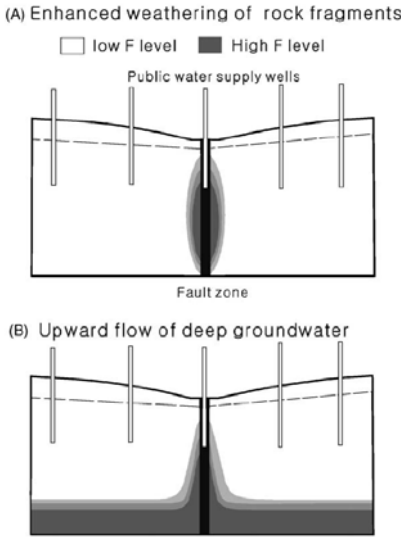

Figure 3-13　断層の垂直方向の高透水性による地下水のフッ素含有量の相違(Kim and Young Jeong, 2005)

3.1.15 台湾

水の拡散係数が水圧変化を左右することにより、破断の際の有効垂直応力を支配する。1999 年のマグニチュード 7.6 のチチ地震のモデル計算によると断層が十分にシールされていたとすれば、大きなずれが起きた箇所で断層内の水圧が高まったことにより高周波の揺れが抑制される現象の好例であることが示された。Doan ら(2006)はこれらのモデルの鍵となるパラメーターである水の拡散係数を干渉井を使って原位置で計測した。その結果地震の際の Chelungpu 断層で予想される値に矛盾しない $D = (7 \pm 1) \times 10^{-5}$ m^2/s という低い値を得た。殆どの多孔質弾性体では水の貯留係数 S は 10^{-7} から 10^{-5} の間の値であることを鑑みると断層沿いの水の透過率 T は 10^{-11} から $10^{-9} m^2/s$ であることになる。それ

に対応する透水係数は 10^{-18}－10^{-16} m^2/s となり、母岩のコアから計測された透水係数の最大 100 倍大きい。すると断層ゾーンの圧力は 0.06 から 6MPa 加圧されたことになり、これは地盤圧力の 0.2%から 20%と計算される。

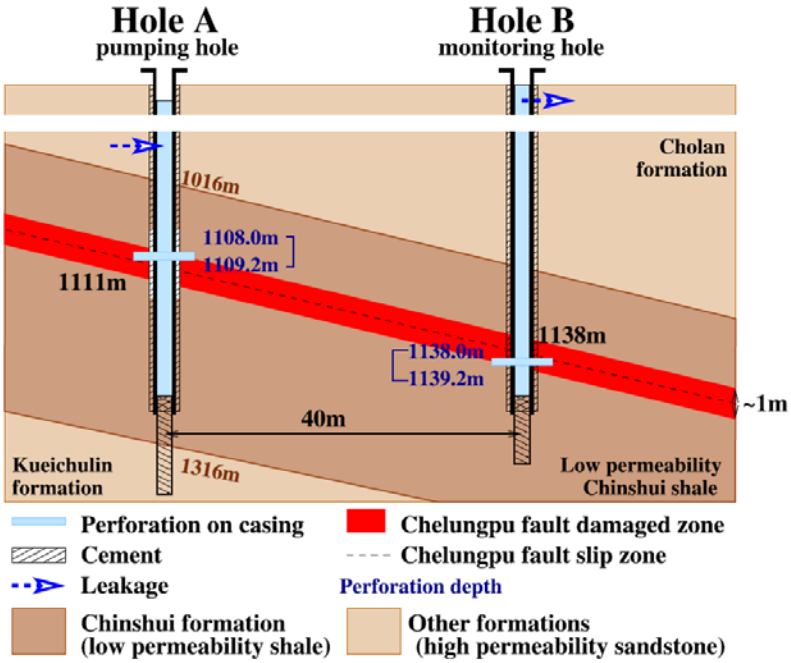

Figure 3-14　Doanら(2006)による Chelungpu 断層の水の拡散率の測定の際のボアホール配置

3.1.16 FAIRBANKS, ALASKA

熱分解ガスクロマトグラフィー/質量分析(py-GC/MS) は地下水中の溶存有機物（DOM）を使った地下水の起源の指紋捜査の手段として有効である。White ら(2002)は Py-GC/MS 分析を使った実例として、アラスカ州フェアバンクスの永久凍土に覆われた複雑な地下水理構造を解明した。彼らは２つの分水界地域の関連性を調べる為に地下水、湧き水、小川の水などのサンプルの指紋捜査的分析を行った結果、分水嶺の反対側同士の湧き水は同じ水源であることが明らかになったとしている。また、DOM の指紋的特徴のみを使って地下水の起源や種類の分類が可能であると説いた。これにより、DOM 解析が複雑な分水界地域の水みちの解明や汚染物質の移行に関する役割といった DOM の重要な特性の評価に繋がる可能性ができた。

3.1.17 BLUE RIDGE PROVINCE, VIRGINIA

Seaton と Burbey (2004)はバージニア州の Blue Rige Province の地下 300m 以深にある断層は大きな貯留能力を持ち、多大な量の地下水を井戸に供給することが可能だと説いた。さらに、これらの断層は深部の帯水層をコンパートメントに仕切っていると考えられる。深部の帯水層への水の涵養と帯水層からの流出は上部の封圧層からゆっくり漏れるか、あるいは過去の変成期に高い濃度のクォーツが生成し、後の変形エピソードに割れ目が発達した局所的な裂け目ゾーンを通って起こると考えれる。彼らはこの地域の逆断層の重要性を説き、Blue Ridge Province の水理モデルに古い断層構造を取り入れることを提唱した。結晶岩環境の中の断層は周辺の水理に影響を及ぼすと言うより、地域の水理特性を支配すると述べている。

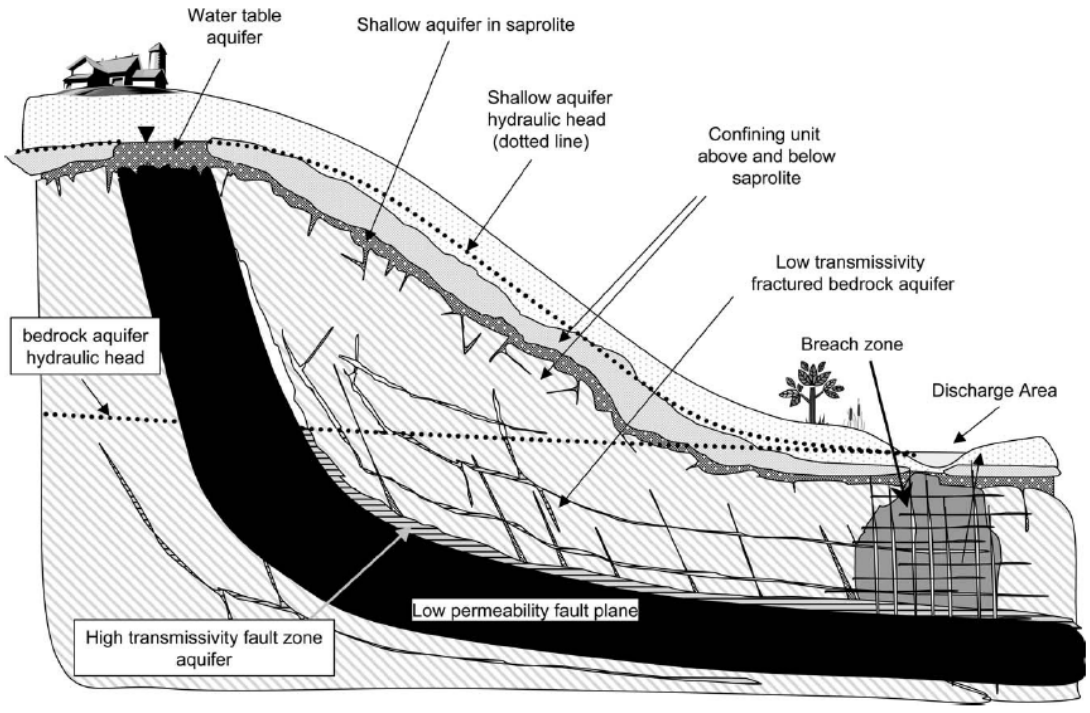

Figure 3-15　Blue Ridge Province の逆断層の高い貯留能力(Seaton and Burbey, 2004)

3.1.18 ルイジアナ州

Bense と Person(2006)は珪質砕屑堆積岩の帯水層で頻繁に観測される断層ゾーンの高透水性と難透水性の二面性は断層が水理学的に極端な非等方構造を呈すると解釈する事が可能であると説いた。断層の水理学的非等方性は粘土スミア、砂の引きずり、粒子の再配列、断層の垂直方向の分断など種々のメカニズムが成因となる。Bense と Person は断層ゾーンの幅、岩相の不均質性、水理的非等方性を予測するアルゴリズムを提唱した。

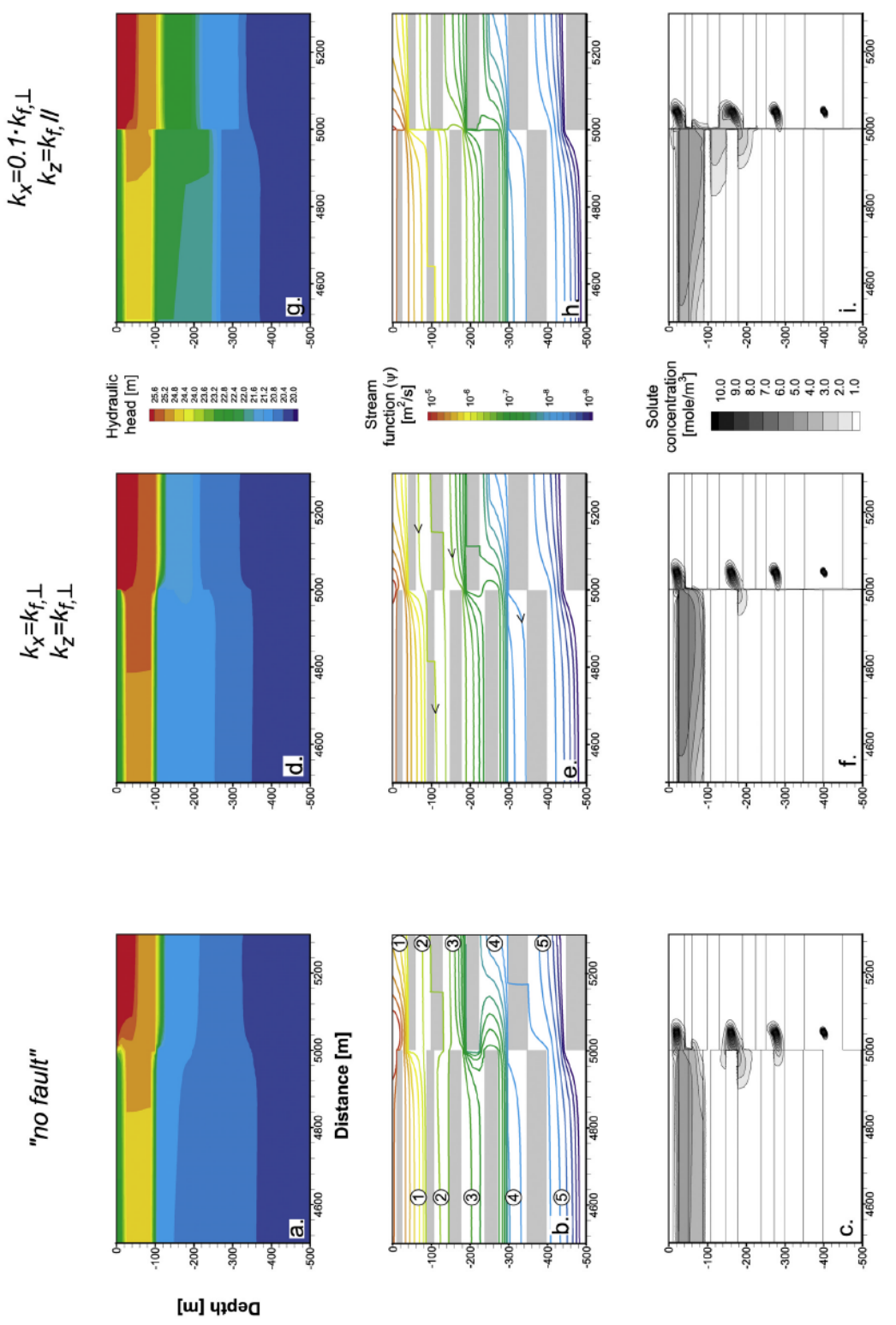

Figure 3-16　　モデル化した 3 種類の断層を横切る流れと物質移行（Bense and Person, 2006）

3.1.19 アルボード、オレゴン、米国

Heffner と Fairley (2006)は米国オレゴン州のアルボード盆地の断層の水理構造の研究を行い、断層は空間的、時間的に不均質であり、断層内を流れる水に対して高透水性、低透水性、あるいはその両方の性状を同時に呈することを示した。彼らは正断層に沿った 702 箇所の泉や地表面で測定された温度分布を基に地球統計学的手法を使って、活動的正断層の透水係数の分布のモデルを構築した。断層面に平行する方向の流れは広い範囲で低い透水性から中程度の透水性を示すが、数多くの個別の流れの水みちが存在することを発見した。この結果は結晶岩や強く岩石化した堆積岩の断層の概念モデルとは良く一致するが、アルボード盆地のような沖積層や軽度に岩石化した堆積岩内の断層に予測される性状と大きく異なり、一層の研究の必要性を説いている。

.

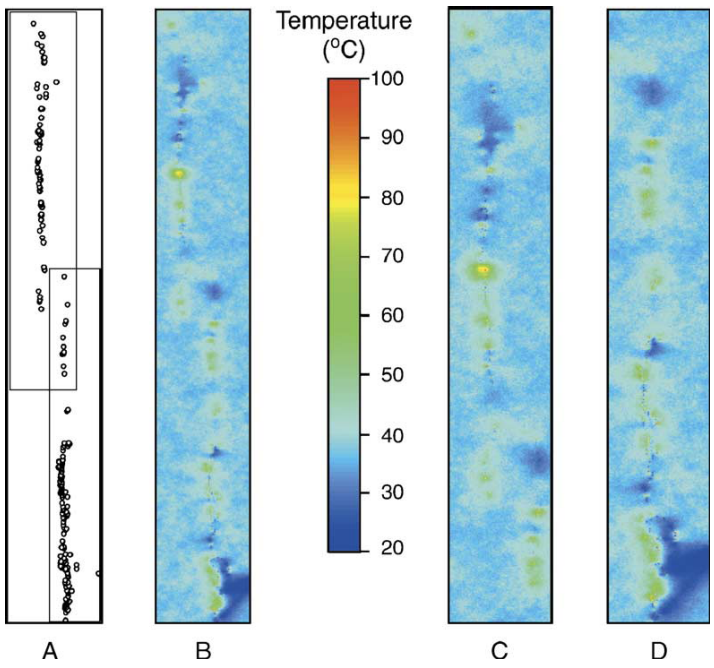

Figure 3-17　断層沿いの湧き水の温度分布と地球統計学手法を使ったシミュレーション (Heffner and Fairley, 2006)

また、Fairley と Hinds(2004a, 2004b)は断層のステップオーバー付近では複雑な 3 次元的な流れの循環挙動を示すことを発見した。こういった現象は正確な断層付近の流れの概念モデルや数値モデルを構築する際に非常に重要であると説いている。

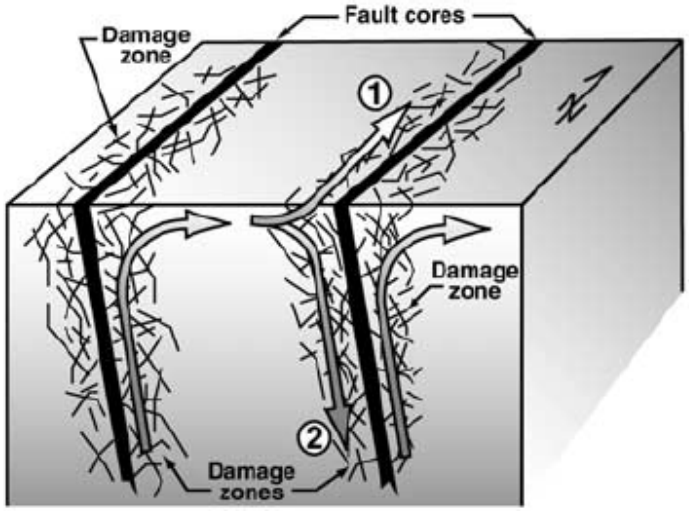

Figure 3-18　断層のステップオーバー内の地下水の 3 次元的流れ(Fairley and Hinds2004a, 2004b)

3.1.20 ワシャキエ山脈、ワイオミング州

Evans ら(1997)は花崗岩中の逆断層ゾーンの露頭の各部分、各方向から岩石のコアを採取し、応力下および非応力下で透水性の計測を行った。その結果、少なくとも岩石コアのスケールでは断層のダメージゾーンは母岩と断層コア部の間に位置する透水性の高い部位であることが判明した。ダメージゾーンのコアは応力下でも母岩やコア部のコアに比べて透水係数の減少度が低い。これらの結果は花崗岩に関する過去の原位置での水の流れの観測結果と一致するとしている。ダメージゾーンとコア部の 2 つの部分からなる構造は断層全体としての水の流れに対して非等方性を形成する。ダメージゾーンの発達した断層ゾーンは断層面に平行で比較的薄い平板状の部分で流れが卓越する。一方、断層コア部は断層を横切る方向の流れに対して透水性が低い。

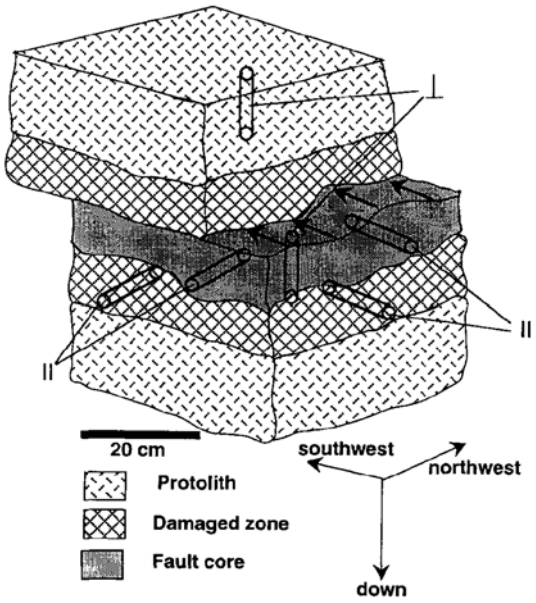

Figure 3-19　Evansら(1997)の採取した逆断層ゾーン内のコアサンプルの位置と方向

3.1.21 ハンナ盆地、ワイオミング州

Johnson と Huntoon(1994)によれば、ワイオミング州のハンナ盆地のシャーリー逆断層の上盤沿いの地下水の流れは概ね地層に沿っている。異なる帯水層間の層序を横切る地下水の流れは加圧層や透水層を分断する正断層や亀裂を伝ってのみ流れる。こうった層序に平行、垂直な構造が高地の涵養域から流出域までの水みちの構造を形成する。シャーリー山脈のマジソン層から涵養された水は水頭の低い方向へ流れるが、Tensleep 帯水層に上昇し、低地に達する前に正断層を伝ってハンナ盆地の上辺付近の Tensleep 砂岩が露頭する辺りで地表に流出する。

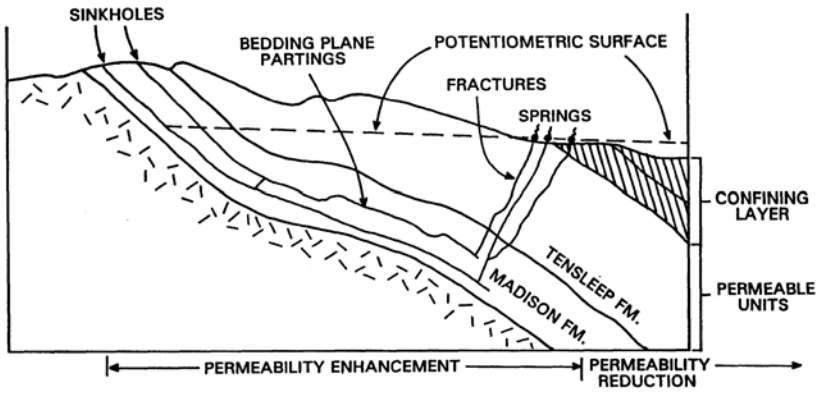

Figure 3-20　シャーリー逆断層周辺の地下水の流れ(Johnson and Huntoon, 1994)

3.1.22 リオグランデリフト、ニューメキシコ州

Mailloux ら(1999)は断層ブロックのテクトニックによる動きと断層の透水構造がニューメキシコ州ソッコーロ市に近いリオグランデリフトの過去と現在の水理地質に及ぼす影響を数値モデルを使って解析した。La Jencia と Soccoro 盆地の過去と現在の地下水の流れのパターンと温泉形成の解明を目的としている。数値モデル解析結果と過去現在の流れのデータが最も一致したのは断層の水理性状を高透水性でも低透水性でもないと仮定し、2km の長さの亀裂性の結晶岩に中程度の透水性を持たせたケースであった。定性的には地下水盆の中の地下水の流れの変化は主として帯水層や封圧層が途切れたり、つながったりすることに因ってもたらされる。山脈フロントの涵養水の約 5%が堆積岩下 2.8km の深度まで浸入していると考えられた。これまでは地下水源としてリオグランデリフト谷の浅部の堆積層のみ対象としていたが、新たな地下水源として期待できる可能性がある。

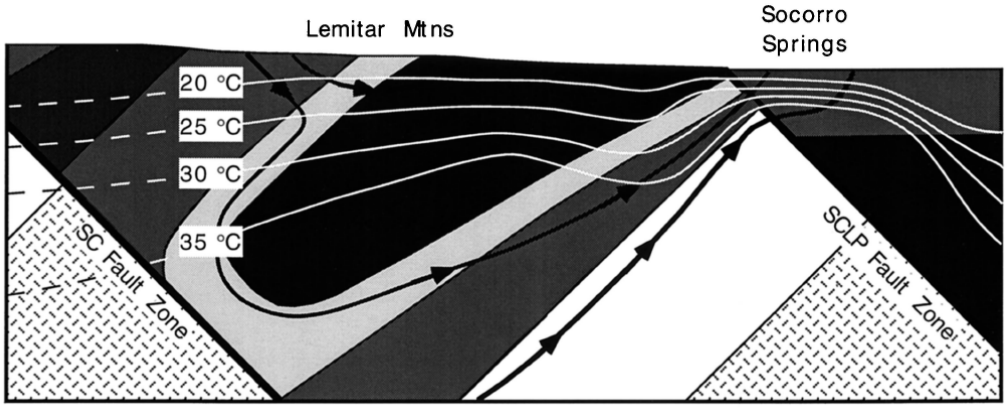

Figure 3-21　　リオグランデリフトの断層ブロック沿いの地下水の流れ (Maillouxら, 1999)

3.1.23 ロスアラモス、ニューメキシコ

ロスアラモス地域の地下水の涵養の物理的プロセスは未だに解明されていない。特に、Pajarito 断層ゾーンが地下水の涵養に与える影響（水みちまたは反対の障壁なのか）に関して殆ど判っていない。断層水理に関するデータが殆ど存在しない為に地域の地下水モデルも不完全と言わざるを得ないと Dale ら(2005)は述べている。Dale らは 2000 年 5 月に起きた Cerro Grande 山火事によって地下水にもたらされたトレーサーを使って断層の露頭（PA-106）および下流の湧水点の地化学的組成を比較し、涵養水の源を推定することが可能であった。山火事とその夏のモンスーンによる洪水によって、PA-106 に於いて HCO_3, SO_4, Ca, K, Mg, Mn, Sr,さらに TDS が 4 倍に膨らんだ。その 1 ヶ月以内に Homestead と Starmer Springs に於いて同様の痕跡が確認されたことから、Pajarito 断層ゾーンが地下水の涵養に重要な役割を担っている事が推定される。上記以外に解析に使った地化学成分は ^3H, ^4He, Ar, Ne, δD, $\delta^{18}O$ であった。

また、Howley(2005)によれば Estancia 流域に全体於いて小流域を区切る断層に伴う亀裂と溶解プロセスによってもたらされた間隙率と透水係数は基盤岩中の地下水の流動と特質に明白に影響をもたらす。Koning(2005)は同地域において、航空磁気測量のリニアメントが断層の特定に役立つことを示した。多くの場合航空磁気測量データとマッピン

グの結果が一致して理う。これらの断層が地下水流動と帯水層のコンパートメント化に対して絶大な影響を及ぼしていることは疑いがないとしている。

Rodrigues and Williams は 16 の MT ステーションを使って北西の Pajarito 断層と南東の La Bajada 断層で区切られる La Bajada 収縮内の地下構造を探った。MT 測量はそれぞれの年代の岩石に予測される電気抵抗値を元に基盤岩の相対位置と古生代 - 中生代 - 第三期の堆積岩の厚さを推定した。例えば粘土鉱物の少ない、水で飽和した第三期の堆積岩は比較的低い抵抗値(10 to 50 ohm-m)であり、一方、中生代の頁岩は 1 から 5 ohm-m といった非常に低い値を示す。地表近くの第三期の玄武岩、安山岩と流紋火山岩は非常に高い 100 から 5,000 ohm-m の抵抗値を示し、埋没した古生代の炭酸塩堆積物は 200 から 500 ohm-m である。

3.1.24 EAST TINTIC MOUNTAINS ユタ州

Hamaker(2005)は Eureka Lilly 断層ゾーンは East Tintic 鉱山地区の地下水流に対して不透水バリアとなっていると結論した。断層の両側の地下水が異なった温度、組成、さらに水頭圧であるというのが根拠である。断層のダメージゾーンは開口割れ目の卓越した連結したネットワークを形成しており、断層の交差する箇所は水みちとなっている。断層のコアブレッチアは再セメント化し、鉱化して空隙を埋めていることにより、厚い不透水ゾーンを形成している。これにより、断層が両側の地下水の仕切りとなっている。このコンパートメント化により、従来の流域モデルのコンセプトが不正確で当てはまらないと結論した 。

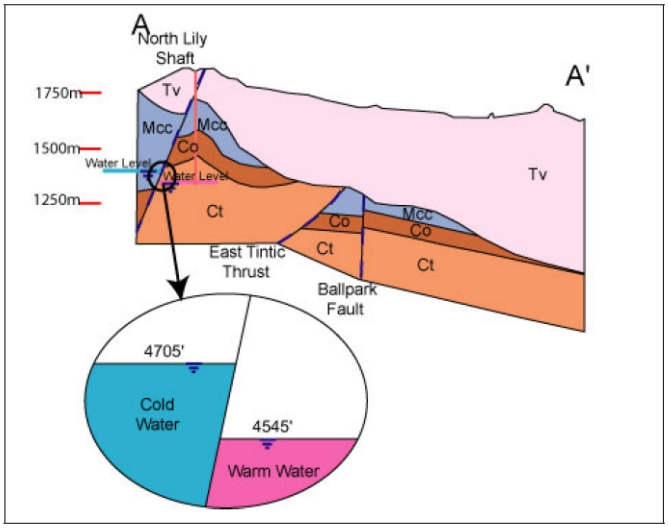

Figure 3-22　　不透水バリアとなっている正断層の両側の水頭と水温(Hamaker，2005)

3.1.25 ハリケーン、ユタ州

ユタ州、ハリケーン市近くの Timpoweap Canyon にハリケーン断層コア部とダメージゾーンの理想的とも言える露頭が存在している。さらにこの谷ではダメージゾーンの各所から湧水してバージン川に流れ込んでおり、断層ゾーンからの湧き水の研究に最適である。ハリケーン断層は急傾斜の活動正断層で、長さが 250km、ずれが 2500m である。Timpoweap Canyon のダメージゾーンの亀裂性石灰岩からは~40°C の温水が 260 L/s、二酸化炭素が 4 L/s の流量で湧き出ている。また、湧き水中のδ^2H と δ^{16}O の組成から地下水は約 3km 深の基盤岩にから出ていると考えられる。一般の断層ではダメージゾーンの亀裂密度は断層から遠くなるにつれ減少する傾向にあり、湧水量もそれに伴って減ると考えられているが、Timpoweap Canyon のダメージゾーンはその法則に従わない。これは Laramide と Sevier 造山運動の応力によって形成された既存の亀裂が原因だと考えられる。ジプサムの溶解による陥没構造と大きな亀裂が湧水箇所を決定している (Dutson, 2005)。

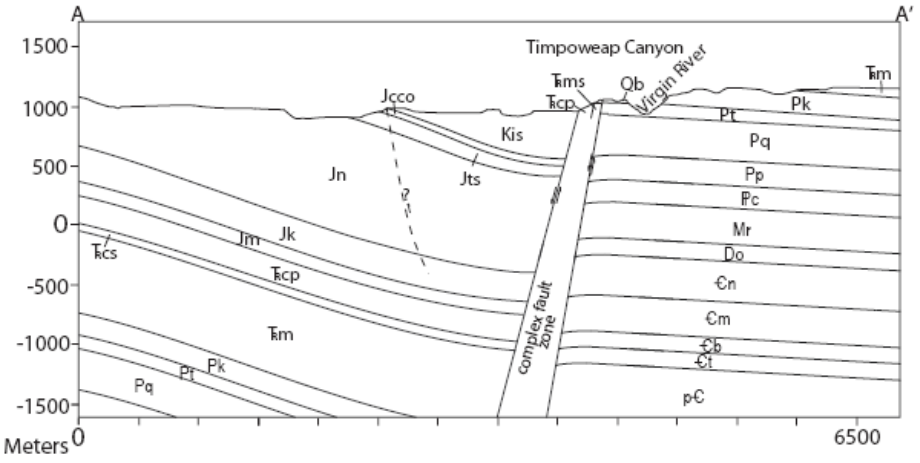

Figure 3-23　　ユタ州 Timpoweap Canyon のハリケーン断層の断面図(Dutson, 2005)

3.1.26 BIG HOLE FAULT、ユタ州

Shipton ら(2002)は露頭と 4km の長さの Big Hole 正断層を貫く 5 本のボーリング孔(数十ｍスケール)から断層の構造と透水係数の分布を調べた。Big Hole 断層はユタ州中央部のジュラ紀の Navajo 砂岩に露頭している。ずれが 8m と 3~5ｍの 2 箇所にサイトから合計 363.2 m のコアを採取した。断層コア部は最大 30cm の幅で著しく粉砕された空隙率の低い融合された変形帯で片側、または両側にすべり面が確認される。Probe permeameter を使った計測では断層に近づくにつれ、2000md から 0.1md に減少した。断層コア部のコアを使った計測ではコア部は 1md 以下の透水係数であった。これらのデータを使い、Shipton らは断層のバルクの透水係数を計算した。それによれば、5m~10m のスケールでは 30-40md で、母岩の 1~4%の透水係数であった。複数の断層が複雑に折り重なったケースを想定した場合 7–57 md であった。断層を横切る透水係数は断層のパラメーターの内、一番大きなばらつきを示す断層コア部の厚さに最も大きく左右されることが明らかになった。

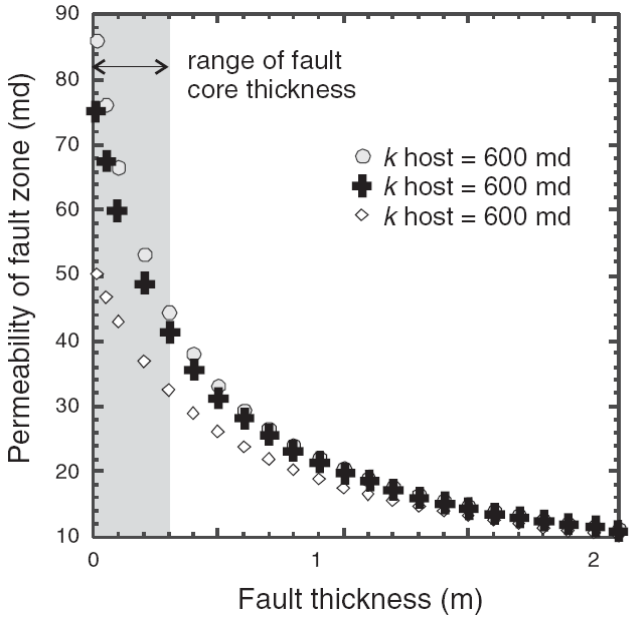

Figure 3-24　断層の厚さと断層のバルクの透水係数の関係(Shiptonら、2002)

3.1.27 エルクホーン、コロラド州

Marler と Ge (2007)はコロラド州 South Park 市の Elkhorn 断層の水理性状と断層が広域水理に及ぼす影響を調べた。Elkhorn 断層は傾斜のゆるい逆断層で先カンブリア時代の結晶岩が South Park Basin の堆積層に押し上げられている。Elkhorn 断層は断層を横切る方向の透水性が低く、結晶岩の帯水層と South Park Basin の堆積層の地下水を分断していると考えられている。Marler と Ge は断層の水理性状を特定する為にボアホール試験に加えて、直流電気抵抗試験を行い、断層の不均質性の構造を調査した。さらに、数値モデルを使って地下水の流れのシミュレーションを行った。その結果、断層は 3m の厚さの低透水のコア部と高透水性のダメージゾーンで形成され、断層を横切る方向の流れは極めて制限されていることが判明した。

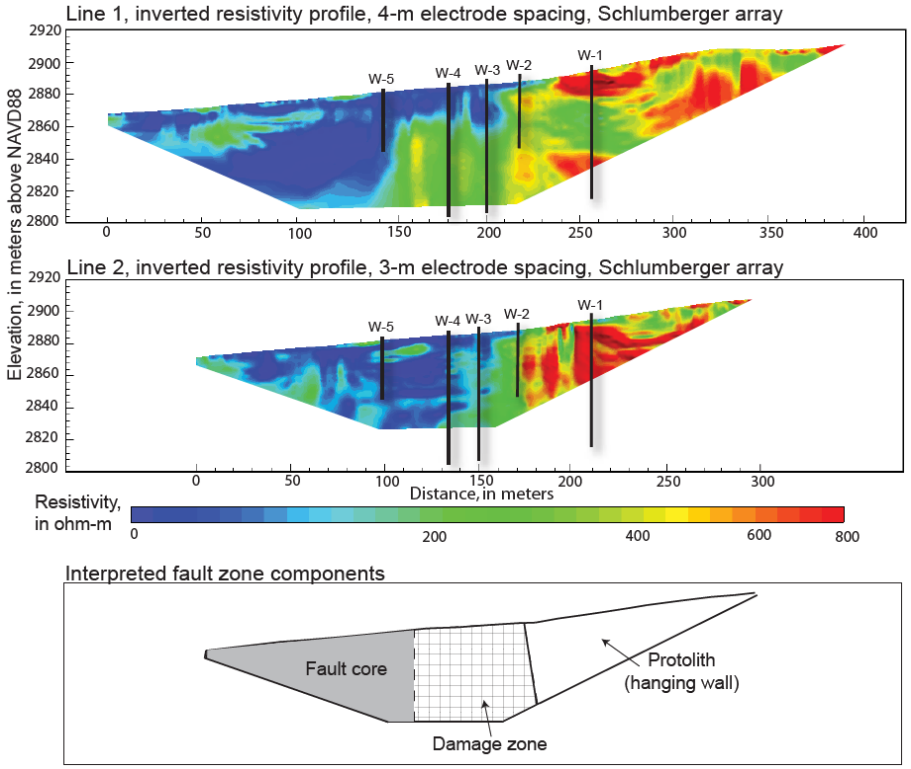

Figure 3-25　ユタ州エルクホーン断層の電気抵抗トモグラフィー解析結果 (MarlerとGe, 2007)

3.1.28 MEDINA, テキサス

Clark と Journey (2006)はテキサスの Medina 郡北部のリレーランプとそれらに関連する断層が地下水の流れを 4 つの個別の流れの経路に分けて南西方向に流していると説いた。Medina の北西の流路は北側に Woodard Cave 断層が在り、南は Parkers Creek 断層が存在する。地下水は Seco Creek 沿いの直交する断層に突き当たるまで地層の傾斜方向である南西に向かって流れる。その後この断層が難透水性である為、一部あるいは殆どの地下水を南向きに流す。

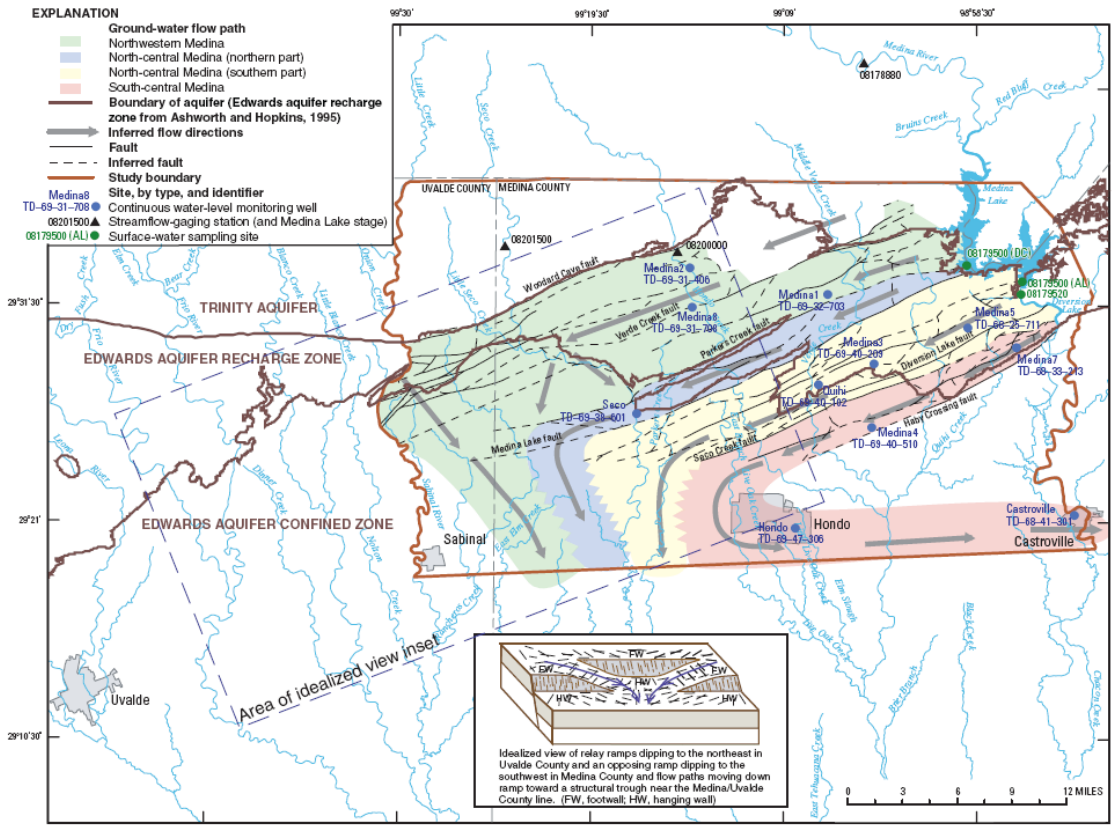

Figure 3-26　テキサス州 Medina 群の断層にコントロールされた 4 つの地下水流(Clark and Journey，2006)

3.1.29 HIDDEN VALLEY FAULT, TEXAS

SWRI は近年洪水により露出したテキサスの南部中央に存在する白亜紀の Glen Rose 地層を切る Hidden Valley 断層を使って断層の性状評価のプロジェクトを立ち上げた。Hidden Valley 断層は炭化水素の油田にありがちな代表的構造であり、このサイトは断層構造、岩種と断層ゾーンの水理性状の相関性を調査できる類のないサイトである。当該サイトでは以下のような研究計画が立てられている。

1. 層序学的、岩相学的特性評価
   - 上盤と下盤の詳細な断面マップの製作
   - 自然ガンマ線計測ログ
   - 母岩の岩相、表面性状と粘土含有量の定量化
2. 地質構造の解析
   - 層序の力学的な解析
   - 露頭スケールの構造的要因の詳細なマップ

- 微細構造解析
- 地質マッピングとボアホールデータからデジタル地質構造モデルを構築

3. ボアホール関連
   - 掘削、コア採取、検層の後、上盤側と下盤側の多区間に水圧計を設置
4. 水理学的特性評価
   - Canyon 湖と近辺の井戸の水位データの収集
   - 地表の泉、地表水の浸出点、侵入点のモニタリング
   - Canyon Lake 渓谷 の流水量測定
   - 観測井内の多区間での水圧モニタリング
5. 力学的特性評価
   - 断層の露頭部の岩の力学的性状の解析、試験
   - 有限要素法を使った Hidden Valley 断層の応力変形解析

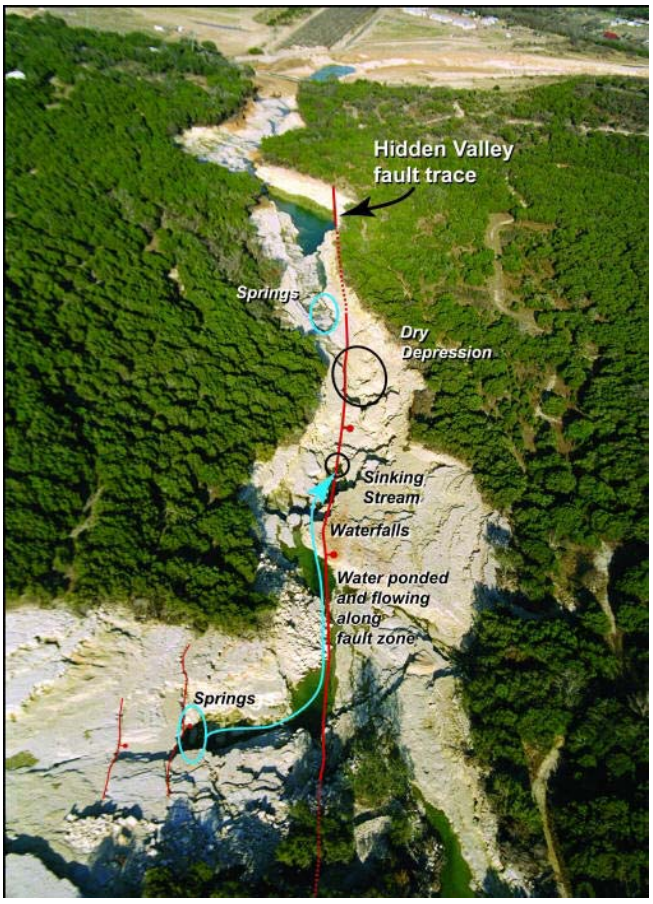

Figure 3-27　テキサス州、Hidden Vally 断層の露頭トレース（SWRI, 2008）

3.1.30 YUUCA MOUNTAIN、ネバダ

Bredehoeft (1997)はネバダ州ヤッカマウンテン付近の地下水面の温度の分布からヤッカマウンテンの東側と西側の両側の主だった断層沿いに地下水が深部から上昇して来ていると推察した。Bredehoeft はこれらの断層の透水係数が非常に重要であるにも拘らずデータが不足していると述べている。

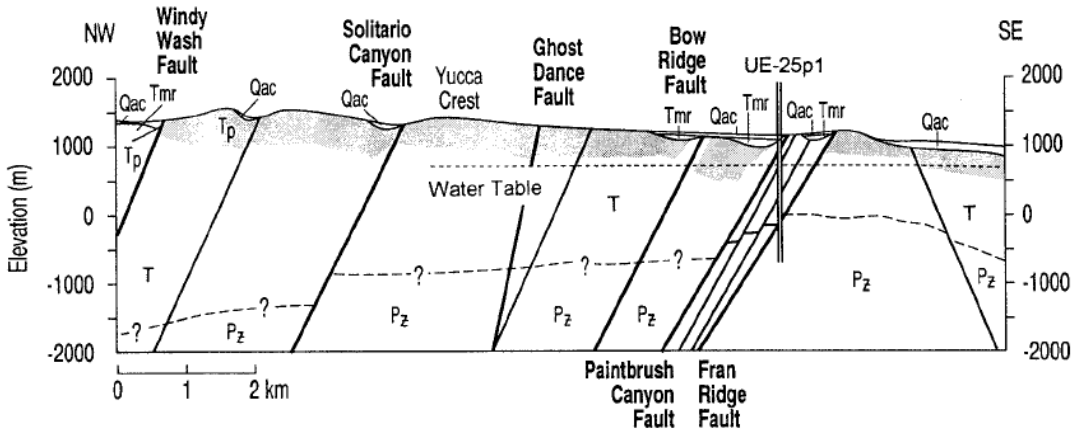

Figure 3-28　ヤッカマウンテンの断層群(Bredehoeft, 1997)

Blakely ら(2000)は地下の複雑な地質構造を探る目的でヤッカマウンテンの南の Amargosa 砂漠とその付近で高精度の航空磁気測量を行った。測量は面積にしておよそ 7,700 km^2 (2,970 mi^2)をカバーし、ネバダ州 Beaty からカリフォルニア州 Shoshone までの Nevada 核実験場とデスバレー国立公園を含む広い範囲であった。航空磁気測量の測線は東西に 400m 間隔で高度 150m、もしくは安全とされるぎりぎりの高度で飛行した。特徴的な磁気異常は Yucca Mountain や Greenwater Range などの火山岩地形と Bare Mountain や Black Mountains.のような原生代基盤岩で観測される。火山岩の断層によるずれが磁気異常のリニアメントの原因となり、浅い断層の詳細なマッピングが可能となる。特に興味深いのは Devils Hole と Pahrump Valley に見られる堆積層での磁気異常である。泉の存在箇所が磁気異常のリニアメントと一致することから、これらは断層が深部の磁性岩をずらし、堆積層も切っており、地下水流動に大きな影響を与えていると考えられる。Funeral Mountains 上の磁気異常のリニアメントは一般に非磁性の Stirling 珪岩を切っている先カンブリア時代の北-北東方向の走行の断層群と一致する。これらの磁気異常の箇

所と方向を Furnace Creek の北に位置する湧水箇所と比較して考えると、断層は北から Death Valley 方向へは水みちとなっていると考えられる。しかし、この磁気異常の鉱物学的な説明はついていない。

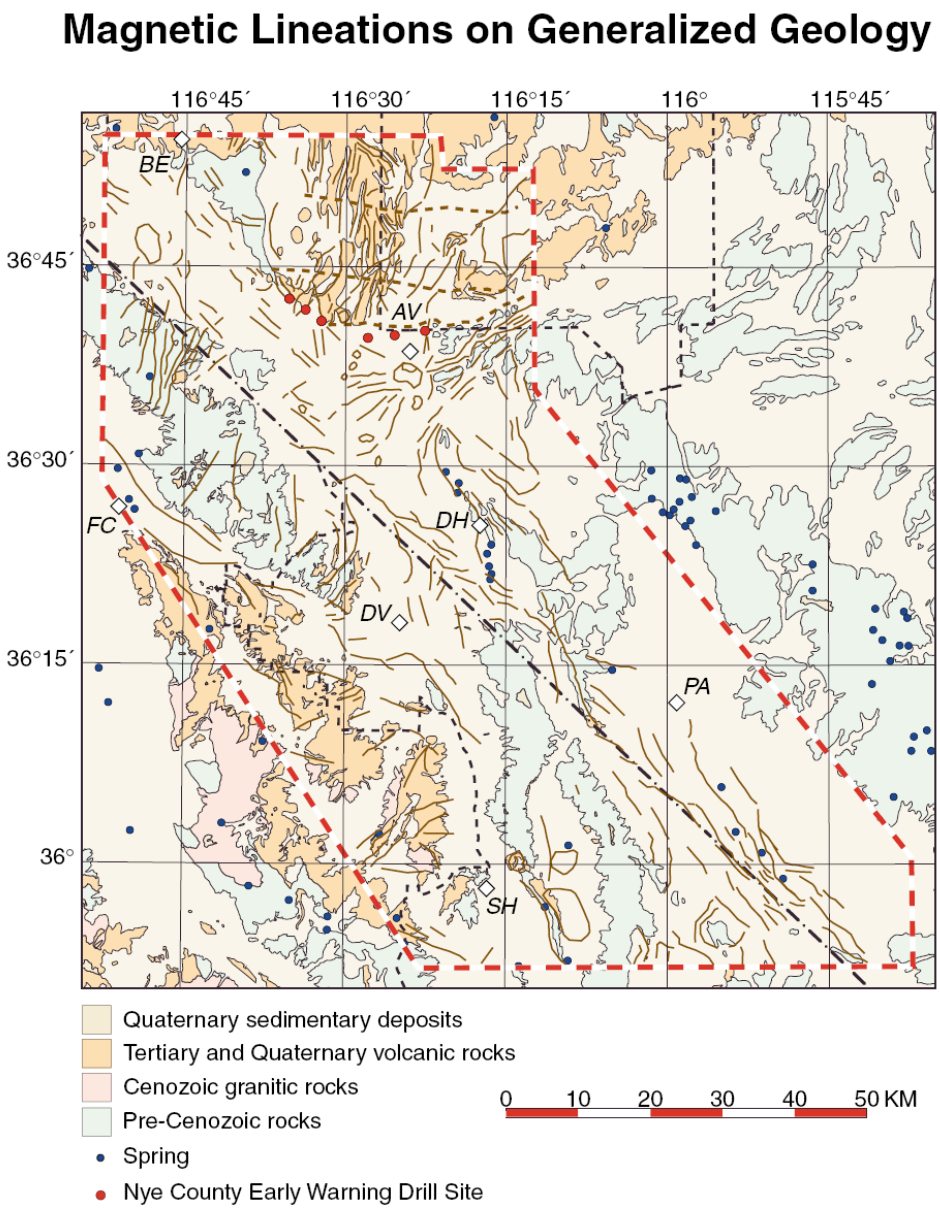

Figure 3-29　　ヤッカマウンテン南西の断層による磁気異常のリニアメント(Blakely ら、2000)

Flint ら(2001)のヤッカマウンテンの概念モデルでは断層は地表から処分場レベルを通って地下水面までの水の流れの直線的な経路になっているとした。未固結の Paint Brush

(PTn)と呼ばれる凝灰岩地層そのものは難透水性であり、天水は傾斜にそってほぼ平行に流れるが、断層が PTn 地層を切っている部分で断層に入り、地下水面への最短路であ

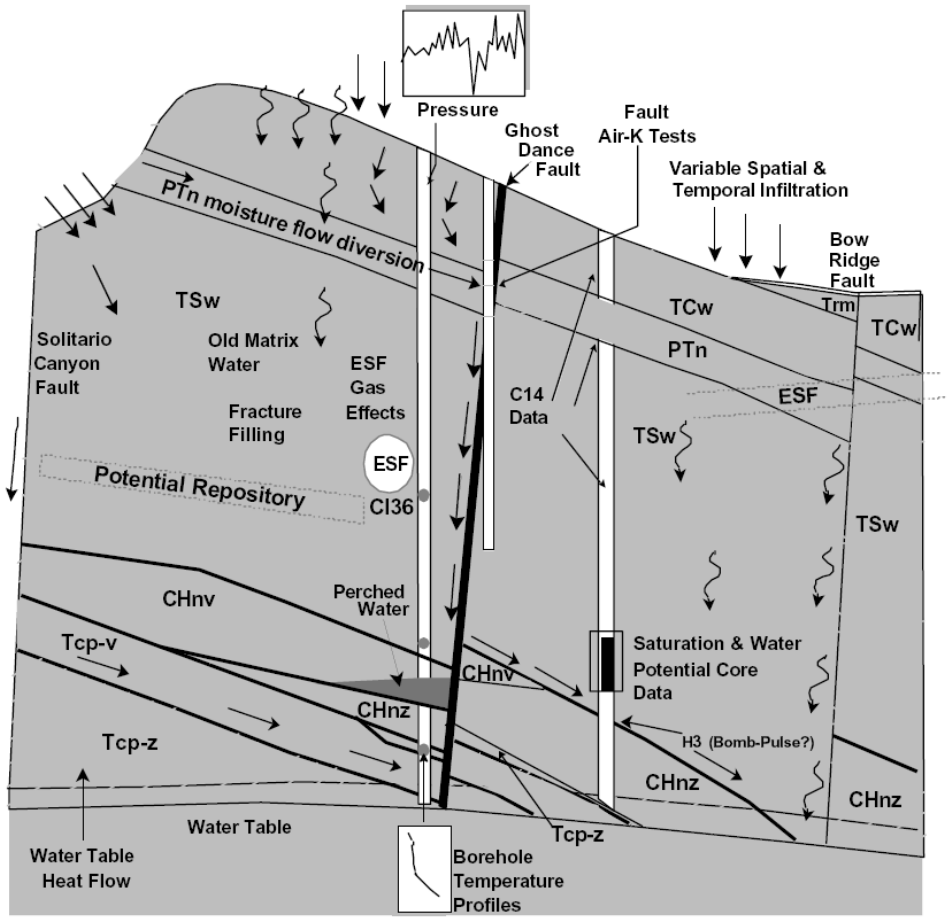

る断層を伝わって飽和領域へと流れる。処分場レベル以深では断層が地下水の流れと物質移行を支配してる。

Figure 3-30　Flint ら(2001)のヤッカマウンテンの不飽和部の概念モデル。断層が早い水みちとなっている。

IAEA(2002)はヤッカマウンテンの飽和領域の特性評価のレビューにおいて地下水の流れに対する断層の役割が未だに不明であり、その結果重要な地下水の流動経路に関して未解明である事に大きな懸念を示した。

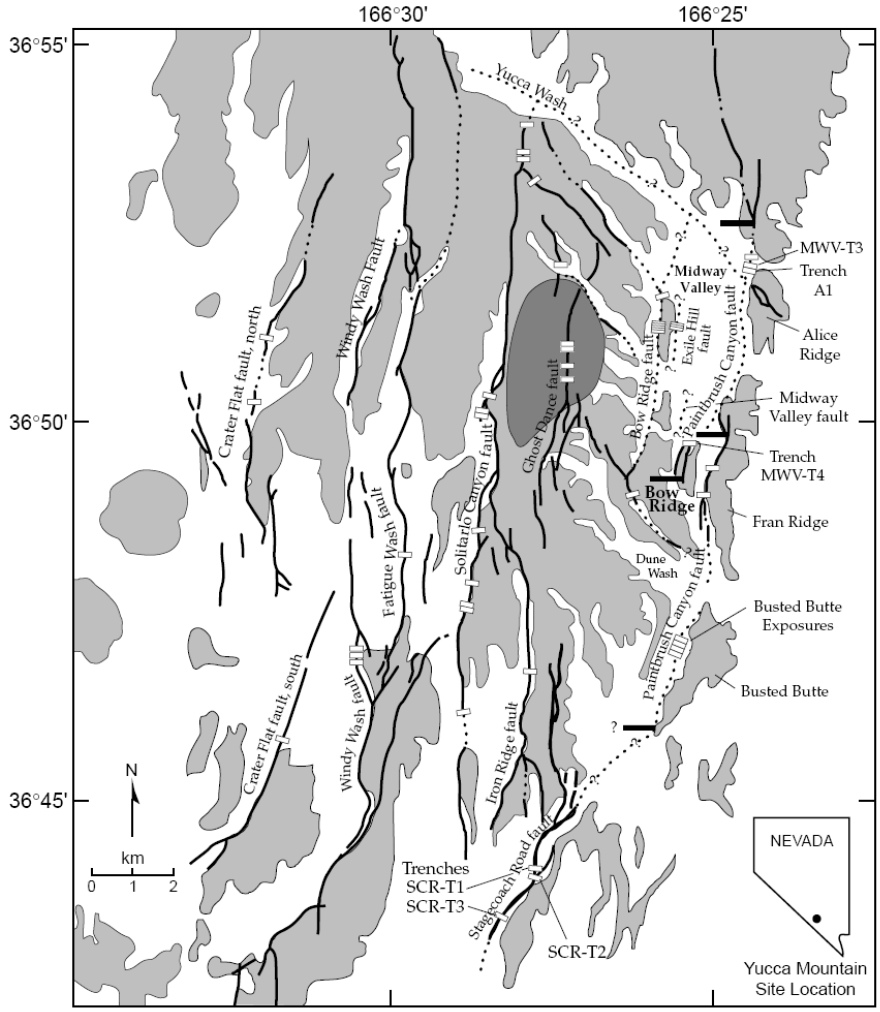

Figure 3-31　　ヤッカマウンテン周辺の主要断層とトレンチの位置 (IAEA, 2002)

Simmons ら(2004)によれば、地表からの概要調査の為の物理探査手法を用いて断層の存在、地層の分布、さらに埋没している火山の形や大きさ(Ponce, 1996; Sikora et al., 1995)に関する情報を得た。ヤッカマウンテンサイトで第一義的に解決するべく努力すべき問題は処分場ブロック中の断層の数、スタイル、深さと連続性の解明である為、種々の物理探査の手法を用い、どの手法が最も断層のイメージの取得に有効か比較検討された。その結果、どの１つも有効と言えず、正確な地下構造の情報を把握する為には、いろいろな手法を組み合わせる必要があることが明らかになった。

重力探査や磁気探査のような広域の物理探査データは火山岩の構造、異なった岩相のコンタクトと断層のオフセットの同定に使われた(Langenheim, 2000c)。地震探査の屈折波（S 波と P 波の速度）は上部地殻、ヤッカマウンテンとその周辺の速度構造をモデル化する為に使われた(Smith ら, 2000d)。近年行われた航空磁気測量は地域の多くの埋没した火山の大きさと形の同定に使われ、ヤッカマウンテン周辺の火山災害の予知に役立った(Smith and Keenan, 2005)。物理探査は少なくとも数十メートルのオフセットのある断層の検知に役立ったが、断層の存在の検証には複数の手法の組み合わせが必要となった。埋没した断層とその他の地質の不均質構造を検知する為にマグネトテルリック法（MT 法）を試みたが、他の手法と組み合わせなければあまり有用でないことが判った。一般的な結論としては、断層を検知するにはスタンダードな物理探査手法を用いた場合、断層のオフセットが少なくとも数十メートルはある必要がある(Simmons ら, 2004 Section 4.6.5.3).。

ヤッカマウンテンサイトに於いて、断層の水理データはあまり取得されていない。透気性、間隙率やトレーサーの移行のデータを取得する為に空気のインジェクション試験やトレーサー試験が Ghost Dance 断層や Bow Ridge 断層で行われた(BSC, 2004b, Section 2.2.3)程度である。断層は地下水の流れに対して、主要な水みちになったり、横切る方向に不透水性であったりし、その結果、宙水層を形成したりする(Flint ら., 2001)。

岩石や鉱物の地化学性状は主として異なった岩相沿いの岩と水の相互作用と断層やフラクチャー沿いに析出する二次鉱物に影響を受ける。これらの相互作用は岩石鉱物の溶解反応、イオン交換反応、加水分解反応、析出反応、酸化反応その他の変化や反応である。断層の鉱物学的性状は水と物質の移行の評価に重要である。断層沿いの鉱化が皆無であったり、希少であれば断層は高透水性である可能性が高い。以下、ヤッカマウンテンでの断層の検知や特定に有効であった手法を列挙する。

- 衛星イメージデータ(レーダー、スペクトル解析等)
- 異なったスケールの物理探査
- 広域、地表地質調査
- リニアメントマッピング
- 岩石サンプルの取得

- 間隙水や宙水中の地化学データおよび同位体の痕跡（Cl, ^{3}H 濃度）と充填鉱物
- トレーサーインジェクションテスト

此処で特筆すべきは、上記リストの最後のトレーサーテストは我が国の概要調査では全く実施すべきでないと考える。ヤッカマウンテンでのトレーサー試験は候補地が 1 つに絞られた後の精密調査段階で行われたものであり、極めて小さいスケールの調査であった。

3.1.31 NEVADA

Hammond と Evans(2002)は Keno 断層ゾーンの地化学的痕跡と断層構造が鉱石鉱化成分を含んだ流体の流れに対する影響、及び露頭している鉱石を使って正断層の構造と成因に関連するプロセスの調査を行った。当該断層は北部ネバダ州の中央付近に位置し、シルト岩およびシルトを含んだ石灰岩中のる 55m から 100m の傾斜方向にずれた、傾斜の緩やかな正断層である。走行を横切る方向に 180m、傾斜方向に 65m、走行方向に 350m の露頭があり、岩相の混在する炭酸塩堆積岩で、断層、フラクチャーと地下水が如何に相互作用してるかの研究に理想的なサイトである。断層の上盤も下盤もフラクチャーが極めて多いが、フラクチャーの密度は断層からの距離によってさほど変化していない。断層のずれは 100%傾斜方向のずれから 100%走行方向のずれに変化している。また、1m から数十 m のスケールでは鉱物化のパターンとフラクチャーの密度に相関性が見られない。断層は高透水性と難透水性を併せ持っていると考えられ、断層は断層が形成された時期に発達したフラクチャーと鉱物を含んだ水をつなげる役割を果たしたと考えられる。その後断層は局所的に炭化水素を含むカルサイトの鉱脈を形成する水みちとなった。断層の性状は短距離、鉱床スケール、貯留層スケールの距離で激変する。大きなスケールでは可能性があるが、詳細スケールではダメージゾーンの存在と断層の地化学的区分とは相関性が無いことが判明した。

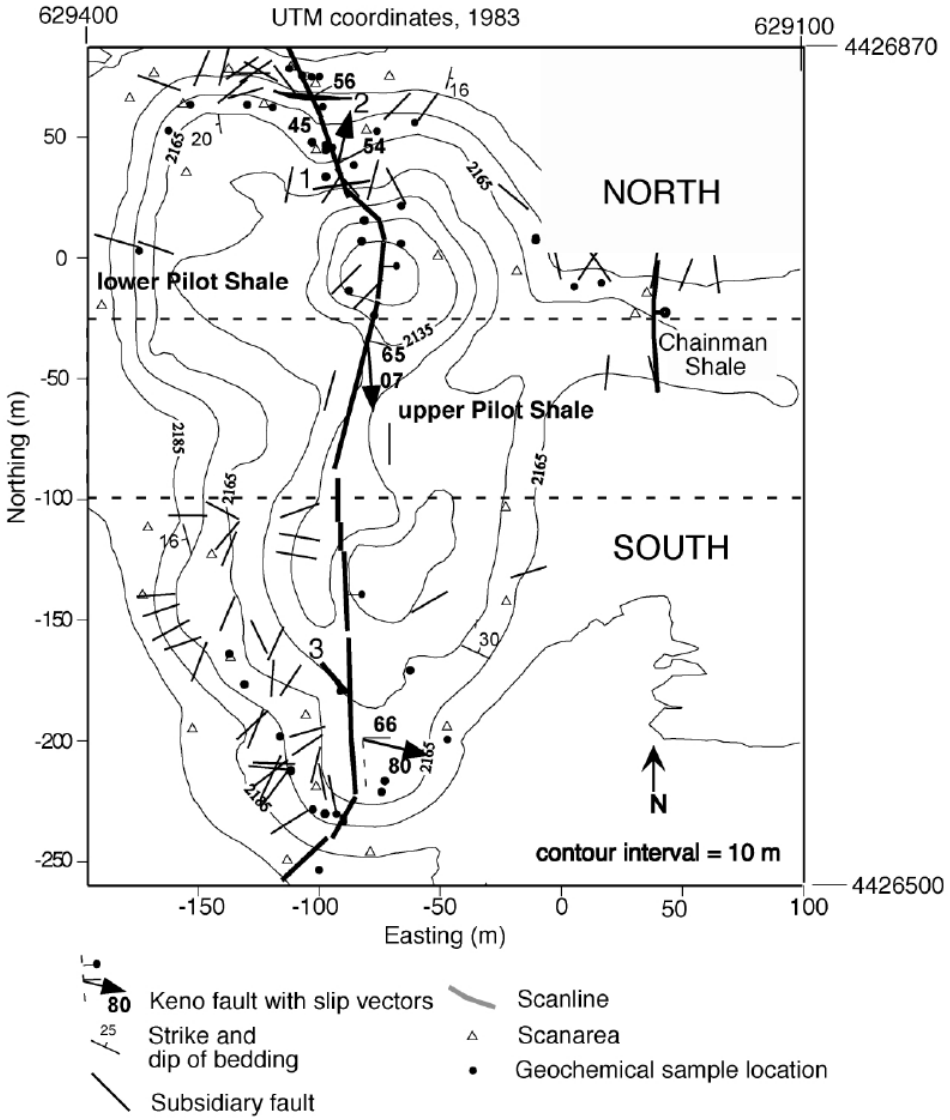

Figure 3-32　　ネバダ州 Keno 断層ゾーンとスキャンライン(Hammond and Evans, 2002)

3.1.32 VALLEY OF FIRE, NEVADA

Jourde ら(2002)は詳細なスケールの現地調査データを使って大きなスケールの横ずれ断層の等価な透水係数を計算した。彼らは既存のネバダ州の Valley of Fire 州立公園内の断層の特性評価データと個々のフィーチャーの性状データを利用した。当該断層(複数)は亀裂ゾーンの横ずれによって形成され、粒子の細かい断層岩（ガウジ）と変形バンドと周辺のジョイントとずれジョイントの発達したダメージゾーンから成る。詳細な断層ゾーンのマッピングと実データにキャリブレートされたイメージデータに基づく透水係

数を使って差分法を使って断層ゾーンの数値モデルを構築した。ずれの長さがそれぞれ 6m、14m、150m のケースの断層をモデル化した。何れの場合も断層ゾーンの透水係数は強い非等方性を示した。場所によっては断層に平行な方向に母岩の 10 倍の大きさの透水係数が認められた。一方、断層に直交する方向では母岩より 2 オーダー低い透水係数となった。ずれの大きな断層ほど直交する方向で透水係数が低いことが分かった。代表的な断層域では、断層に平行な方向の透水係数は亀裂の開口幅に大きく影響されるが直交方向では全く影響が無い。Jourde らは彼らの提唱する手法は詳細な構造と透水係数データが入手、あるいは推定可能なあらゆるタイプの断層にも有効であるとしている。

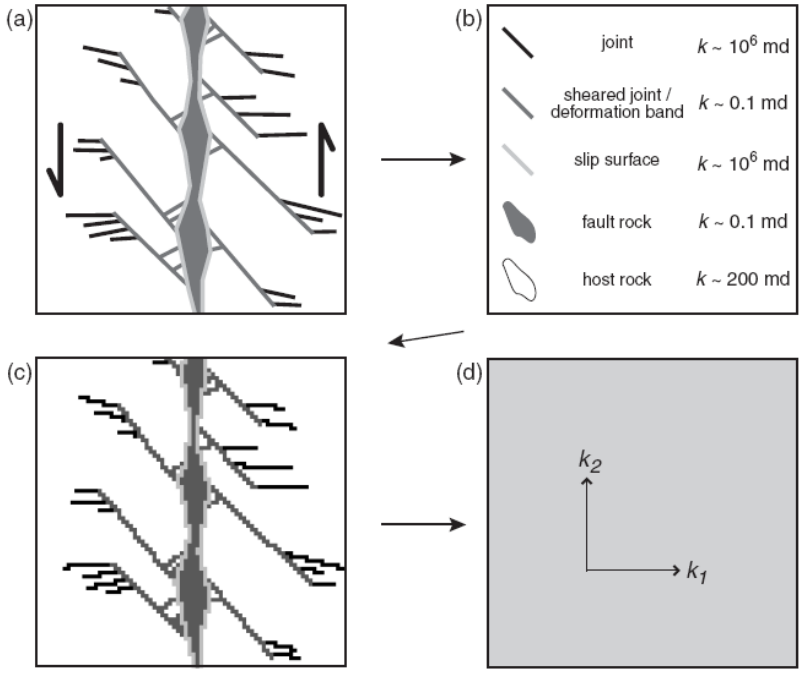

Figure 3-33　詳細な断層ゾーンのマッピングと実データにキャリブレートされたイメージデータに基づく透水係数を使った等価な数値モデル(Jourde et al., 2002)

Burbey(2007)はネバダ州の Mesquite で厚い堆積層に新たに掘削された公共井戸を使った 62 日間の帯水層試験中に GPS ネットワークを使って水平方向と垂直方向の地表面変位のモニタリングデータを採取した。当初は放射方向と接線方向の変位から非等方性の帯水層だと結論されたが、新たな InSAR（Interferometric Synthetic Aperture Radar）データによる地盤沈下の広がりを解析した結果、当該サイトは傾いた正断層によって北西側

に境界があり、南側の沈下も井戸の中心からずれていると考えられる。有限要素法を使い観測された水平方向の変位に合わせるように断層の位置と水圧と応力特性パラメータを推定した。数値シミュレーションの結果、井戸と他の GPS ステーションで観測された変位の大きさと方向が推定される断層から遠ざかる南東方向である場合、断層の幅は 5m で高い透水性と貯留係数を持ち、北東から南西に伸びていると推測される。変位のシミュレーション結果は観測データと良く一致することから、断層の存在の推測が正しい事を示している。帯水層の揚水試験中に水平方向の変位データをモニタリングすることで断層の存在や境界条件について貴重な情報が得られることが示された。

3.2 我が国の事例

3.2.1 超深地層研究所近辺

岐阜県瑞浪市に JAEA（日本原子力研究開発機構）によって瑞浪深地層研究所が建設されつつある。その主立孔付近には NNW 断層と呼ばれる断層が存在し、掘削や揚水試験に対する水頭の応答データや地震の際の水位変化、傾斜計データ等の様々な調査データを元に、Takeuchi ら(2007a)はシーケンシャル水理試験（竹内ら、2007b）及び、高精度傾斜計（中谷ら、2007）を使い NNW 断層は断層を横切る方向に低透水性であると推定した。

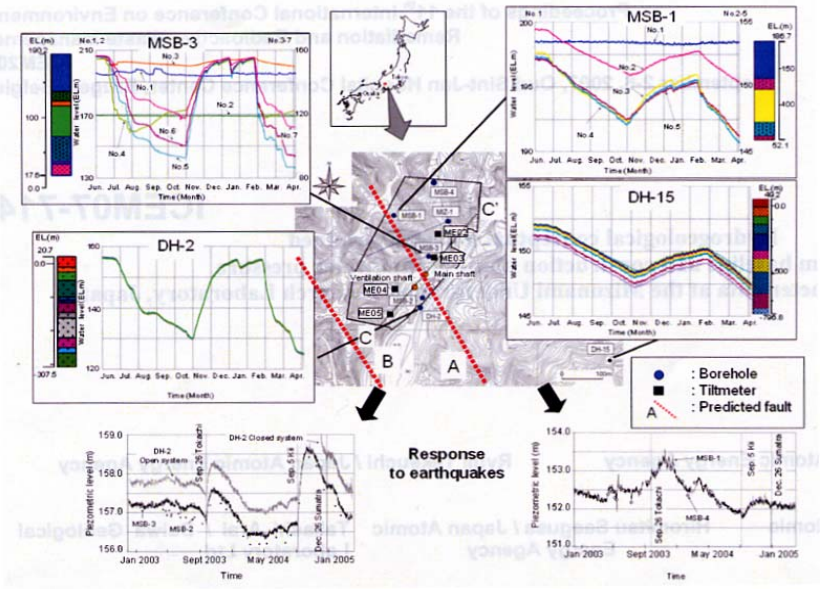

Figure 3-34　NNW 断層を挟んだ両側の地下水頭応答挙動の違い(Takeuchi et al. 2007)

また、深地層研究所の北には月吉断層が存在する。月吉断層は東西に伸びる長さ約 10km 程度とされる逆断層である。月吉断層が横切る JAEA の正馬様サイトでは前身の JNC によって月吉断層の水理性状の調査がなされた。その結果、上盤と下盤では約 40m の水頭差が存在し、断層を横切る方向では低透水性であることが確認された。また、断層の両側に断層に平行に割れ目帯が発達し、高い透水性を示す事が確認された。Sawada ら(2005)はこれらの水理地質データを用いて複数の研究機関がそれぞれ独自のモデルを使った場合のモデル予測の不確実性の検討を行った。また、Doughty and Karasaki (2003) は月吉断層をコア部と両側のダメージゾーンからなるサンドイッチ構造の断層と仮定し、9km×9km×2km の 3 次元水理地質モデルを構築し、パッカー除去時の複数のボアホール内の圧力応答分布と温度分布データを使って断層のコア部とダメージゾーンの透水係数を推定した。

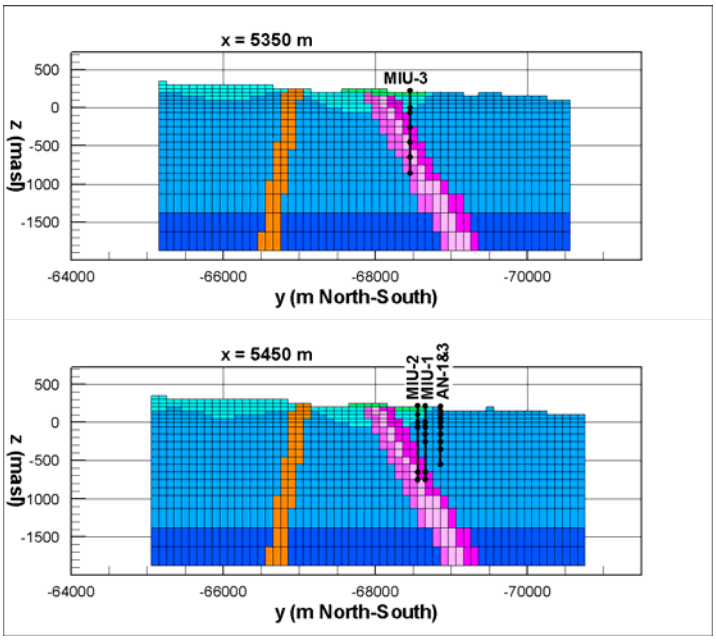

Figure 3-35　Doughty and Karasaki (2003) がモデル化した 9km×9km×2km の東濃地区のモデルの断面。月吉断層はサンドイッチ構造となっている。

3.2.2 幌延深地層研究サイト

伊藤ら (2005) は幌延深地層研究計画サイト周辺地域の間隙水圧分布データを観測データとして用いた逆解析手法の適用性の検討を行った。その結果、断層の水理地質構造によって断層近傍において涵養された地下水の流動状況が大きく異なることが示された。また、深部の水頭値を観測することによって断層の水理地質構造が推定できる可能性を示した。

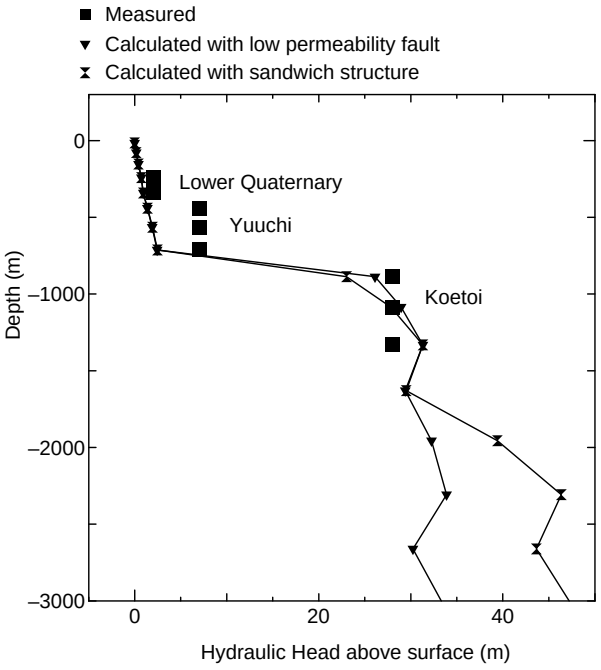

Figure 3-36　低透水ゾーン断層モデルとサンドイッチ構造断層モデルの逆解析水頭値分布の比較 (伊藤ら、2005)

また、石井ら (2006) は北海道北部、幌延地域の大曲断層の三次元分布とその水理特性を反射法地震探査と AMT(Audio Frequency Magnetotelluric)法を使って推定した。その結果、大曲断層は幌延深地層研究センター近辺において地表部で over-step し、地下では収斂する 3 次元構造を持っていると推定した。また、大曲断層は地下 1km 以浅において高透水ゾーンとして機能していると推定した。

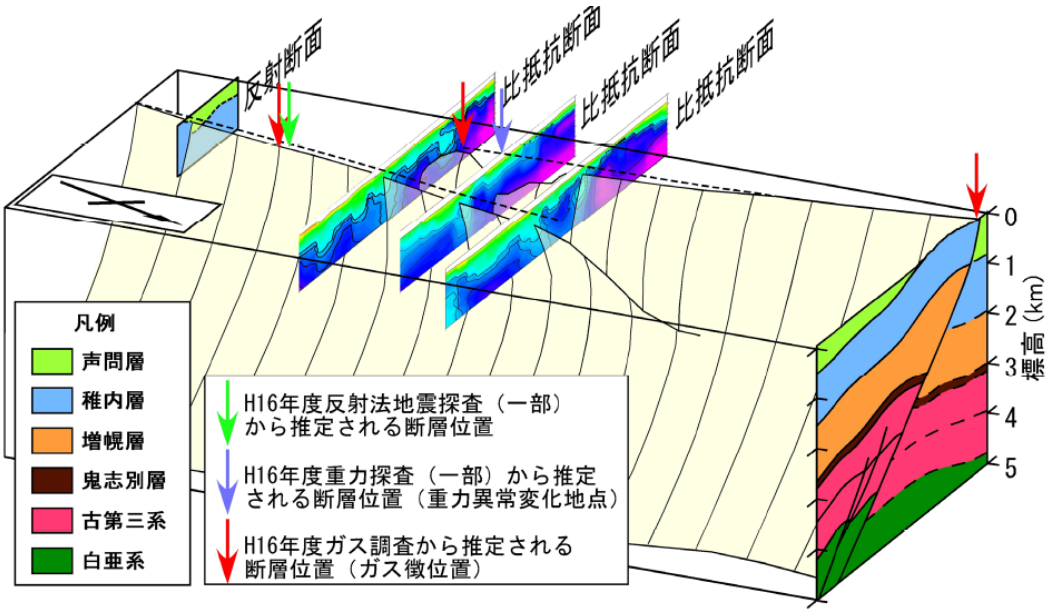

Figure 3-37　石井ら (2006) が反射法地震探査と AMT 法を使って推定した大曲断層の 3 次元構造

3.3　ALSM (Airborne Laser Swath Mapping)

ALSM は空中レーザー地形計測を意味し、近年注目を浴びている技術である（Carter ら、2007）。ALSM は LIDAR (LIght Detection And Ranging あるいは Laser Imaging Detection And Ranging) とも呼ばれる。１ｍ以下の観測点密度を誇り植生の影響をさほど受けずに精密な地表面のデジタル標高マップの取得が可能であり、未知の断層の発見や地すべり危険地域の特定に有用であると考えられる。原理としては航空機搭載のスキャニングレーザーレンジファインダー及びディファレンシャル GPS と慣性ナビゲーションシステムを組み合わせる事によって、木の枝葉を避けてレーザーの斜め方向からの地面からの反射波を捉える。Kondo ら（2008）は糸魚川－静岡構造線に沿って LiDAR 測量を行い、断層の痕跡を確認する事に成功した。また、米国でのデータではあるが、1 平方マイルあたりおよそ$400 から$1,000 の費用で 100 万点のデータが採取可能であり、コスト的にも非常に有利である。従来の写真測量法に比べて 1 オーダー程度精度が高い。ただし、植生の影響を受けにくいが、冬の晴れた日に測量するのが望ましい。

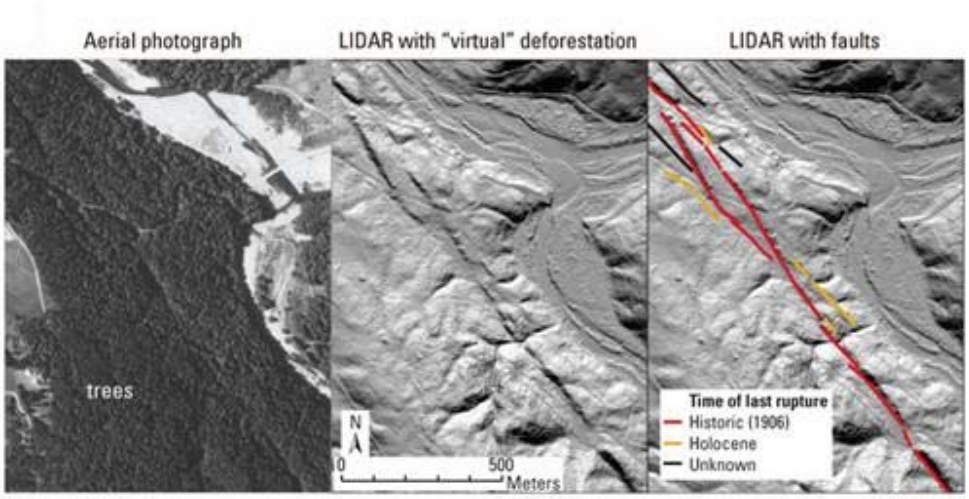

Figure 3-38　（左） 通常の空中写真　（中） フィルターを掛けて植生を取り除いた DEM、（右）断層トレースを重ねた図。
http://geomaps.wr.usgs.gov/sfgeo/quaternary/stories/find_faults.html

3.4　断層水理の解析解と数値モデル

3.4.1　断層のある井戸試験の解析解

Anderson (2006)は解析解を用いて断層を横切る方向に透水性の低い断層と透水性の高い断層のどちらの場合も断層をまたいだ反対側での圧力応答は揚水試験に対して遮水的な応答を示すと結論付けた。この結果は直感と相反するが、事実である。多くの場合どちらの性状の断層が存在する場合も同様な圧力応答を示す。従って、水頭分布から断層の性状を定性的、定量的に推定することが一般に行われているが、解析解のような理想的な条件下でさえ、断層の水理性状の推定が困難であることから、現場試験で限られた数の観測井の圧力応答から断層が高透水性であるか、低透水性であるかを判断することは極めて困難であることが提示された。よって、断層の水理性状を正確に把握する為には、断層のコア部とダメージゾーンを直接試験し、観測点を設置する必要がある。無論、東濃地区の月吉断層に見られるように自然の水頭差があれば、少なくとも直交方向には低透水性だと推測することが可能である。

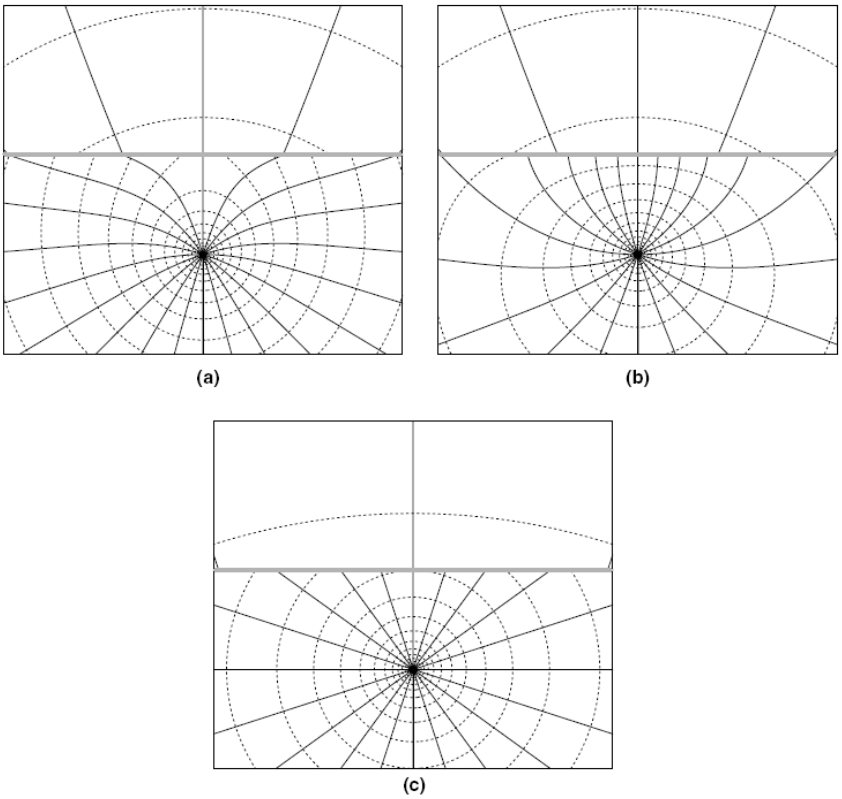

Figure 3-39　揚水試験に対する(a)低透水性 (b)高透水性 (c) 二面性の断層の反対側の水頭応答分布。何れも似通った水頭分布を示している。(Anderson, 2006)

3.4.2 不均質な断層のシミュレーション

Lopez と Smith (1996) は断層内部の不均質性がもたらす地下水の複雑な流れと地温勾配の変化を数値解析を用いて調べた。これらの不均質性は断層の内部と地表面の断層トレースの高い透水性の箇所の連続性によってもたらされている。彼らは不均質な断層内の流れのチャンネリングは均質なケースに比べて最高流出温度に関してはさほどの差は無いが、地下水の流量が大きくなる為、ローカルな熱流量に関しては大きな差異が出ることを示した。

続く第 4 章では、断層内のフラクチャーや小空洞等の不均質性をモデル化して、応力、熱、二相流の連成的な物理プロセスを具現化する手法を詳しく述べた。

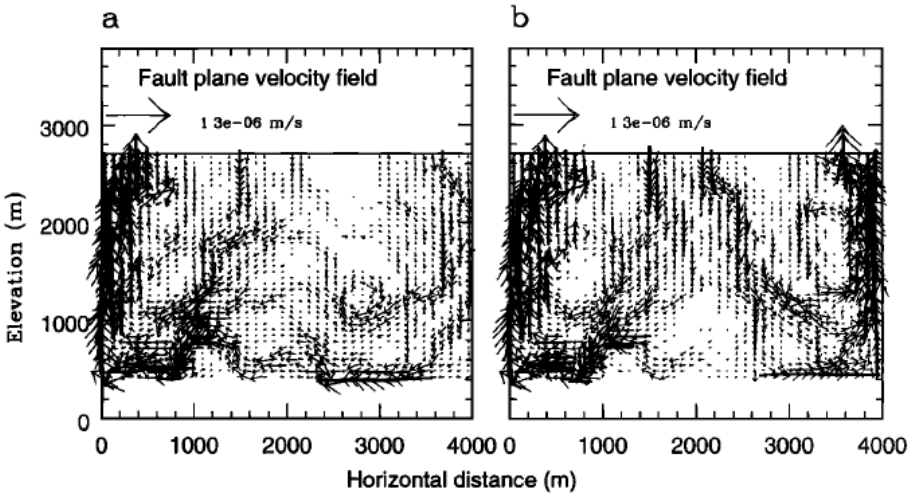

Figure 3-40　不均質な断層内の流れのパターン。(a)は母岩の平均透水係数が $10^{-19}m^2$、(b)は $10^{-16}m^2$ のケース。(Lopez and Smith，1996)

3.4.3 断層を跨いだ水理試験

セクション 3.1 ~ 3.2 で明らかになったように、断層の水理性状は種々の地質情報や断層パラメーター、物理探査データからある程度の類推が可能であるが、透水係数分布や透水係数の絶対値を確認する為には水理試験が欠かせない。ところが、3.4.1 で述べたように、解析解を用いた研究では断層を跨いだ水理試験では断層の性状を把握するのが困難であることが示された。本セクションでは 2 次元の数値モデルを使って断層の近傍で水理試験を行った場合、断層の性状によって水理応答がどのように時系列変化するかを調べた。

断層の性状については、（1）透水係数が母岩に比べて 2 オーダー低い低透水性断層、（2）2 オーダー高い高透水性断層、（3）コア部とダメージ部からなるサンドイッチ構造の断層の 3 つのケースについて調べた。Figure 3-41 にシミュレーションに使用した 2 次元の数値モデルメッシュを示す。Figure 3-42 に 7 日後の圧力分布を示す。Figure 3-43 に各ケースの揚水井と観測井における圧力降下の経時変化を示す。直感的には低透水性の断層がある場合観測井での圧力変化が少なく、高透水性の場合は、圧力変化が伝わり易いと考えがちであるが、図から明らかなように、断層の透水性の性状に拘らず、断層を挟んで揚水井の反対側では圧力が伝わりにくくなっている。

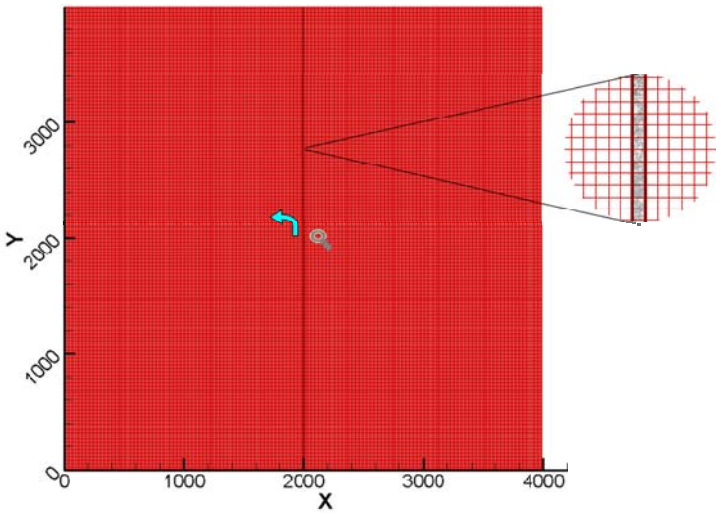

Figure 3-41　断層を跨いだ水理試験の数値モデル。4km×4km、10m 格子グリッド。拡大図は断層の構造を示す。揚水井（矢印）、観測井（虫眼鏡）はそれぞれ断層から 100m の距離。

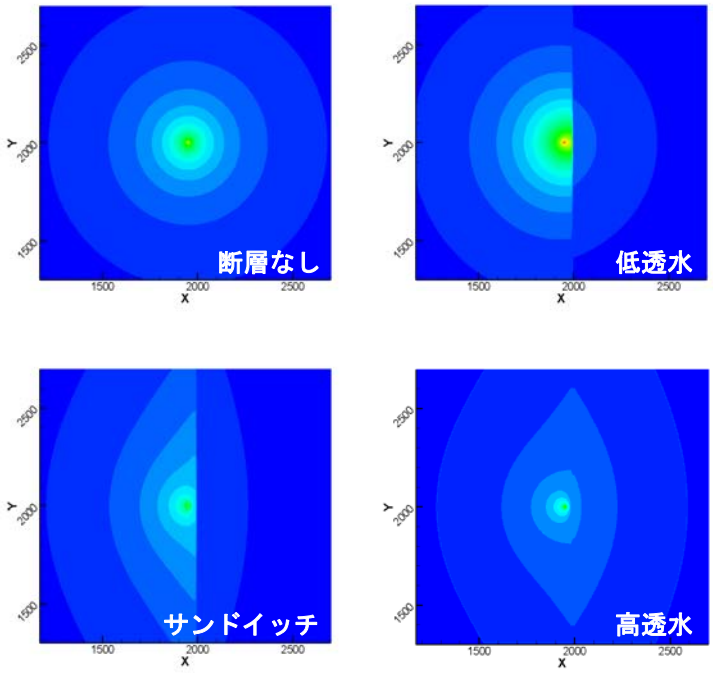

Figure 3-42　それぞれの断層のケースの揚水に対する圧力分布。断層がある場合は何れの場合も断層の反対側に圧力が伝わりにくいことがわかる。

.

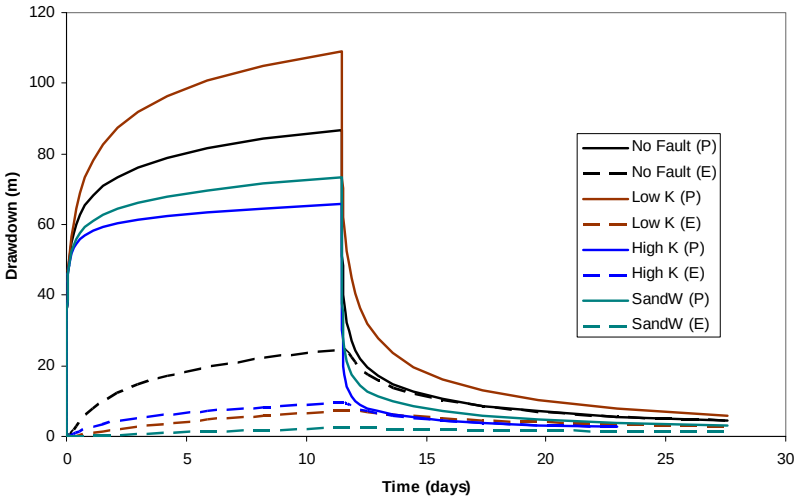

Figure 3-43　各ケースの圧力降下の時間変化。観測井では何れのケースも断層がないケースに比べて圧力降下度が低いことがわかる。

3.5　まとめ

本章では断層の性状の調査事例や、調査技術の実例をまとめた。断層の種類や地質によって、あるいはその地域によって断層性状の特定に有効である各種の技術が見られた。特に、我が国に於いて概要調査で求められるスケールでは、物理探査技術においては、AMT（Acoustic frequency Magneto Telluric）、反射法地震波探査、LIDAR (LIght Detection And Ranging) が断層の特定に有効であった例が多く見られた。また、断層は地域の水理場に大きな影響を及ぼしているので、地域の水頭分布が精密に得られれば、断層の水理性状が推定できることが判った。さらに、地化学的情報や、温度分布から断層性状が推定出来た事例が幾つか見られた。しかしながら、従来の方法や配置では、揚水試験を行っても揚水井や観測井の圧力降下の経時変化のみからは断層の存在そのものは推定できる可能性はあるが、性状の推定は難しい事が明らかになった。

References

AECL, 1994a. An approach to underground characterization of a disposal vault in granite (R.A. Everitt, C.D. Martin, P.M. Thompson) AECL-10560, COG-94-38

AECL, 1994b. Environmental Impact Statement on the Concepts for Disposal of Canada's Nuclear Fuel Waste. AECL -10711, COG-93-1, 496p.

Anderson, Erik I., Analytical solutions for flow to a well through a fault, Advances in Water Resources, 29(12), Pages 1790-1803, 2006.

Antonio, Fernando and Leal Pacheco, Response to pumping of wells in sloping fault zone aquifers, Journal of Hydrology, 259, 116-135, 2002.

Bense, V. F. and H. Kooi, Temporal and spatial variations of shallow subsurface temperature as a record of lateral variations in groundwater flow, Journal of Geophysical Research, Vol. 109, B04103, doi:10.1029/2003JB002782, 2004.

Bense, V. F. and Ronald Van Balen, The effect of fault relay and clay smearing on groundwater flowpatterns in the Lower Rhine, Embayment Basin Research (2004) 16, 397–411, doi: 10.1111/j.1365-2117.2004.00238.

Bense, V. F. and Ronald Van Balen, Hydrogeological aspects of fault zones on various scales in the Roer Valley Rift System, Journal of Geochemical Exploration 78-79, 317-320, 2003.

Bense, V. F.and M. A. Person, Faults as conduit-barrier systems to fluid flow in siliciclastic sedimentary aquifers, Water Resources Research, 42, W05421, doi:10.1029/2005WR004480, 2006.

Blakely, Richard J., Victoria E. Langenheim, David A. Ponce, and Gary L. Dixon: Aeromagnetic Survey of the Amargosa Desert, Nevada and California: A Tool for Understanding Near-Surface Geology and Hydrology, U.S. Geological Survey Open-File Report 00-188, 2000.

Borgnea, T. Le, O. Bour, F.L. Paillet and J.-P. Caudal, Assessment of preferential flow path connectivity and hydraulic properties at single-borehole and cross-borehole scales in a fractured aquifer, Journal of Hydrology, Volume 328, Issues 1-2, 347-359, 2006,

Bredehoeft, John D.: Fault permeability near Yucca Mountain, Water Resources Research, 33(11), 2459-2463, 1997.

BSC 2004b. Technical Basis Document No. 2: Unsaturated Zone Flow Revision I: May 2004. Bechtel SAIC Company, Las Vegas, Nevada.

Burbey, Thomas J., Fault Characterization using InSAR, GPS, and Deformation Modeling, 2007 GSA Denver Annual Meeting , October 28–31, 2007.

Caine, Jonathan Saul, James P. Evans, and Craig B. Forster, Fault zone architecture and permeability structure, Geology; November 1996; v. 24; no. 11; p. 1025-1028.

Carter, E.W., R.L. Shrestha, and K. C. Slatton, Geodetic laser scanning, Physics Today, S-0031-9228-0712-020-2, December, 2007.

Carvalho João, João Cabral, Rui Gonçalves, Luís Torres and Luís Mendes-Victo, Geophysical methods applied to fault characterization and earthquake potential assessment in the Lower Tagus Valley, Portugal, Tectonophysics, Volume 418, Issues 3-4, Pages 277-297, 2006.

Clark, Allan K. and Celeste A. Journey: Flow Paths in the Edwards Aquifer, Northern Medina and Northeastern Uvalde Counties, Texas, Based on Hydrologic Identification and Geochemical Characterization and Simulation, USGS Scientific Investigations Report 2006–5200, 2006.

Dai, X.Y., D. White, and C.L. Ping, Comparing bioavailability in five Arctic soils by pyrolysis-gas chromatography/mass spectrometry,

Dale, M., F. Goff, K. Granzow, P, Longmire, and D, Counce: Assessing Ground-Water Recharge Through The Pajarito Fault Zone, Uppper Pajarito Canyon, Los Alamos, New Mexico, Geologic and Hydrogeologic Framework of the Española Basin –Proceedings of the 4th Annual Española Basin Workshop, Santa Fe, New Mexico, March 1-3, 2005.

do Nascimento, A. F., R. J. Lunn, and P. A. Cowie, Modeling the heterogeneous hydraulic properties of faults using constraints from reservoir-induced seismicity, J. Geophys. Res., 110, B09201, doi:10.1029/2004JB003398. 2005.

Doan M. L., E. E. Brodsky, Y. Kano, K. F. Ma, In situ measurement of the hydraulic diffusivity of the active Chelungpu Fault, Taiwan, Geophys. Res. Lett., 33, L16317, doi:10.1029/2006GL026889, 2006.

Doan, M. L., and F. H. Cornet, Thermal anomaly near the Aigio fault, Gulf of Corinth, Greece, maybe due to convection below the fault, Geophys. Res. Lett., 34, L06314, doi:10.1029/2006GL028931, 2007.

Doughty C, and K. Karasaki, Constraining Hydrologic Models Using Thermal Analysis, 岩盤力学に関するシンポジウム講演論文集, 地盤工学会, 32, 377-382, 2003.

Dutson, Sarah Janeen, Effects of Hurricane Fault Architecture on Groundwater Flow in the Timpoweap Canyon of Southwestern Utah, M.S. Thesis, Brigham Young University, 2005.

Evans, James P., Craig B. Forster and James V. Goddard, Permeability of fault-related rocks, and implications for hydraulic structure of fault zones, Journal of Structural Geology, Volume 19, Issue 11, Pages 1393-1404, 1997.

Fairley, Jerry P. and Jennifer J. Hinds, Field observation of fluid circulation patterns in a normal fault system, Geophysical Research Letters, Vol. 31, L19502, doi:10.1029/2004GL020812, 2004a.

Fairley, Jerry P. and Jennifer J. Hinds, Rapid transport pathways for geothermal fluids in an active Great Basin fault zone, Geology, Vol. 32, No. 9, 825-828, 2004b.

Flint, A.L., Flint, L.E., Bodvarsson, G.S., Kwicklis, E.M. and Fabryka-Martin, J., Evolution of the conceptual model of unsaturated zone hydrology at Yucca Mountain , Nevada. Journal of Hydrology 247 p.p. 1-30, 2001.

Hamaker, Sandra M., Relationship between Fault Zone Architecture and Groundwater Compartmentalization in the East Tintic Mining District, Utah, M.S. Thesis, Brigham Young University, 2005.

Hammond, K. Jill and James P. Evans, Geochemistry, mineralization, structure, and permeability of a normal-fault zone, Casino mine, Alligator Ridge district, north central Nevada, Journal of Structural Geology, Volume 25, Issue 5, Pages 717-736, May 2003.

Hawley, John W., Hydrogeologic Cross Sections of The Estancia Groundwater Basin, Central New Mexico, Geologic and Hydrogeologic Framework of the Española Basin –Proceedings of the 4th Annual Española Basin Workshop, Santa Fe, New Mexico, March 1-3, 2005.

Heffner, James and Jerry Fairley, Using surface characteristics to infer the permeability structure of an active fault zone, Sedimentary Geology 184, 255–265, 2006.

International Atomic Energy Agency, An International Peer Review of the Yucca Mountain Project TSPA-SR Total System Performance Assessment for the Site Recommendation (TSPA-SR), OECD Publications, 2002.

石井英一、安江健一、田中竹延、津久井朗太、松尾公一、杉山和稔、松尾重明、北海道北部、幌延地域における大曲断層の三次元分布と水理特性、地質学雑誌、112、５、301-314、2006.

伊藤一誠、唐崎建二、畑中耕一郎、内田雅大、間隙水圧観測結果を用いた逆解析による堆積岩地域の水理地質構造把握―幌延深地層研究計画サイトへの適用―、応用地質、45、3、125-134、2004

Jeong, Woo-Chang and Dominique Bruel and Tim Hicks, Modelling the Influence of Fault Zone Heterogeneity on Groundwater Flow and Radionuclide Transport,

Johnson, Scott A. and Peter W. Huntoon, Permeability Architecture and Groundwater Circulation Along a Fault-Severed Margin, Northern Hanna Basin, Carbon County, Wyoming, WWRC-94-27, 1994.

Jourde, Herve, Eric A. Flodin, Atilla Aydin, Louis J. Durlofsky, and Xian-Huan Wen, Computing permeability of fault zones in eolian sandstone from outcrop measurements, AAPG Bulletin, v. 86, no. 7, pp. 1187–1200, 2002.

Kessler, John and Robin McGuire, Yucca Mountain Total System Performance Assessment, Phase 3, TR-107191, 3055-02, 1996.

Kim, Kangjoo and Gi Young Jeongb, Factors influencing natural occurrence of fluoride-rich groundwaters: a case study in the southeastern part of the Korean Peninsula, Chemosphere, 58(10), Issue 10, Pages 1399-1408, 2005.

H. Kondo, S. Toda, K. Okumura, K. Takada, T. Chiba, A fault scarp in an urban area identified by LiDAR survey: A Case study on the Itoigawa–Shizuoka Tectonic Line, central Japan, Geomorphology, doi:10.1016/j.geomorph.2008.02.012, 2008.

Langenheim, V., 2000c, Constraints on the Structure of Crater Flat, Southwest Nevada, Derived from Gravity and Magnetic Data. In: Geologic and Geophysical Characterization Studies of Yucca Mountain, Nevada, A Potential High-Level Radioactive-Waste Repository, By John W. Whitney and William R. Keefer, Scientific Editors, U.S. Geological Survey Digital Data Series 058, p.11.

Labaume, P., S. Sheppard, and I. Moretti, Structure and hydraulic behaviour of cataclastic thrust fault zones in sandstones, Sub-Andean Zone, Bolivia, Journal of Geochemical Exploration 69–70, 487–492, 2000.

Leckenby, Robert J., David J. Sanderson and Lidia Lonergan, Estimating flow heterogeneity in natural fracture systems, Journal of Volcanology and Geothermal Research, Volume 148, Issues 1-2, Pages 116-129, 2005.

Lopez, Dina L. and Leslie Smith, Fluid flow in fault zones: Influence of hydraulic anisotropy and heterogeneity on the fluid flow and heat transfer regime, Water Resources Research, Vol. 32, no. 10, 3227-3235, 1996.

Mailloux, Brian J., Mark Person, Shari Kelley, Nelia Dunbar, Steve Cather, Luther Strayer, and Peter Hudleston, Tectonic controls on the hydrogeology of the Rio Grande Rift, New Mexico, Water Resources Research, Vol. 35, No. 9, pp2641–2659, 1999.

Marler J, and Ge S, The permeability of the Elkhorn fault zone, South Park, Colorado, Ground Water. May-Jun;41(3):321-32, 2003.

Micarelli, Luca, Isabelle Moretti, Manon Jaubert, and Hakim Moulouel, Fracture analysis in the south-western Corinth rift (Greece) and implications on fault hydraulic behavior, Tectonophysics 426, 31–59, 2006.

中谷勝哉、松木浩二、新井孝志、大村一夫、竹内真司、新井靖、堀本誠記、傾斜計を用いた地下水流動評価法の開発とモデル解析、Journal of MMJ, 23, 17-25, 2007.

Nguyen, F., S. Garambois, D. Chardon, D. Hermitte, O. Bellier and D. Jongmans, Subsurface electrical imaging of anisotropic formations affected by a slow active reverse fault, Provence, France, Journal of Applied Geophysics, Volume 62, Issue 4, Pages 338-353, 2007.

Rawling, Geoffrey C., Laurel B. Goodwin, and John L. Wilson: Internal architecture, permeability structure, and hydrologic significance of contrasting fault-zone

types, Geology
29(1), 43-46, DOI: 10.1130/0091-7613, 2001.

Ponce, D.A., 1996, Interpretive geophysical fault map across the central block of Yucca Mountain, Nevada: U.S. Geological Survey Open-File Report 96-285, 15 p.

Posiva Oy, Olkiluoto Site Description 2004, Posiva Report, 2004.

Pugetsound Lidar Consortium, http://pugetsoundlidar.ess.washington.edu

Rodrigues, B., and J. Williams: Preliminary Electrical Resistivity Model Across the La Bajada Constriction for Hydrogeologic Framework Studies in the Espanola and Santo Domingo Basins, New Mexico, Geologic and Hydrogeologic Framework of the Española Basin –Proceedings of the 4th Annual Española Basin Workshop, Santa Fe, New Mexico, March 1-3, 2005.

Sawada, A., H. Saegusa, and Y. Ijiri, Uncertainty in Groundwater Flow Simulations Caused by Multiple Modeling Approaches, at the Mizunami Underground Research Laboratory, Japan, International Symposium on Dynamics of Fluids in Fractured Rock No2, Berkeley, CA , ETATS-UNIS (02/2004) vol. 162, 213p, 2005.

Seaton, William J., and Thomas J. Burbey, Influence of Ancient Thrust Faults on the Hydrogeology of the Blue Ridge Province, Groundwater, Vol. 43, No. 3, 301–313, 2005.

Shipton, Zoe K., James P. Evans, Kim R. Robeson, Craig B. Forster, and Stephen Snelgrove, Structural heterogeneity and permeability in faulted eolian sandstone: Implications for subsurface modeling of faults, AAPG Bulletin, v. 86, no. 5, pp. 863–883, 2002.

Sikora, R.F., Campbell, D.L, and Kucks, R.P., 1995, Aeromagnetic surveys across Crater Flat and part of Yucca Mountain, Nevada: U.S. Geological Survey Open-File Report 95-812, 13 p.
at http://wrgis.wr.usgs.gov/docs/gump/sikora/95-812.html)

Simmons, A.S., J. Houseworth, R. Keefer, E. Kwicklis, G. LeCain, J. Luellen, D. O'Leary, J. Paces, Z. Peterman, R. Price, R. Quittmeyer, B. Robinson, L. Scheibel, S. Sharpe, J. Stuckless, P. Tucci, and J. Whitney. 2004. Yucca Mountain Site Description. TDR-CRW-GS-000001 REV 02 ICN 01. Volume I: Section 1-5. Bechtel SAIC Company, Las Vegas, Nevada.

Smith K.D., Li L., Brune J. N., Anooshehpoor R., and. Savage M. K, 2000d - Preliminary Results from the NPE-Ryan Reversed Refraction Profile in Geologic and Geophysical Characterization Studies of Yucca Mountain, Nevada, A Potential High-Level Radioactive-Waste Repository, By John W. Whitney and William R. Keefer, Scientific Editors, U.S. Geological Survey Digital Data Series 058, p.9.

Sultan, M., A. Wagdy, N. Manocha, W. Sauck, K. Abdel Gelil, A.F. Youssef, R. Becker, A. Milewski, Z. El Alfy and C. Jones, An integrated approach for

identifying aquifers in transcurrent fault systems: The Najd shear system of the Arabian Nubian shield, Journal of Hydrology, Volume 349, Issues 3-4, Pages 475-488, 2008.

SWRI, http://www.swri.edu/4ORG/d20/deps/consortium/default.htm

Takeuchi, S., R. Takeuchi, W. Salden, H. Saegusa, T. Arai, K. Matsuki, Hydrogeological conceptual model determined from baseline and construction phase groundwater pressure and surface tiltmeter data at the Mizunami Underground Research Laboratory, Japan, Proceedings of the 11th International Conference on Environmental Remediation and Radioactive Waste Management ICEM2007, September 2-6, 2007.

竹内真司、中野勝志、平田洋一、進士喜英、西垣誠、深層岩盤を対象としたシーケンシャル水理試験手法の開発と適用、地下水学会誌、49，1、17-32、2007.

US Nuclear Waste Technical Review Board, Panel on the Natural System Unsaturated Zone Flow and Radio Nuclide Transport, March 9, 2004

White, Daniel, Kenji Yoshikawa and D. Sarah Garland, Use of dissolved organic matter to support hydrologic investigations in a permafrost-dominated watershed, Cold Regions Science and Technology, Volume 35, Issue 1, Pages 27-33, 2002.

4 Conceptualization and Modeling of Fault Zones

4.1 Introduction

Since the 1960s, a number of numerical approaches and techniques have been developed and applied for modeling flow and transport processes in fractured reservoirs (e.g., Kazemi, 1969; Pruess and Narasimhan, 1985; Wu and Pruess, 1988). Even with the significant progress that has been made towards understanding and modeling of flow and transport processes in fractured rock so far, most studies have focused primarily on naturally fractured reservoirs, without explicitly taking faults into consideration. Recently, characterizing the fractured rock of faults or fault zones has received attention, because fault zones are found to be closely associated with, and may dominate, flow and transport processes in fractured reservoirs (Wu et al., 2004; 2006a; 2007a).

Mathematical approaches developed for modeling flow through fractured reservoirs rely in general on continuum approaches. Such approaches involve developing conceptual models, incorporating the geometrical information of a given fracture-matrix system, setting up mass and energy conservation equations for fracture-matrix domains, and then solving discrete nonlinear algebraic equations of mass and energy conservation. The commonly used mathematical methods for modeling flow through fractured rock include: (1) an explicit discrete-fracture and matrix model (Snow, 1965), (2) a dual- and multiple-continuum method, including double- and multiporosity, dual-permeability, or the more general "multiple interacting continua" (MINC) method (Warren and Root, 1963; Kazemi, 1969; Pruess and Narasimhan, 1985; Wu and Pruess, 1988), and (3) an effective-continuum method (ECM) (Wu, 2000a).

In addition to the traditional double-porosity concept, a number of triple-porosity or triple-continuum models have been proposed (Closemann, 1975; Wu et al., 2004a; Kang et al., 2006) to describe flow through fractured rocks. In particular, Liu et al. (2003) and Camacho-Velazquez et al. (2005) present several new triple-continuum models for single-phase flow in a fracture-matrix system that include cavities within the rock matrix (as an additional porous portion of the matrix). In general, these models have focused on handling the heterogeneity of the rock matrix or fractures, e.g., subdividing the rock

matrix or fractures into two or more subdomains with different properties. In concept, all these approaches can be applied to modeling flow and transport in highly dense fractures in fault zones.

Dual-continuum or multiple-continuum approaches for modeling flow in fractured porous media, as applied in this study, include the classical double-porosity model (Barenblatt et al., 1960; Warren and Root, 1963), the dual-permeability concept, the more rigorous dual-continuum generalization of the MINC (Pruess and Narasimhan, 1985) and the multicontinuum model (Wu and Pruess, 1988). In the double-porosity model, a flow domain is composed of matrix blocks with low permeability, embedded in a network of interconnected fractures. Global flow and transport in the formation occur only through the fracture system, conceptualized as an effective continuum. This model treats matrix blocks as spatially distributed sinks or sources to the fracture system without accounting for global matrix-matrix flow. In comparison, the MINC concept is able to describe gradients of pressures, temperatures, or concentrations near the matrix surface and inside the matrix—by further subdividing individual matrix blocks with one- or multidimensional strings of nested meshes. Therefore, the MINC model in general provides a better numerical approximation for transient fracture-matrix interactions than the double-porosity model. Because of its computational efficiency and its ability to match many types of observed fault-flow data (e.g., Wu et al., 2004; 2007a), the dual-continuum models as exemplified in the double-porosity and dual-permeability concepts—which have perhaps been the most widely used methods in petroleum and geothermal engineering, as well as in groundwater hydrogeology—will be used for this study.

In this section, a physically based fault conceptual model is presented for modeling multiphase flow and transport processes in the fractured rock of fault zones. In particular, we discuss a general mathematical framework model for dealing with fracture-matrix interactions, which is applicable to both continuum and discrete fracture conceptualization in fault zones. The multicontinuum, physically based conceptual mathematical model includes the effects of various scaled fractures, vugs, or cavities on water and heat flow processes in fault zones.

In this continuum model, faults or fault zones of formations is conceptualized as a multiple-continuum medium, consisting of (1) highly permeable, large-scale and well-connected fractures, (2) low-permeability rock matrix, and (3) various-sized vugs (if existing). Similar to the conventional double-porosity model, the large-scale, well-connected fracture continuum is responsible for global flow within faults, while vuggy and matrix continua, providing storage space, are locally connected to each other (and interacting with globally connecting fractures). In addition, the flow along faults is also interacting laterally with formation layers on both sides of the fault zone.

In this approach, a subsurface fault domain consisting of fractures, rock matrix, vugs, or other large pores is discretized using an unstructured grid with regular or irregular meshes, followed by time discretization carried out using a backward, first-order, finite-difference method. The final discrete nonlinear equations are handled fully implicitly, using Newton iteration. In addition, the fracture medium is handled using a general dual-continuum concept with continuum or discrete modeling approaches.

We demonstrate that with this unified approach, modeling a particular process of fracture or porous-medium flow and transport in fault zones becomes simply a matter of defining types of media (i.e., fractures, matrix, vugs, or other large pores) with a set of state variables, along with their interactions on the interfaces between continua. The proposed numerical scheme is applicable to simulating water and heat flow, as well as solute transport, through fractured fault zones and their interaction with surrounding rock layers.

4.2 Conceptual Model of Fractured Faults

Faults may consist of a single fracture or multiple scale fractures, or highly dense fractured zones. In general, faults or fault zones belong typically to fractured rock and can be classified as a special case of fractured reservoirs. A typical fractured reservoir, as shown in **Error! Reference source not found.** (Warren and Root, 1963), consists of large-scale fractures, a low-permeable rock matrix, and a number of various sized cavities or vugs. Figure 4-2 shows a formation of outcrops with a vertical fault (Wu et al., 2006), and the fractured system is conceptualized using vertical and horizontal fracture networks with vugs along the vertical fault in the figure.

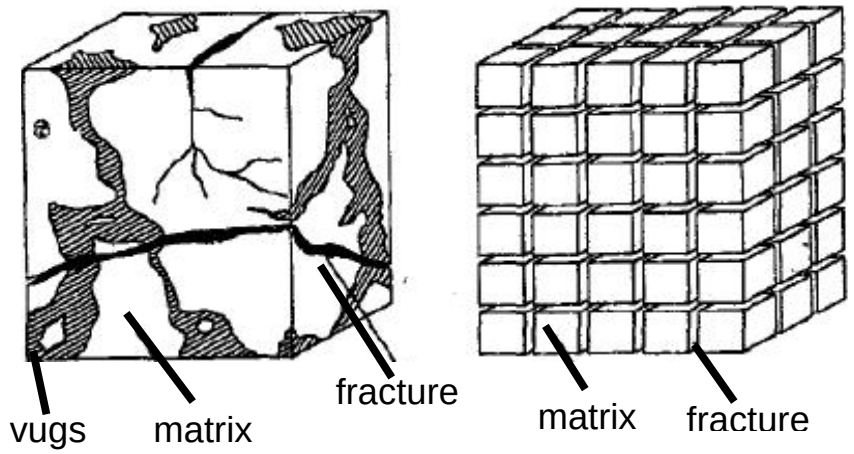

Figure 4-1 Schematic of conceptualizing fractured formation using the double-porosity conceptual model (Warren and Root, 1963).

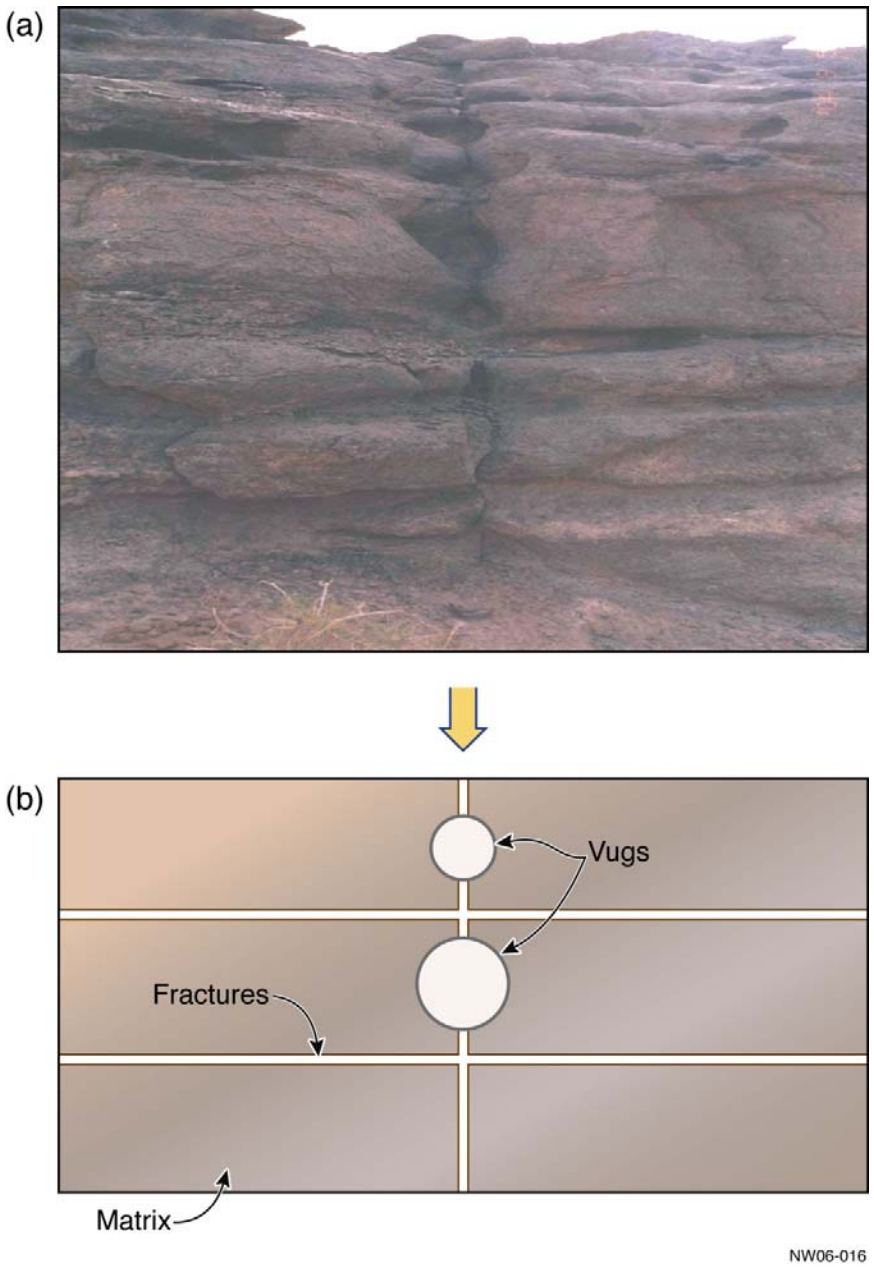

Figure 4-2 Schematic of conceptualizing vuggy fractured formation as a discrete fracture system with well connected, (a) outcrop pictures and (b) conceptual model (Wu et al. 2006).

As shown in

Figure **4-1** and Figure 4-2, different types of fractured rock in fault zones can be described using a multicontinuum concept. The multicontinuum conceptual model considers large fractures as main pathways for the global flow. Vuggy and matrix continua, locally connected to each other as well as directly or indirectly interacting with globally connecting fractures, provide storage space as sinks or sources to fractures. Note that vugs directly connected with fractures could be considered part of the fracture continuum. More specifically, we conceptualize the fractured-vug-matrix system of fault zones as consisting of (1) a fracture continuum—"large" fractures (or fractures), *globally connected* on the scale of a model domain, providing flow paths to injection and production wells; (2) a vuggy continuum—various-sized vugs or large pore space cavities, which are *locally connected* to fractures either through "small" fractures or *isolated* by rock matrix; (3) a matrix continuum—rock matrix, which may contain a number of cavities, *locally connected* to large fractures and/or to vugs; and (4), small-scale fractures (Wu et al., 2004a).

In principle, the proposed multiple-continuum model for fault zones is a natural extension of the generalized multiple-continuum (MINC) approach (Pruess and Narasimhan, 1985; Wu and Pruess, 1988). In this approach, an "effective" porous medium is used to approximate fractures, vugs (if any), rock matrix continuum, or any large pores. The triple- or multiple-continuum conceptual model assumes that approximate thermodynamic equilibrium exists locally within each of the continua at all times. Based on this local equilibrium assumption, we can define thermodynamic variables, such as pressure, fluid saturation, concentration, and temperature, for each continuum. Note that the multiple-continuum model is not limited to the orthogonal idealization of the fracture system, or uniform size, regular shape, or distribution of vugs and cavities, as illustrated in

Figure **4-1** and Figure 4-2. Irregular and stochastic distributions of fractures and cavities can be handled numerically, as long as the actual distribution patterns are known (Pruess, 1983).

4.3 Mathematical Model

The physical processes associated with flow and transport in fractured porous media in fault zones are governed by the same fundamental conservation laws as those used in other branches of science and engineering: conservation of mass, momentum, and energy governs the behavior of fluid flow, chemical transport, and heat transfer in porous or fractured rock. These physical laws are often represented mathematically on the macroscopic level by a set of partial differential or integral equations, called governing equations. These governing equations are generally nonlinear as long as compressible fluid flow or heat transfer is involved and needed to quantitatively model the flow and transport processes occurring in porous or fractured media. Based on the general conservation laws, we present a set of generalized governing equations for fluid flow, multicomponent transport, and heat transfer in porous and fractured media, providing a framework for numerical formulations to cover all possible scenarios for flow and transport in porous media.

We consider the following physical processes in fault zones: (1) single-phase aqueous phase flow, (2) solute (multiple minerals) transport, and (3) ambient heat flow, driven by geothermal gradient. Let us consider a nonisothermal system consisting of one aqueous fluid phase, which in turn consists of a number of mass components. To derive a set of generalized governing equations for fluid flow, multicomponent transport, and heat transfer, we assume that these processes can be described using a continuum approach within a representative elementary volume (REV) in a porous or fractured medium. In addition, a condition of local thermodynamic equilibrium is assumed, so that at any time temperatures, phase pressures, densities, viscosities, enthalpies, internal energies, and component concentrations (or mass fractions) are the same locally in each REV of the porous medium.

According to mass and energy conservation principles, we can write a generalized conservation equation of mass components and energy in a porous continuum, as follows:

$$\frac{\partial M^k}{\partial t} = G^k + q^k + F^k \qquad (1)$$

where superscript k is the index for the components k = 1, 2, 3,…, N_c, with N_c being the total number of mass components and k = N_c+1 for an energy "component" (note that heat energy is here regarded as a component for convenience); M is the accumulation term of component k; G^k is the decay or internal generation (reaction) term of mass or energy components; q^k is an external source/sink term or fracture-matrix exchange term for mass or energy component k and energy; and F^k is the "flow" term of mass or energy movement or net exchange from single-phase flow, or diffusive and dispersive mass transport, or heat transfer, as discussed below.

In addition to the conservation or continuity equations of mass and thermal energy, shown in Equation (1), we also need specific relationships or *mechanisms* that describe why and how fluid flow, solute transport, and heat transfer occur in porous and fractured media. This is to define the "flow" term in Equation (1), and the following specific laws act as such mechanisms by governing local fluid flow, component transport, and heat transfer processes in porous media.

4.3.1 SINGLE-PHASE DARCY FLOW

For single-phase liquid flow, the accumulation terms in Equation (1) for water phase is evaluated as

$$M^w = \rho_w \phi \tag{2}$$

where ρ_w is the density of water phase; and ϕ is the porosity of porous or fractured media. Note that in this special case, the decay or generation term is negligible with

$$G^w = 0 \tag{3}$$

The mass flow term is determined by

$$F^w = \nabla \bullet (\rho_w \mathbf{v}_v) \tag{4}$$

where $\mathbf{v}_w$ is a vector of the Darcy's velocity or volumetric flow of water, defined by Darcy's law to describe the flow of single fluid as

$$\mathbf{v}_w = -\frac{k}{\mu}(\nabla P_w - \rho_w g \nabla z) \tag{5}$$

where P_w, μ, and g are pressure, viscosity of water phase, and gravitational constant, respectively; z is the vertical coordinate; k is absolute or intrinsic permeability (a tensor in general).

4.3.2 MASS TRANSPORT

The movement of dissolved mass components or chemical species in a fluid-rock-medium system can also be handled as a special case of Equation (1). The accumulation terms for component k is

$$M^k = \phi\rho_w X_w^k + (1-\phi)\,\rho_s\,\rho_w\,X_w^k\,K_d^k \quad (k = 1, 2, 3,\ldots, N_c) \quad (6)$$

where X_w^κ is the mass fraction of component k in water, ρ_s is the density of rock solids; and K_d^k is the distribution coefficient of component k between the aqueous phase and rock solids to account for adsorption effects.

In the case in which components are subject to a first-order radioactive decay, the decay/generation term is

$$G^k = \phi\lambda_k\left(\rho_w X_w^k + (1-\phi)\,\rho_s\,\rho_w\,X_w^k\,K_d^k\right) \quad (k = 1, 2, 3,\ldots, N_c) \quad (7)$$

where λ_k is the radioactive decay constant of component k.

The mass component transport is governed in general by processes of advection, diffusion, and dispersion, and is also subject to other processes such as radioactive decay, adsorption, dissolution and precipitation, mass exchange and partition between phases, or chemical reactions. Advective transport of a component or solute is carried by flow of a fluid, and diffusive and dispersive flux is contributed by molecular diffusion and mechanical dispersion, or hydrodynamic dispersion. These processes are described using a modified Fick's law for transport through a single-phase porous medium (Wu, 2004b). Then, the total mass flow term for a component k, by advection and dispersion, is written as

$$F^k = -\nabla\bullet\left(\rho_w\,X_w^k\,\mathbf{v}_w\right) + \underline{D}_w^k\bullet\nabla\left(\rho_w X_w^k\right) \quad (k = 1, 2, 3,\ldots, N_c) \quad (8)$$

Equation (8) indicates that the mass flow consists of two parts: the first part, i.e., the first term on the right-hand side of (8), is contributed by advection in water flow; and

the second part [the second term on the right-hand side of (8)] is the diffusive flux by hydrodynamic dispersion. In Equation (8), $\underline{D}_w^k$ is the hydrodynamic dispersion tensor accounting for both molecular diffusion and mechanical dispersion for component k in the water phase, defined by an extended dispersion model (Scheidegger, 1961),

$$\underline{D}_w^k = \alpha_T |\mathbf{v}_w| \delta_{ij} + (\alpha_L - \alpha_T) \frac{\mathbf{v}_w \mathbf{v}_w}{|\mathbf{v}_w|} + \phi \tau d_w^k \delta_{ij} \quad (k = 1, 2, 3, \ldots, N_c) \quad (9)$$

where α_T and α_L are transverse and longitudinal dispersivities, respectively, in the water phase of porous or fractured media; τ is tortuosity of the porous medium; d_w^k is the molecular diffusion coefficient of component k within the water phase; and δ_{ij} is the Kronecker delta function ($\delta_{ij} = 1$ for i = j, and $\delta_{ij} = 0$ for $i \neq j$), with i and j being coordinate indices.

4.3.3 HEAT TRANSFER

The accumulation term for the heat equation is usually is defined as

$$M^{N_c+1} = \phi \rho_w U_w + (1 - \phi) \rho_s U_s \quad (10)$$

where U_β and U_s are the internal energies of water phase and rock solids, respectively.

Heat transfer in porous and fractured media is in general a result of both convective and conductive processes. Heat convection is contributed by thermal energy carried mainly by bulk flow of water. On the other hand, heat conduction is driven by temperature gradients and may follow Fourier's law. Then the combined, overall heat-flux term, owing to convection, conduction, and radiation in a multiphase, multicomponent, porous medium system, may be described as:

$$F^{N_c+1} = -\nabla \bullet (h_\beta \rho_\beta \mathbf{v}_\beta) + \nabla \bullet (K_T \nabla T) \quad (11)$$

where h_w are the specific enthalpies of the water phase, K_T is the overall thermal conductivity; and T is temperature;

4.3.4 CONSTITUTIVE RELATIONSHIPS

To complete the mathematical description of water flow, multicomponent transport, and heat transfer in porous and fractured media, Equation (1), a generalized mass- and energy-balance equation, needs to be supplemented with a number of constitutive equations. These constitutive correlations express the interrelationships of, and constraints on, physical processes, variables, and parameters, and allow the evaluation of secondary variables and parameters as functions of a set of primary unknowns or variables selected to make the governing equations solvable. Many of these correlations for estimating properties and interrelationships are determined by experimental studies.

4.4 Numerical Formulation and Solution

The methodology for using numerical approaches to simulate subsurface flow and transport, and heat transfer, consists in general of the following three steps: (1) spatial discretization of mass and energy conservation equations, (2) time discretization; and (3) iterative approaches to solve the resulting nonlinear, discrete algebraic equations. Among various numerical techniques for simulation studies, a mass- and energy-conserving discretization scheme, based on finite or integral finite-difference or finite-element methods, is the most commonly used approach and is discussed here.

4.4.1 DISCRETE EQUATIONS

The component mass- and energy-balances represented in Equation (1) are discretized in space using a control-volume concept. The control-volume concept provides a general spatial discretization scheme that can represent a one-, two- or three-dimensional domain using a set of discrete meshes. Each mesh has a certain control volume for a proper averaging or interpolation of flow and transport properties or thermodynamic variables. The control volume concept includes the conventional finite-difference scheme (Aziz and Settari, 1979; Narasimhan and Witherspoon, 1976; Pruess et al., 1999), an integral finite-difference method (Figure 4-3), a control-volume finite element (Forsyth, 1994), and Galerkin finite-element methods (Huyakorn et al., 1994).

These are the most widely used discretization schemes for subsurface flow and transport simulation.

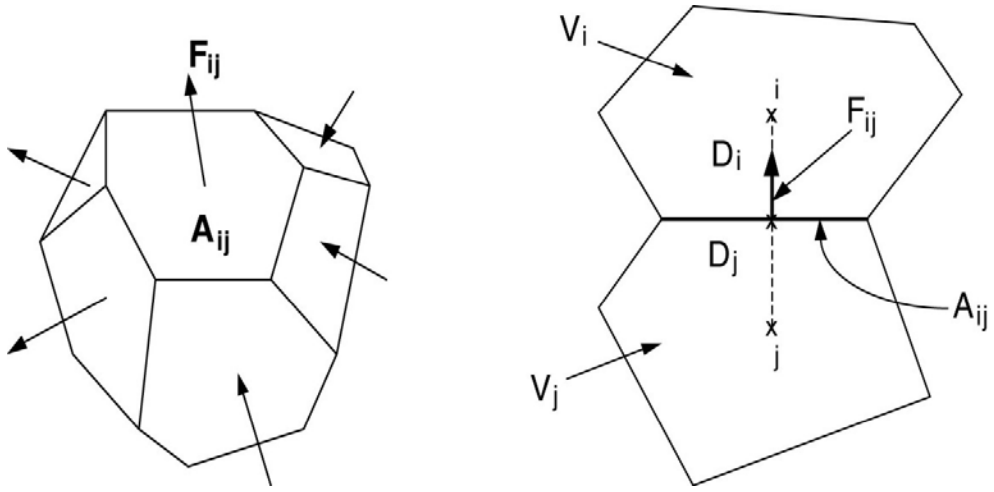

Figure 4-3 Space discretization and flow-term evaluation in the integral finite difference method (Pruess et al., 1999)

As shown in Figure 4-3, the spatial discretization of Equation (1) is carried out using the integrated finite difference scheme, and time discretization is carried out using a backward, first-order, fully implicit finite-difference scheme. The discrete nonlinear equations for components of water, other mass components, and heat at gridblock or node i can be written in a general form:

$$\left\{M_i^{k,n+1} + G_i^{k,n+1}\Delta t - M_i^{k,n}\right\}\frac{V_i}{\Delta t} = \sum_{j\in\eta_i} \text{flow}_{ij}^{k,n+1} + Q_i^{k,n+1} \qquad (12)$$

$(k = 1, 2, 3, \ldots, N_c, N_c+1)$ and $(i=1, 2, 3, \ldots, N)$

where superscript k serves also as an equation index for all mass components with k = 1, 2, 3, …, N_c and k = N_c+1 denoting the heat equation; superscript n denotes the previous time level, with n+1 the current time level to be solved; subscript i refers to the index of gridblock or node i, with N being the total number of nodes in the grid; Δt is the time step size; V_i is the volume of node i; η_i contains the set of direct neighboring nodes (j) of node i; and A_i^k, G_i^k, flow_{ij}^k, and Q_i^k are the accumulation and decay/generation terms, respectively, at node i.

The "flow" term between nodes i and j, and the sink/source term at node i for component k or thermal energy, respectively, are defined below. Equation (12) has the same form regardless of the dimensionality of the system, i.e., it applies to one-, two-, or three-dimensional flow, transport, and heat-transfer analyses within and outside fault zones.

The accumulation and decay/generation terms for mass components or thermal energy are evaluated using Equations (6), (7), and (10), respectively, at each node i. The "flow" terms in Equation (12) are generic and include mass fluxes by advective and dispersive processes, as described by Equation (4) or (8), as well as heat transfer, described by (11).

The mass flow term of Equation (12) for single-phase water flow is described by a discrete version of Darcy's law, i.e., the mass flux of water phase along the connection is given by

$$\text{flow}_{ij}^{w} = \lambda_{w,ij+1/2}\gamma_{ij}\left[\psi_j - \psi_i\right] \tag{13}$$

where $\lambda_{w,i\,j+1/2}$ is the mobility term to water phase, defined as

$$\lambda_{w,i\,j+1/2} = \left(\frac{\rho_w}{\mu}\right)_{ij+1/2} \tag{14}$$

In Equation (13), γ_{ij} is transmissivity and is defined differently for finite-difference or finite-element discretization. If the integral finite-difference scheme (Pruess et al., 1999) is used, the transmissivity is evaluated as

$$\gamma_{ij} = \frac{A_{ij}k_{ij+1/2}}{D_i + D_j} \tag{15}$$

where A_{ij} is the common interface area between connected blocks or nodes i and j (Figure 4-3); and D_i is the distance from the center of block i to the interface between blocks i and j (Figure 4-3). The flow potential term in Equation (13) is defined as

$$\psi_i = P_{w\,i} - \rho_{w,ij+1/2}\,g\,Z_i \tag{16}$$

where Z_i is the depth to the center of block i from a reference datum.

For mass-component transport, the flow term, or the net mass flux by advection and hydrodynamic dispersion of a component along the connection of nodes i and j, is determined by

$$\text{flow}_{ij}^{k} = F_{A,ij}^{k} + F_{D,ij}^{k} \quad (k = 1, 2, 3, \ldots, N_c) \tag{17}$$

where $F_{A,ij}^{k}$ and $F_{D,ij}^{k}$ are the net mass fluxes by advection and hydrodynamic dispersion along the connection, respectively, with

$$F_{A,ij}^{k} = A_{ij}\left(X_{\beta}^{k}\right)_{ij+1/2} \text{flow}_{ij}^{w} \tag{18}$$

and

$$F_{D,ij}^{k} = -\mathbf{n}_{ij} \bullet A_{ij}\underline{D}_{w}^{k} \bullet \nabla\left(\rho_{w} X_{w}^{k}\right) \tag{19}$$

where $\mathbf{n}_{ij}$ is the unit vector along the connection of the two blocks i and j.

The total heat flux along the connection of nodes i and j, including advective and conductive terms, can be also evaluated, when using a finite-difference scheme, by

$$\text{flow}_{ij}^{N_c+1} = \left(h_{w}\right)_{ij+1/2} \text{flow}_{ij}^{w} + A_{ij}\left(K_{T}\right)_{ij+1/2}\left[\frac{T_j - T_i}{D_i + D_j}\right] \tag{20}$$

In evaluating the "flow" terms in the above Equations (13)–(16), (18), and (20), subscript ij+1/2 is used to denote a proper averaging or weighting of fluid flow, component transport, or heat-transfer properties at the interface or along the connection between two blocks or nodes i and j. The convention for the signs of flow terms is that flow from node j into node i is defined as "+" (positive) in calculating the flow terms. Wu and Pruess (2000b) present a general approach to calculating these flow terms associated with advective and dispersive mass transport and heat transfer in a multiphase system, using an irregular and unstructured, multidimensional grid.

The mass or energy sink/source in Equation (12) at node i, Q_i^k, is defined as the mass or energy exchange rate per unit volume of rock or soils. It is normally used to treat boundary conditions, such as surface infiltration, pumping, and injection through wells. Note that we present explicit, discrete expressions for estimating all the flow terms above, except for dispersive fluxes in Equation (18). This is because of the numerical difficulties

introduced in handling the hydrodynamic tensor of dispersion, which is treated very differently with different numerical approaches, such as finite difference or finite element. In most formulations for solute transport, the off-diagonal terms and contributions of the dispersion tensor are ignored, and dispersive transport is considered only along the principal directions. However, a general procedure for using the integral finite difference to incorporate a full dispersion tensor is presented by Wu and Pruess (2000b).

Note that Equation (12) presents a precise form of the balance equation for each mass component and heat in a discrete form. It states that the rate of change in mass or energy accumulation (plus decay/generation, if existing) at a node over a time step is exactly balanced by inflow/outflow of mass and energy, and also by sink/source terms, when existing for the node. As long as all flow terms have flow from node i to node j equal to and opposite to that of node j to node i for fluids, components, and heat, no mass or energy will be lost or created in the formulation during the solution. Therefore, the discretization in (12) is conservative.

4.4.2 NON-DARCY AND OTHER COMPLEX FLOW

The flow regime may be more complicated within faults or fault zones, because of (1) the high permeability of fractures and (2) large pores, such as vugs and larger-aperture fractures, in fault zones.

Non-Darcy Flow: In addition to Darcy flow, as described in Equations (5) or (13), non-Darcy flow may also occur between and among the multiple continua within fault zones. A general numerical approach for modeling non-Darcy flow (Wu, 2002) can be directly extended to the multiple-continuum model of this work for flow in fault zones. Volumetric flow rate (namely Darcy velocity for Darcy flow) for non-Darcy flow of each fluid may be described using the multiphase extension of the *Forchheimer* equation:

$$-\left(\nabla P_w - \rho_w \mathbf{g}\right) = \frac{\mu}{k}\mathbf{v}_w + \beta\rho_w \mathbf{v}_w\left|\mathbf{v}_w\right| \qquad (21)$$

β is the non-Darcy flow coefficient, intrinsic rock property, with a unit m^{-1} for water phase under flow condition.

Note that for no matter what type of flow, (i.e., Darcy flow, non-Darcy flow, or the following pipe-type flow), the discrete mass- and energy-balance equation of (12) is always valid. For the case of non-Darcy's flow, the flow term (flow_{ij}^{w}) in Equation (13) along the connection (i, j), between elements i and j, is numerically replaced by (Wu, 2002):

$$\text{flow}_{ij}^{w} = \frac{A_{ij}}{2(k\beta)_{ij+1/2}}\left\{-\frac{1}{\lambda_\beta}+\left[\left(\frac{1}{\lambda_\beta}\right)^2-\bar{\gamma}_{ij}\left(\psi_{\beta j}-\psi_{\beta i}\right)\right]^{1/2}\right\} \tag{22}$$

$$\bar{\gamma}_{ij} = \frac{4\left(k^2\rho_w\beta\right)_{ij+1/2}}{D_i + D_j} \tag{23}$$

Flow in Parallel-Wall Fracture or Tube: In general, flow along connecting paths of large-aperture fractures or vugs through narrow pores or fractures may be too fast, or openings may be too large to describe using Darcy's law. In particular, when these large-aperture fractures vuggy connections could be approximated as a single (or parallel) fracture or tube within fault zones, solutions of flow through a parallel-wall, uniform fracture or Hagen-Poiseuille tube-flow solution (Bird et al., 1960) may be extended to describe such flow in Equation (13):

$$\gamma_{ij} = \frac{wb^3}{12\left(D_i + D_j\right)} \qquad \text{for fracture-type connection} \tag{24}$$

and

$$\gamma_{ij} = \frac{\pi r^4}{8\left(D_i + D_j\right)} \qquad \text{for tube-type connection} \tag{25}$$

where b is fracture aperture, w is fracture width, and r is tube radius. Similarly, flow solutions for both laminar and turbulent flow through simple geometry of vug-vug connections can be used for flow between these vuggy connections.

4.4.3 EFFECT OF ROCK DEFORMATION

Based on the observation from experimental results (Wu et al., 2008) and previous research (Terzaghi, 1943), the effective porosity and permeability of porous and

fractured rock in an isothermal system are assumed to correlate with the mean effective stress (σ'_m), defined as:

$$\sigma'_m = \sigma_m(x, y, z, P_w) - \alpha P_w \qquad (26)$$

where σ_m is mean total stress; and α is Biot's effective parameter (Biot, 1941) and is treated as constant in space or in general estimated by

$$\sigma_m(x,y,z,P_w)=(\sigma_x(x,y,z,P)+\sigma_y(x,y,z,P)+\sigma_z(x,y,z,P_w))/3 \qquad (27)$$

where σ_x, σ_y, and σ_z are total stress in x, y, and z- directions, respectively.

With the definition of the mean effective stress of Equation (26), the effective porosity of fractures and rock matrix in fault zones is defined as a function of mean effective stress only,

$$\phi = \phi(\sigma'_m) \qquad (28)$$

Similarly, intrinsic permeability is related to the effective stress as,

$$k = k(\sigma'_m) \qquad (29)$$

To incorporate rock-deformation effects at a given site, the proposed models, derived from Equations (28) and (29), need to be determined from laboratory or field studies. The key for applicability of these models, in fault flow simulations coupled with rock deformation, is that the distribution of effective stress or total stress field must be predetermined as a function of spatial coordinates and pressure fields, as in Equations (26) and (27). In practice, the stress distribution may be estimated analytically, numerically, or from field measurements, because in reservoirs, changes in effective stress are primarily caused by changes in pressure.

When the functions of (28) and (29) are determined, then the two equations are used in flow and transport calculations. For example, Equation (28) is used in (6) and (10) for accumulation terms, while (29) is used in (13) or (22) for flow calculation to incorporate effect of rock deformation of fault flow.

4.4.4 HANDLING FRACTURE-VUG-MATRIX INTERACTION IN FAULTS

The technique used in this work for handling flow through vuggy fractured rock follows the dual- or multiple-continuum methodology (Warren and Root, 1963; Pruess and Narasimhan, 1985; Wu and Pruess, 1988). With this dual-continuum concept, equations for fluid and heat flow and mass transport discussed above can be used to describe flow along fractures and inside matrix blocks, as well as fracture-matrix-vug interaction. However, special attention needs to be paid to interporosity flow in the fracture-matrix-vug continua. Flow terms of interporosity between fracture-matrix, fracture-vug, vug-vug, and vug-matrix connections are all evaluated using Equation (13) or (22). However, the transmissivity of (15) will be evaluated differently for different types of interporosity flow. For fracture-matrix Darcy flow, γ_{ij}, is given by (Wu et al., 2006b).

$$\gamma_{FM} = \frac{A_{FM} k_M}{l_{FM}} \tag{30}$$

where A_{FM} is the total interfacial area between fractures (F) and the matrix (M) elements; k_M is the absolute matrix permeability; and l_{FM} is the characteristic distance for flow crossing fracture-matrix interfaces. For fracture-vug flow, γ_{ij} is defined as

$$\gamma_{FV} = \frac{A_{FV} k_V}{l_{FV}} \tag{31}$$

where A_{FV} is the total interfacial area between the fracture and vugs (V) elements; l_{FV} is a characteristic distance for flow between fractures and vugs; and k_V is the absolute vuggy permeability, which should be the permeability of small fractures that control flow between vugs and fractures. Note that for the domain in which vugs are isolated from fractures, no fracture-vug flow terms need to be calculated, because they are indirectly connected through the matrix.

For vug-matrix flow, γ_{ij} is evaluated as:

$$\gamma_{VM} = \frac{A_{VM} k_M}{l_{VM}} \tag{32}$$

where A_{VM} is the total interfacial area between the vug and matrix elements; and l_{VM} is a characteristic distance for flow crossing vug-matrix interfaces. Similarly, the transmissivity between vugs, when they are connected through narrow fractures or tube can be defined.

Note that Table 4-1 summarizes several simple models for estimating characteristic distances in calculating interporosity flow within fractures, vugs, and the matrix. In such cases, we have regular one-, two-, or three-dimensional large fracture networks, each with uniformly distributed small fractures connecting vugs or isolating vugs from fractures, based on the quasi-steady-state flow assumption of Warren and Root (1963).

In practical application of the proposed modeling approach, the MINC concept (Pruess, 1983; Pruess and Narasimhan, 1985) is extended to modeling flow through fractured-vuggy rock. Using this approach, we start with a primary or single-continuum medium mesh that uses bulk volume of formation and layering data. Then, geometric information for the corresponding fractures and vugs within each formation subdomain of fault zones and their surrounding rock is used to generate integrated finite-difference meshes from the primary grid. Fractures are lumped together into the fracture continuum, while vugs with or without small fractures are lumped together into the vuggy continuum. The rest is treated as the matrix continuum. Connection distances and interface areas are then calculated accordingly (e.g., using the relations discussed above and the geometric data of fractures and vugs). Once a proper mesh for a multiple-continuum system is generated, fracture, vuggy, and matrix blocks are specified, separately, to represent fracture or matrix continua.

Table 4-1. Characteristic distances* for evaluating flow terms between fractures, vugs, and matrix systems

Fracture Sets	Dimensions of Matrix Blocks (m)	Characteristic F-M Distances (m)	Characteristic F-V Distances (m)	Characteristic V-M Distances [1] (m)	Characteristic V-M Distances [2] (m)
1-D	A	$l_{FM} = A/6$	$l_{FV} = l_x$	$l_{VM} = a/6$	$l_{VM} = (A - d_c)/2$
2-D	A, B	$l_{FM} = AB/4(A+B)$	$l_{FV} = \frac{l_x + l_y}{2}$	$l_{VM} = ab/4(a+b)$	$l_{VM} = \frac{A+B-2d_c}{4}$
3-D	A, B, C	$l_{FM} = 3ABC/10/(AB+BC+CA)$	$l_{Ff} = \frac{l_x + l_y + l_z}{3}$	$l_{VM} = 3abc/10/(ab+bc+ca)$	$l_{Ff} = \frac{A+B+C-3d_c}{6}$

* Note in Table 4-1, A, B, and C are dimensions of matrix blocks along x, y, and z directions, respectively.

[1] Characteristic V-M distances are estimated for the case that vuggy-matrix connections are dominated by small fractures, where dimensions a, b, and c are fracture-spacings of small fractures along x, y, and z directions, respectively.

[2] Characteristic V-M distances are used for the case that vugs are isolated from fractures.

In addition to discretization techniques discussed above, the following assumption may be also used: there is equilibrium within vugs, i, e., no flow calculations are needed within vugs.

4.5 Numerical Solution Scheme

A number of numerical solution techniques have been developed in the literature over the past few decades to solve the nonlinear, discrete equations of reservoir simulations. When handling coupled flow, transport, and heat transfer in a subsurface system, the predominant approach is to use a fully implicit scheme. This scheme is best because of the extremely high nonlinearity inherent in those discrete equations, and the many numerical schemes with different levels of explicitness that fail to converge in practice. In this section, we discuss a general procedure to solve the discrete nonlinear Equation (12) fully implicitly, using a Newton iteration method.

Let us write the discrete nonlinear Equation (12) in a residual form as:

$$R_i^{k,n+1} = \left\{M_i^{k,n+1} + G_i^{k,n+1} - M_i^{k,n}\right\}\frac{V_i}{\Delta t} - \sum_{j\in\eta_i} flow_{ij}^{k,n+1} - Q_i^{k,n+1} = 0 \qquad (33)$$

$$k = 1, 2, 3, \ldots, N_c+1;\ \ i = 1, 2, 3, \ldots, N).$$

Equation (33) defines a set of $(N_c+1) \times N$ coupled nonlinear equations that need to be solved for every balance equation of mass components and heat, respectively. In

general, (N_c+1) primary variables per node are needed to use the Newton iteration for the associated (N_c+1) equations per node. The primary variables are usually selected among fluid pressures, mass (mole) fractions of components in fluids, and temperatures. The rest of the dependent variables—such as viscosity and densities, partitioning coefficients, specific enthalpies, thermal conductivities, dispersion tensor, and nonselected pressures and mass (mole) fractions—are treated as secondary variables, which are calculated from selected primary variables.

In terms of the primary variables, the residual equation, Equation (22), at a node i is regarded as a function of the primary variables at not only node i, but also at all its direct neighboring nodes j. The Newton iteration scheme gives rise to

$$\sum_m \frac{\partial R_i^{k,\,n+1}\left(x_{m,p}\right)}{\partial x_m}\left(\delta x_{m,p+1}\right) = -R_i^{k,n+1}\left(x_{m,p}\right) \qquad (34)$$

where x_m is the primary variable m with m = 1, 2, 3, …, N_c+1, respectively, at node i and all its direct neighbors; p is the iteration level; and i =1, 2, 3, …, N. The primary variables in Equation (34) need to be updated after each iteration:

$$x_{m,p+1} = x_{m,p} + \delta x_{m,p+1} \qquad (35)$$

The Newton iteration process continues until the residuals $R_n^{k,n+1}$ or changes in the primary variables $\delta x_{m,p+1}$ over an iteration are reduced below preset convergence tolerances.

Numerical methods are generally used to construct the Jacobian matrix for Equation (34), as outlined in Forsyth et al. (1995). At each Newton iteration, Equation (34) represents a system of (N_c+1) × N linearized algebraic equations with sparse matrices, which are solved by a linear equation solver.

4.6 Treatment of Initial and Boundary Conditions

A set of initial conditions is required to start a transient simulation, i.e., a complete set of primary variables need to be specified for every gridblock or node. A commonly used procedure for specifying initial conditions is the restart option, in which

a complete set of initial conditions or primary unknowns is generated in a previous simulation, with proper boundary conditions described.

When using a block-centered grid, first-type or Dirichlet boundary conditions can be effectively treated with the "inactive cell" or "big-volume" method, as normally used in the TOUGH2 code (Pruess et al., 1999). In this method, a constant pressure/concentration/temperature node is specified with an inactive cell or with a huge volume, while keeping all the other geometric properties of the mesh unchanged.

With finite-element or edge-centered finite-difference grids, first-type boundary conditions and Neuman boundary conditions can be treated using a generalized, sink/source term approach (Wu et al., 1996). Certain flux-type boundary conditions are easy to handle for a situation in which flux distribution along the boundary is known, such as in dealing with surface infiltration. However, a description of more general types of flux or mixed boundaries, such as seepage faces and multilayered wells, is part of the solution, and general procedures for handling such boundary conditions are discussed in Wu et al. (1996).

4.7 Simulation Example

In this section, we demonstrate the application of the mathematic model discussed above. The reservoir simulator used is the modified TOUGH2 code-EOS3 module, incorporating density-dependent variation in the water pressure or head. In modeling, we use the modified TOUGH2-EOS3 to simulate nonisothermal flow of single-phase water with density dependence on mineral compositions, in addition to pressure and temperature in the two wells, HDB-7 and HDB-8. The two wells are located close to each other, but are possibly separated by a fault (Figure 4-4).

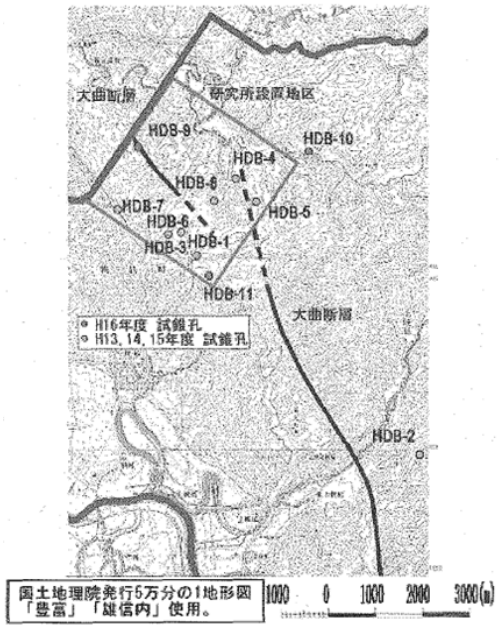

Figure 4-4 HDB boreholes at the Horonobe URL site (Yabuuchi et al., 2006)

The basic assumption in the modeling exercise is that the system is in steady-state condition for water flow, solute transport, and heat flow. In particular, the aqueous mineral-concentration distribution is assumed at steady state as a function of elevation or depth only for each well. Therefore, the water density is correlated to mineral compositions by extrapolating and interpolating the measured mineral compositional data from the two wells, in addition to its dependence on pressure and temperature.

The two wells are represented using two 1-D column grids of 600 m with uniform column grid of 5 m grid spacing, starting from zero depth at ground surface, using a single-continuum, multilayered modeling approach. The geologic units/layers associated with the two 1-D models are shown in Table 4-2 and **Error! Reference source not found.**, respectively, for Well HDB-7 and HDB-8. For Well HDB-7, the 1-D model grid starts from zero depth at ground surface (elevation of 43.752 m) down to 600 m in depth—the geologic unit (Table 4-2) associated from 0 to 400 m is the Yuuch F, and from 400 m down, it is the Koetoi unit. For Well HDB-8, the 1-D model covers from the surface, at elevation of 70.051 m, down to a 600 m depth, with the top layer of 140 m

belonging to the Koetoi unit and the unit below belonging to the Wakkanai F. (**Error! Reference source not found.**).

Table 4-2. Geologic units/layers and measured temperature and pressure data for Well HDB-7

Geologic Units/Layers	Depth (m)	Thickness (m)	Temperature (^{o}C)	Pressure (KPa)
Yuuchi F.	45.35	97.71	8.55	549.27
Yuuchi F.	143.06	48.74	12.2	1600.14
Yuuchi F.	191.80	15.26	14.11	2099.64
Yuuchi F.	207.06	15.04	14.62	2259.53
Yuuchi F.	222.09	10.76	15.13	2414.1
Yuuchi F.	232.86	98.02	15.55	2529.13
Yuuchi F.	330.88	25.77	19.53	3522.07
Yuuchi F. /Koetoi F.	356.64	91.53	20.56	3790.36
Koetoi F.	448.17	75.33	24.51	4709.45

Table 4-3 Geologic units/layers and measured temperature and pressure data for Well HDB-8

Geologic Units/Layers	Depth (m)	Thickness (m)	Temperature (^{o}C)	Pressure (KPa)
Koetoi F.	65.48	31.74	31.74	680.89
Koetoi F.	97.22	10.75	10.75	996.56
Koetoi F. / Wakkanai F.	107.97	69.01	69.01	1103.02
Wakkanai F.	176.98	29.75	29.75	1784.73
Wakkanai F.	206.73	73.74	73.74	2077.55
Wakkanai F.	280.43	10.72	10.72	2734.68
Wakkanai F.	291.15	100.48	100.48	2938.81
Wakkanai F.	391.64	49.5	49.5	3944.4
Wakkanai F.	441.13	32.33	32.33	4433.35

Table 4-4 lists the measured total mineral concentrations of the liquid water and depth data, as well as calculated density factors used in the simulation to modify liquid densities. The porosity and permeability data for the well models are listed in Table 4-5. Note that permeability values in Table 4-5 are converted using a constant liquid density of 1000.1 (kg/m^3) and a constant viscosity of 0.0011 (Pa•s).

A series of simulations for the two 1-D models are conducted as follows:

1. Simulations using hydrostatic conditions (i.e., no vertical flow conditions) are first carried out for determining top and bottom boundary conditions, in terms of pressures and temperatures, by matching the measured temperature and pressure data of Table 4-2 and Table 4-3. The results of the steady-state simulations are then used as base models for flow-scenario analysis.
2. Water is injected from the top or bottom boundaries of the two well models, with different injection rates. This is to estimate downward flow or upward flow conditions, while keeping constant temperature data on both top and bottom boundaries.

Table 4-4 Measured total mineral concentrations and calculated density factors used for modifying water density as a function of total concentrations at depth

Well	Depth (m)	Total concentration (ppm)	Density factor
HDB-7	41.61	4,698	1.003
HDB-7	131.13	9,928	1.008
HDB-7	320.52	29,107	1.027
HDB-7	343.42	31,572	1.030
HDB-7	398.90	28,850	1.027
HDB-7	442.20	31,094	1.029
HDB-7	496.25	28,440	1.026
HDB-7	506.64	29,230	1.027
		-	
HDB-8	63.15	3,255	1.001
HDB-8	101.87	4,204	1.002
HDB-8	283.82	11,469	1.009
HDB-8	344.45	12,395	1.010
HDB-8	400.79	12,014	1.010
HDB-8	449.14	13,066	1.011
HDB-8	465.34	15,175	1.013

Table 4-5 Permeability and porosity values for different geologic units/layers

Geologic Unit	Hydraulic conductivity (m/sec)	Permeability (m^2)	Porosity
Quaternery Sediments	1.00E-06	1.10E-13	0.55
Yuuchi F.	5.70E-10	6.27E-17	0.55
Koetoi F.	3.59E-09	3.95E-16	0.55
Wakkanai F.	1.36E-08	1.50E-15	0.45
Masuhoro F.	5.00E-10	5.50E-17	0.4
Cretaceous rock	1.00E-11	1.10E-18	0.4
Fault	1.00E-10	1.10E-17	0.55

In the literature (e.g., Wu et al., 2004; 2007a), geothermal gradients or temperature profiles are very sensitive to and thus useful in estimating water percolation fluxes in the subsurface. Here, we use the measured temperature data to estimate both flow rate and flow directions at the two wells. Figure 4-5 through Figure 4-7 show comparisons between simulated temperature/pressures and measurements for Well HDB-

7. Figure 4-5 shows that at Well HDB-7, if we inject water from the bottom, i.e., water flows up, the simulated temperature data cannot match the measured values. However, if we inject water from the top, Figure 4-6 indicates the measured temperature could be fitted well at a flow rate of 3 mm/yr. Figure 4-7 presents pressure profiles simulated with water injection at the top and indicates that the lower injection rates match measured pressure better. The difference between simulated and measured results in Figure 4-7 results primarily from the 1-D flow assumption in the model, while under field conditions, downwards flow will be subjected to multidimensional flow, find least flow resistance paths, and the top pressure would be lower.

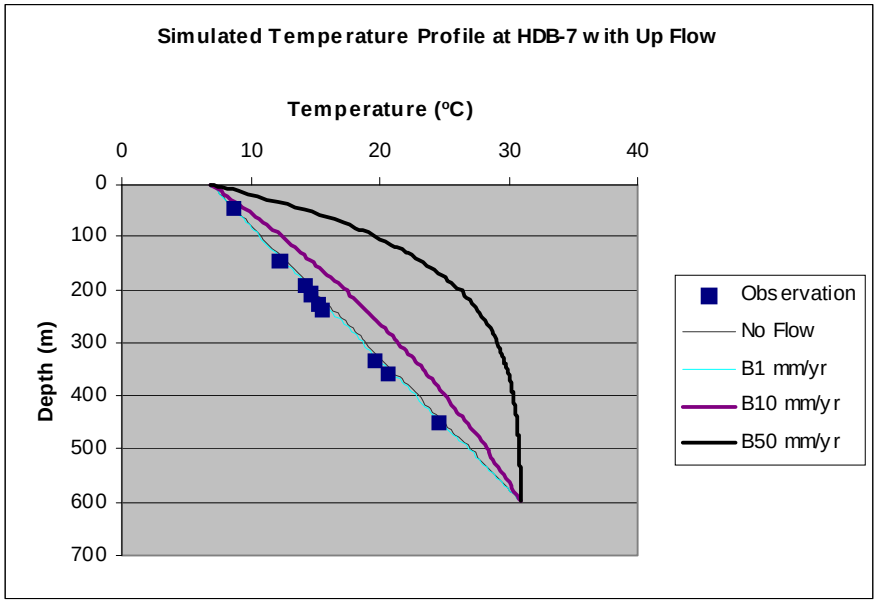

Figure 4-5 Comparison of simulated and measured temperatures at Well HDB-7 with water injected at bottom boundary at a rate of 0, 1 mm/yr, 10 mm/yr, and 50 mm/yr.

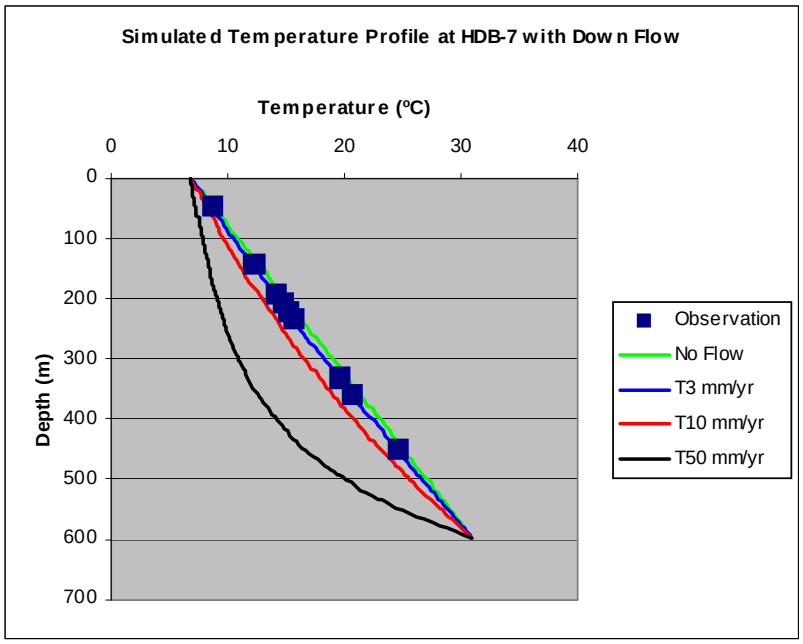

Figure 4-6 Comparison of simulated and measured temperatures at Well HDB-7 with water injected at top boundary at a rate of 0, 3 mm/yr, 10 mm/yr, and 50 mm/yr.

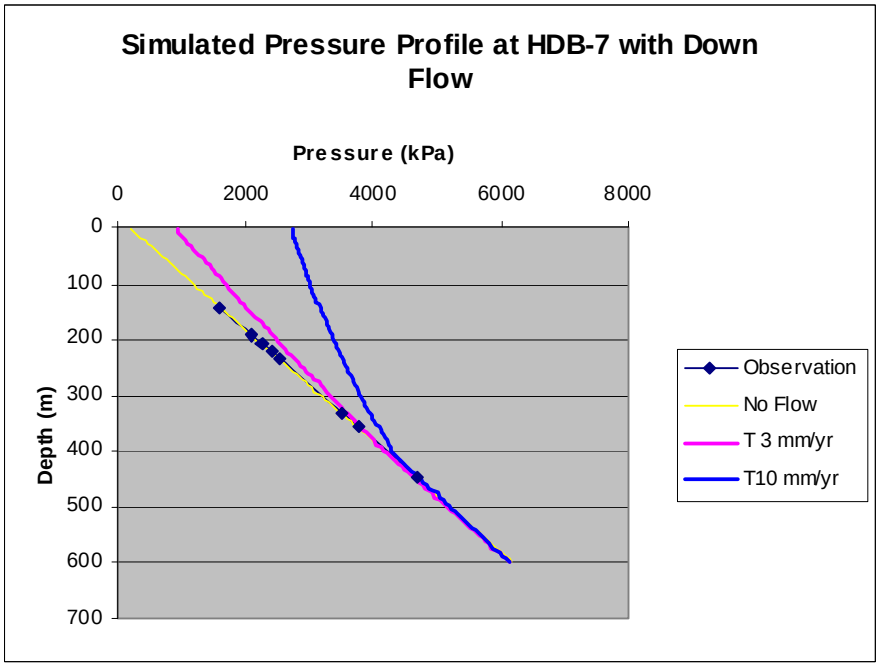

Figure 4-7 Comparison of simulated and measured pressures at Well HDB-7 with water injected at top boundary at a rate of 0, 3 mm/yr, and 10 mm/yr.

Figure 4-8 through Figure 4-10 show the results for Well HDB-8. For this well, Figure 4-8 shows that the best estimated flow rate is at about 6 mm/yr, injected from the bottom boundary. This means upward flow at this location. If injected from the top, Figure 4-9 shows that simulated results cannot match the measured temperature profiles at all. Figure 4-10 shows the results and comparisons of pressures for upward flow, indicating a good agreement for a flow rate of 6 mm/yr.

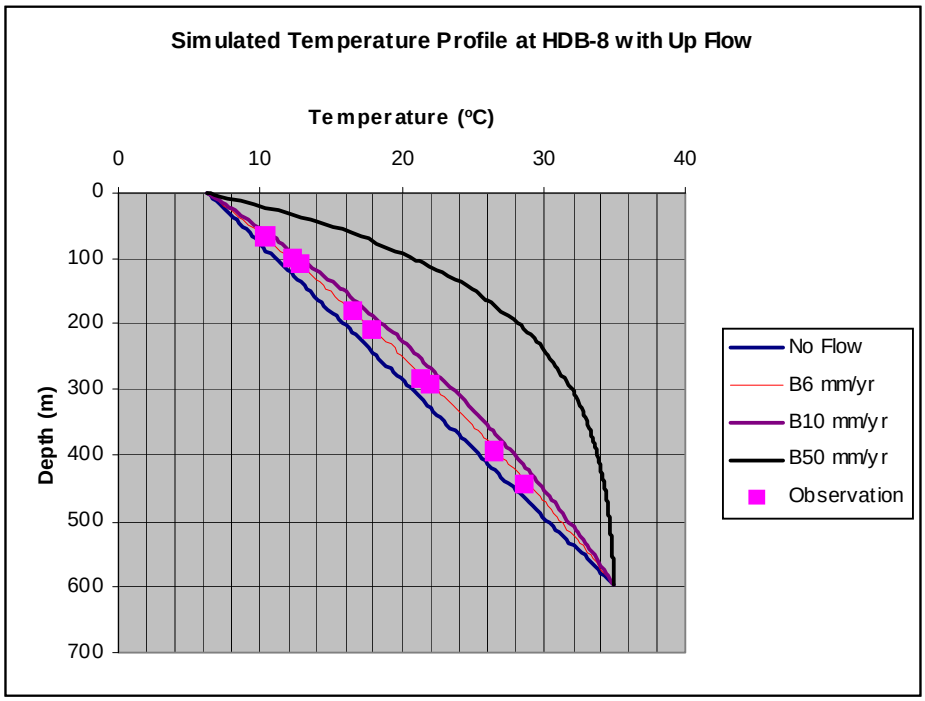

Figure 4-8 Comparison of simulated and measured temperatures at Well HDB-8 with water injected at bottom boundary at a rate of 0, 6 mm/yr, 10 mm/yr, and 50 mm/yr.

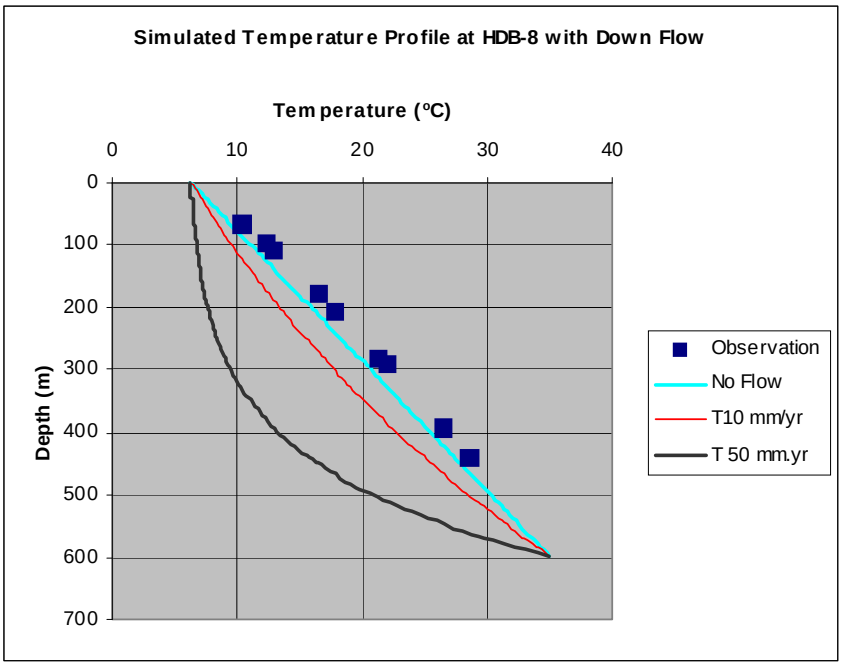

Figure 4-9 Comparison of simulated and measured temperatures at Well HDB-8 with water injected at top boundary at a rate of 0, 10 mm/yr, and 50 mm/yr.

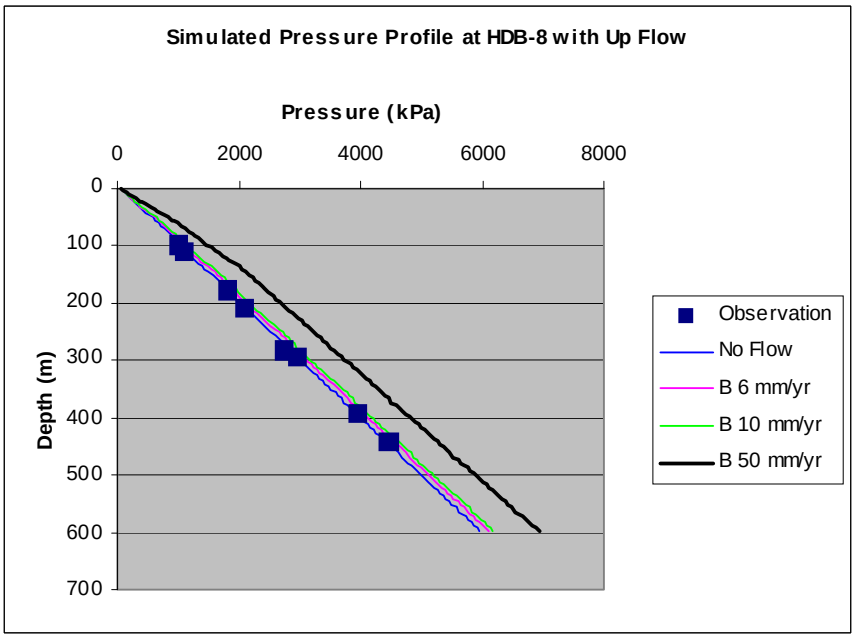

Figure 4-10 Comparison of simulated and measured pressures at Well HDB-8 with water injected at bottom boundary at a rate of 0, 6 mm/yr, 10 mm/yr, and 50 mm/yr.

Note that the two wells, HDB-7 and HDB-8, are close to each other, with HDB 8 further inland. A comparison between simulation results and the measurements of temperature and pressures, discussed above, indicates different flow directions, i.e., flow at HDB-8 is upwards (discharge) and flow at HDB-7 is downwards (recharge). This indicates that there likely exists a fault separating the two wells, and the fault behaves as a closed boundary or low-permeability barrier to flow between the two wells.

4.8 Summary

A physically based conceptual and numerical model is presented for simulating fluid and heat flow and solute transport through fractured fault zones using a multiple-continuum medium approach. The suggested multiple-continuum concept is a natural extension of the classic double-porosity model, with the fracture continuum responsible for conducting global flow, while vuggy (if any) and matrix continua, locally connected and interacting with globally connecting fractures, provide storage space for fluid and solute.

The proposed conceptual model can be implemented into a general multidimensional numerical reservoir simulator TOUGH2 using a control-volume, finite-difference approach, which can be used to simulate single-phase flow, solute transport, and heat transfer in 1-D, 2-D, and 3-D fractured reservoirs. Model application is demonstrated by modeling two well-flow problems at ambient geothermal and water flow conditions. Data from the Horonobe URL site were analyzed to demonstrate the proposed approach and to examine the flow direction and magnitude on both sides of a suspected fault.

4.9 Recommendations for Future Work

We recommend the following future work as a natural extension of the present study.

1. Develop a general-purpose reservoir simulator for single-phase water flow, density-dependent solute transport, and heat transfer, based on the TOUGH2 code.
2. Investigate flow characteristics in typical fault zones with fractured vuggy rock.
3. Incorporate the effects of rock deformation on flow calculation.

4. Perform site-specific characterization modeling studies.

4.10 References

Aziz, K. and A. Settari, *Petroleum Reservoir Simulation*, Applied Science Publishers LTD, London, 1979.

Barenblatt, G. I., Zheltov, I. P., and Kochina, I. N., Basic concepts in the theory of seepage of homogeneous liquids in fissured rocks, PMM, *Sov. Appl. Math. Mech.,* 24(5), 852–864, 1960.

Biot, M. A., General theory of three dimensional consolidation, *J. Appl Phys.*, 12:57-64, 1941.

Bird, R. B., W. E. Steward, E. N. Lightfoot. Transport Phenomena, John Willey & Sons, Inc., New York, London, Sydney, 1960.

Camacho-Velazquez, R., M. Vasquez-Cruz, R. Castrejon-Aivar, and V. Arana-Ortiz, Pressure transient and decline-curve behavior in naturally fractured vuggy carbonate reservoirs, *SPE Reservoir Evaluation & Engineering,* 95-111, April, 2005.

Closemann, P.J., The aquifer model for fissured fractured reservoir, *Soc. Pet. Eng. J.*, 385–398, 1975.

Forsyth, P. A., Y. S. Wu and K. Pruess, Robust numerical methods for saturated-unsaturated flow with dry initial conditions in heterogeneous media, *Advance in Water Resources,* 18, 25-38, 1995.

Forsyth, P. A., Three-dimensional modeling of steam flush for DNAPL site remediation, *International Journal for Numerical Methods in Fluids, Vol.* 19, 1055-1081, 1994.

Huyakorn, P. S., S. Panday and Y. S. Wu, "A three-dimensional multiphase flow model for assessing NAPL contamination in porous and fractured media, I. Formulation," *Journal of Contaminant Hydrology*, Vol. 16, 109-130, 1994.

Kang, Zhijiang, Yu-Shu Wu, Jianglong Li, Yongchao Wu, Jie Zhang, and Guangfu Wang, Modeling multiphase flow in naturally fractured vuggy petroleum reservoirs, PSE-1-2356, Presented at the 2006 SPE Annual Technical Conference and Exhibition, San Antonio, Texas, 24-27 September, 2006.

Kazemi, H., Pressure Transient Analysis of Naturally Fractured Reservoirs with Uniform Fracture Distribution. *SPEJ,* 451–462. Trans., AIME, 246, 1969.

Liu, J. C. G. S. Bodvarsson, and Y. S. Wu, Analysis of pressure behavior in fractured lithophysal reservoirs, *Journal of Contaminant Hydrology*, 62-62, 189-211, 2003

Narasimhan, T. N. and P. A. Witherspoon, An Integrated Finite difference method for analyzing fluid flow in porous media, *Water Resources Research, 12(1)*, 57-64, 1976.

Pruess K., Oldenburg, C., and Moridis, G., TOUGH2 User's Guide, Version 2.0, Report LBNL-43134, Berkeley, California: Lawrence Berkeley National Laboratory, 1999.

Pruess, K. and Narasimhan, T. N., A practical method for modeling fluid and heat flow in fractured porous media, *Soc. Pet. Eng. J.,* 25, 14-26, 1985.

Pruess, K., GMINC-A mesh generator for flow simulations in fractured reservoirs, Report LBL-15227, Berkeley, California: Lawrence Berkeley National Laboratory, 1983.

Scheidegger, A. E., General theory of dispersion in porous media, *J. Geophys. Res.,* Vol. 66, 3273-3278, 1961.

Snow, D. T., A parallel plate model of fractured permeable media, Ph.D. Dissertation, University of California, Berkeley, Californian, 1965.

Terzaghi, K., *Theoretical Soil Mechanics*, John Wiley & Sons Inc., New York, 1943.

Warren, J. E. and Root, P. J., The behavior of naturally fractured reservoirs, *Soc. Pet. Eng. J.,* 245–255, Trans., AIME, 228, 1963.

Wu, Y. S., J. Rutqvist, K. Karasaki, Q. Lei, W. Xiong, J. Yuan, J., and M. Liu, A mathematical model for rock deformation's effects on flow in porous and fractured reservoirs, prepared for presentation at San Francisco 2008, the 42nd US Rock Mechanics Symposium and 2nd U.S.-Canada Rock Mechanics Symposium, held in San Francisco, June 29-July 2, 2008.

Wu, Yu-Shu, Guoping Lu, Keni Zhang, L. Pan, and G. S. Bodvarsson, "Analyzing Unsaturated Flow Patterns in Fractured Rock Using an Integrated Modeling Approach," LBNL-54006, *Hydrogeology Journal*, Vol. 15, pp.553-572, 2007a.

Wu, Yu-Shu, Christine Ehlig-Economides, Guan Qin, Zhijiang Kang, Wangming Zhang Babatunde Ajayi, and Qingfeng Tao, "A Triple Continuum Pressure Transient Model for A Naturally Fractured Vuggy Reservoir," SPE-110044, presented at the 2007 SPE

Annual Technical Conference and Exhibition held in Anaheim, California, 11–14 November 2007b.

Wu, Yu-Shu, S. Mukhopadhyay , K. Zhang, and G. S. Bodvarsson, "A Mountain-Scale Thermal-Hydrologic Model for Simulating Fluid Flow and Heat Transfer in Unsaturated Fractured Rock," LBNL-57921, *Journal of Contaminant Hydrology,* Vol. 86, pp.128-159, 2006a.

Wu, Y. S., G. Qin, Richard E. Ewing, Yalchin Efendiev, Zhijiang Kang and Yulin Ren, "A Multiple-Continuum Approach for Modeling Multiphase Flow in Naturally Fractured Vuggy Petroleum Reservoirs," SPE-104173, Presented at the 2006 SPE International Oil & Gas Conference and Exhibition, Beijing, China, 5–7 December, 2006b.

Wu, Y. S., G. Lu, K. Zhang, and G. S. Bodvarsson, "A Mountain-Scale Model for Characterizing Unsaturated flow and Transport in Fractured Tuffs of Yucca Mountain," LBNL-52524, *Vadose Zone Journal*, Vol. 3, pp.796-805, 2004.

Wu, Y. S., H. H. Liu, And G. S. Bodvarsson, A triple-continuum approach for modeling flow and transport processes in fractured rock, *Journal Of Contaminant Hydrology*, 73, 145-179, 2004a.

Wu, Y. S., A unified numerical framework model for simulating flow, transport, and heat transfer in porous and fractured media, *Developments In Water Science,* Edited By Cass T. Miller, Matthew W. Farthing, William G. Gray, And George F. Pinder, Elsevier, 2004b.

Wu, Y. S., Numerical simulation of single-phase and multiphase non-Darcy flow in porous and fractured reservoirs, *Transport In Porous Media*, Vol. 49, No. 2, pp.209-240, 2002.

Wu, Y. S., On the effective continuum method for modeling multiphase flow, multicomponent transport and heat transfer in fractured rock, Book chapter in *Dynamics of Fluids in Fractured Rocks, Concepts and Recent Advances*, edited by B. Faybishenko, P. A. Witherspoon and S. M. Benson, AGU Geophysical Monograph 122, American Geophysical Union, Washington, DC, 299–312, 2000a.

Wu, Y. S. and K. Pruess, Numerical simulation of non-isothermal multiphase tracer transport in heterogeneous fractured porous media, *Advance in Water Resources*, 23, 699-723, 2000b.

Wu, Y. S., A virtual node method for handling wellbore boundary conditions in modeling multiphase flow in porous and fractured media, *Water Resources Research*, 36 (3), 807-814, 2000b

Wu, Y. S., P. A. Forsyth and H. Jiang, A consistent approach for applying numerical boundary conditions for subsurface flow, *Journal of Contaminant Hydrology*, Vol. 23, 157-185, 1996.

Wu, Y. S. and Pruess K., A multiple-porosity method for simulation of naturally fractured petroleum reservoirs, *SPE Reservoir Engineering*, 3, 327-336, 1988.

5　概要調査地域に於ける断層の調査法に関して

5.1　調査のストラテジー

概要調査においておそらく最も重要な調査対象の１つは断層である。断層は周辺の水理場を支配すると言っても過言ではない。従って、処分場の長期性能評価や安全性から鑑みると断層の水理性状を正確に把握する必要がある。処分場予定地の近くに大きな活断層が存在すれば、場合によっては不適格要因にもなり得る。さらに、対象とする地層に断層を避けて処分場のパネルが余裕を持って配置できるだけのボリュームが存在する事を概要調査の早い段階で確認する必要がある。これらの事から、概要調査段階において断層の性状の特定は最優先課題と言える。本章では断層の地質および水理性状の調査を正確に効率良く行う為の調査ステップについて述べる。

断層は物性に関して大きな不連続面を形成する。母岩と比較して力学的、地質学的な物性の違いもさることながら、水理学的な物性の対比が極端に大きい場合が多々ある。断層は一般にコア部とそれに付随したダメージゾーンに分けられるが、コア部の厚さやダメージゾーンのダメージの度合いとヒーリング、再活動の歴史によって全体の水理学的特性が異なる。

断層に関する情報としては、位置、幅、走行、傾斜などの幾何学的データを始め、タイプ、過去に動いた年代、ずれ幅、岩相や地質等の情報がある。これらの情報はボアホールを掘削する前にリモートセンシング、地表地質調査や物理探査手法を使ってある程度収集が可能である。また、第 2 章と第 3 章に述べたように、これらの情報と断層の水理性状に相関性が見られた事例があったり、文献によっては相関付ける手法を提示している。断層が数多く存在する場合、すべての断層を侵襲的に調査するには莫大な費用が掛かるばかりでなく、ボアホールが流れの場を乱したり、将来の早い水みちになる可能性がある。専門家によって意見の分かれるところではあるが、断層の長さ、ずれ幅、ダメージゾーンおよびコア部の幅の相互の線形的相似スケール則を使うのも有用である。従って、概要調査では主要と考えられる断層は直接水理試験を行う必要があるが、その他の断層に関しては、地質情報などの断層パラメーターと水理性状の相関性を仮定して予め水理性状の予測を行えば、ボアホールを使った効率的な水理試験の計画策定の手掛

かりとなる。しかしながら、主要断層の水理性状の正確な把握には直接的な水理試験は欠かせない。

次のセクションでは概要調査段階における断層の調査ステップについて述べる。

5.2 断層調査のステップ

5.2.1 文献調査

対象とする地域において断層に関する既存の文献調査を行う。断層の位置、性状、地質、さらに水理、地化学特性に関する記述があればデータを抽出しデータベースに加える。この時点で地質情報、形状データなどの情報があれば断層の概念モデルの構築を開始する。ダメージゾーンの大きさ、偏り、地質等の断層に関するパラメーターから大まかな水理性状を予測しておくことが望ましい。

我が国では如何なる概要調査地区であっても複数の断層が存在すると予期されるが、概要調査段階ですべての断層の性状を把握する必要は無い。大まかな地下水の流動方向が予測可能であれば、最優先的に調査すべき断層は候補地点から下流側の大きな断層であると考える。

5.2.2 衛星、空中測量によるリニアメントの抽出

衛星写真や空中写真を使ってリニアメントを抽出する。重力データに関しては、近年 GRACE と呼ばれる 2 個の衛星を使って重力のシグナルの差を読み取る事によって従来の精度より 1 オーダー高い精度の重力データを得ることが可能になった。対象とする地域をカバーするデータが入手可能であれば、前もって衛星による重力データ解析を行う事を勧める。加えて、セクション 3.3 で述べた ALSM (Airborne Laser Swath Mapping) 又は LIDAR(Light Detection and Ranging)と呼ばれるレーザー測量技術を使った空中測量を行って正確な地表面のデジタルマップからリニアメントを判読する事を強く勧める。LIDAR は近年米国で断層のトレースの発見に極めて有効であるとされる技術である。我が国においても断層の痕跡を確認した成功例がある。LIDAR は空中磁気や重力、電磁波などの測量と同時に行える可能性もある。

5.2.3 地上物理探査

リモートセンシングや空中探査で発見されない断層及び地質構造を特定する目的で 3 次元の地震波探査を行うことを提言する。3 次元の地震探査は非侵襲的に地下の内部構造を 3 次元的に推定できる唯一の手法である。一般に地震探査は結晶質岩より堆積岩の方がより良い成果が得られているが、対象とする地層がどの岩種であっても、3 次元の震探を行うべきである。3 次元の震探データから断層を避けながら必要な大きさの処分場パネルが建設できる十分な余裕のボリュームが対象深度の地層に存在するかどうかの手掛かりが得られるはずである。3 次元地震波探査に加えて、AMT（Audio frequency Magneto Telluric）法や SP（Self Potential）等の地表物理探査を行う。AMT は主として地層の空隙率に対比がある際に有効で、SP 法は水の流動を捉える。従って、断層そのものあるいは断層と母岩の空隙率に変化がなく、地下水の流れが極めて遅い場合はどちらの手法を使っても断層を特定できない可能性がある。しかし、AMT や SP で検知できない断層は水理的にはさほど重要でないと言える。

5.2.4 地表地質調査とトレンチング

上記と平行して、あるいは上記の結果から、断層が存在すると考えられる地点での地表地質調査を行う。地質分布や断層の位置、性状などの推定を行う。既存の文献、あるいはリニアメントの調査から主要と思われる断層が地表、あるいは地表近くに存在すれば断層と直交する方向にトレンチを掘り、断層の内部構造を把握する。

断層が普遍的に存在する日本列島の地質環境を鑑みれば、重要な課題の 1 つは、対象とする断層が活断層であるか、あるいは長期に渡って不活断層であるかを見極める事である。地表踏査ならびにトレンチングによって断層周辺の岩質を調査し、最近では何年前に動いたのかを調べる事によって鉱脈や変成などの岩-水の相互作用の程度が推定できる。次に現在の応力場を知る事によって地殻の変形および構造レジームに関する知見が得られる。

種々の地質パラメータや断層形状を計測し、第 2 章で触れたスケール則が当てはまるか検討する。また、断層部のみならず、オーバーステップの地質性状の調査を行う。

5.2.5 ボアホールによる調査

地質調査や物理探査から得られた情報を元にボアホールを掘削する適切な位置を決定する。概要調査段階では断層性状の把握の目的のみの為に本数の限られるボアホールを掘削するのは一考の余地があると考えられがちである。しかしながら、我が国でのこれまでの事例から考えると、（1）結晶岩においては、1 千メートル級のボアホールを掘削すれば大小なりとも必ず断層を貫通する。（2）岩種に拘らず、断層は周辺の水理場を大きく支配する。以上の事から、敢えて断層を避けて掘削する必要は無いし、おそらく避ける事は困難であろう。しかし、幌延の大曲断層の事例のように、断層のダメージゾーンにおいて、場所によっては高い透水性があると考えられ、母岩そのものの透水性が低い場合は、断層を狙ってボーリング孔を打たなければ、大きなスケールでの主要な水理の特性が解明できない恐れがある。如何に少ない数（1~2 本）のボアホールで如何なる試験を行い、如何なる解析手法を用いて最も効率的で正確に断層の水理性状を把握するかが当面の課題でなる。

リニアメント、物理探査、地表地質調査から複数の断層が存在すると推定される場合は、処分場の位置より下流側に存在する断層の中で最も主要と考えられる断層を特定し、その断層を貫通、もしくは上流側のダメージゾーン内にボアホールを掘削するのが最も効率的である。断層周辺の詳しい水理場の特定の為には断層の両側に複数の観測点が必要となる。概要調査段階で掘削するボーリング孔の数を最小限に抑える為には、JAEA の正馬様用地の MIU-2 孔のように断層を貫いて掘削するのが望ましい。断層がほぼ垂直であれば、傾斜掘りも考慮に入れるべきであるが、傾斜掘りはコスト嵩むうえに、モニタリング機器の設置においても垂直孔よりは課題が多い。

次に決定しなければならない問題は全孔コアボーリングをするか否かである。諸外国の処分プログラムに於いてはコアボーリングが日常的に行われているが、我が国の概要調査段階に限って言えばコストパフォーマンスは低い。従って、予算が極めて限られていれば部分的なコアの採取で良いと考える。ただし、その候補地が精査段階に進む可能性が高ければ、全孔コアを採取する価値がある。無論、掘削速度、逸水などの掘削ログや堀屑のサンプリングは当然行うべきである。また、既に常套になっているが、掘削水に SF6 等のトレーサーを混ぜ入れる事を勧める。断層を貫通して掘削する場合、可能であれば断層を貫通した時点で新たなトレーサーの混入が望ましい。

掘削が完了次第、あるいは必要であれば掘削の段階ごとに検層を行う。スタンダードなワイヤーライン検層に加えて、比較的透水係数の低い孔では、孔内水を脱イオン水で置換して測定を行う安価な FEC(Fluid Electric Conductivity) ログを勧める。この手法を使えばボアホールに沿って流入点の特定および、それらの相対的な透水係数の推定が可能である。掘削前や掘削中に断層の位置が特定できない場合は掘削後にボアホール内の物理探査（VSP、リバース VSP 等）を行った事例もあるが、概要調査段階では基本的には不要と考える。

断層の水理性状の推定に最も確度の高い方法は長期揚水試験、続いて長期圧力回復試験を行うことである。その際、表層の堆積層や多区間で揚水試験を行う必要は無い。基本的には基盤岩全体を 1 区間で揚水試験を行ってもよいが、ボーリング孔が断層を貫いている場合は、断層の上側と下側をパッカーで区切って、それぞれ揚水試験を行う。揚水をしていない区間は圧力のモニタリングを行う。その際ボアホールが水の短絡路にならないようにコア部にパッカーを設置する必要がある。東濃地域の月吉断層の例では上盤と下盤でおよそ 40m の水頭差が存在しているが、MIU-2 孔のパッカーを除去した際に水頭の高い下盤側から上盤側に大量の水が流れ込んだ経緯があった。同様に、逸水箇所等、透水性の高い部分が明確な場合はその区間をパッカーで隔離し揚水し、上下の区間でモニタリングを行う。

概要調査段階での揚水試験は基本的には単一孔試験であるが、他にボアホールが存在すれば、モニタリングを行う。この場合も、多区間に区切る必要は無く、断層があればそれらを区切るだけで良い。その理由は、概要調査の目的は大きなスケールでの断層の役割と断層の水理パラメーターを把握する事であり、小さなスケールの不均質性の調査は不要だからである。

揚水試験の際、地下水中の地化学成分を同定する為に揚水した地下水のサンプリングを行う。掘削水に混ぜたトレーサーの検出、イオン濃度（Na, Cl, HCO_3 等）、希ガス、同位体、溶存有機物、その他の成分の分析を行う。これらのデータを元に地下水の起源や年代が推定できれば周辺の地下水流動場の評価につながる。

断層に関わる長期揚水試験において課題となるのは、圧力遷移データの解析の手法である。断層はコア部やダメージ部は平面的な広がりを持つが、基本的に 3 次元構造であ

り、堆積岩では層序に垂直もしくは大きい傾斜角で交わり、水や石油資源の分野で使用されている水平放射状流を前提とした井戸試験の解析手法がそのまま当てはまらない恐れがある。新たな解析手法や数値モデルを使って逆解析を行う必要がある。

5.2.6 長期モニタリング

セクション 3.1 及び 4.7 の事例に見られるようにボアホール沿いの水頭分布や温度分布を測定することによって地下水の流れの方向や流量が推定できる可能性がある。しかし、掘削直後の水頭や温度分布は掘削によって場が乱されている恐れがあることから、掘削後の長期にわたるモニタリングが必要である。また、気候や季節の変動にどのような反応を示すかをモニタリングする事によって断層の水理性状が推定出来た事例もある。概要調査に数年掛ける予定である事を考えると、モニタリングの装置に関しても 5，6 年の期間にわたって性能が保証されるか、メンテナンスが容易である事が望まれる。一般に圧力センサーの寿命はさほど長くない。明らかに故障をしなくてもドリフトが起きて正確なデータが録れなくなる可能性も考えなくてはならない。東濃地域の長期モニタリングプログラムの例を見ても、約半数のボアホールが使用不能となっている。重複してセンサーや機器を設置して故障の場合に備える事が肝要である。電子的なセンサーの故障を 担保する為にピエゾメーター管を埋設する事も考慮すべきである。

ボーリング孔沿いの温度分布は光ファイバーを使った温度センサーを使用することが望ましい。光ファイバーセンサーは全長に渡って連続的に温度測定が可能である。ケーシングを設置する場合はケーシングの外側にファイバーを埋設すれば揚水試験区間や圧力モニタリング区間、孔内の流動に影響されずに温度分布の連続的モニタリングが可能となる。

5.3 フローチャート

Figure 5-1 に前セクション 5.2 で述べた調査のステップのフローチャートを示す。断層の調査は概要調査の一部であるので、概要調査全体のフローに関しては Karasaki ら（2006）を参考にされたい。

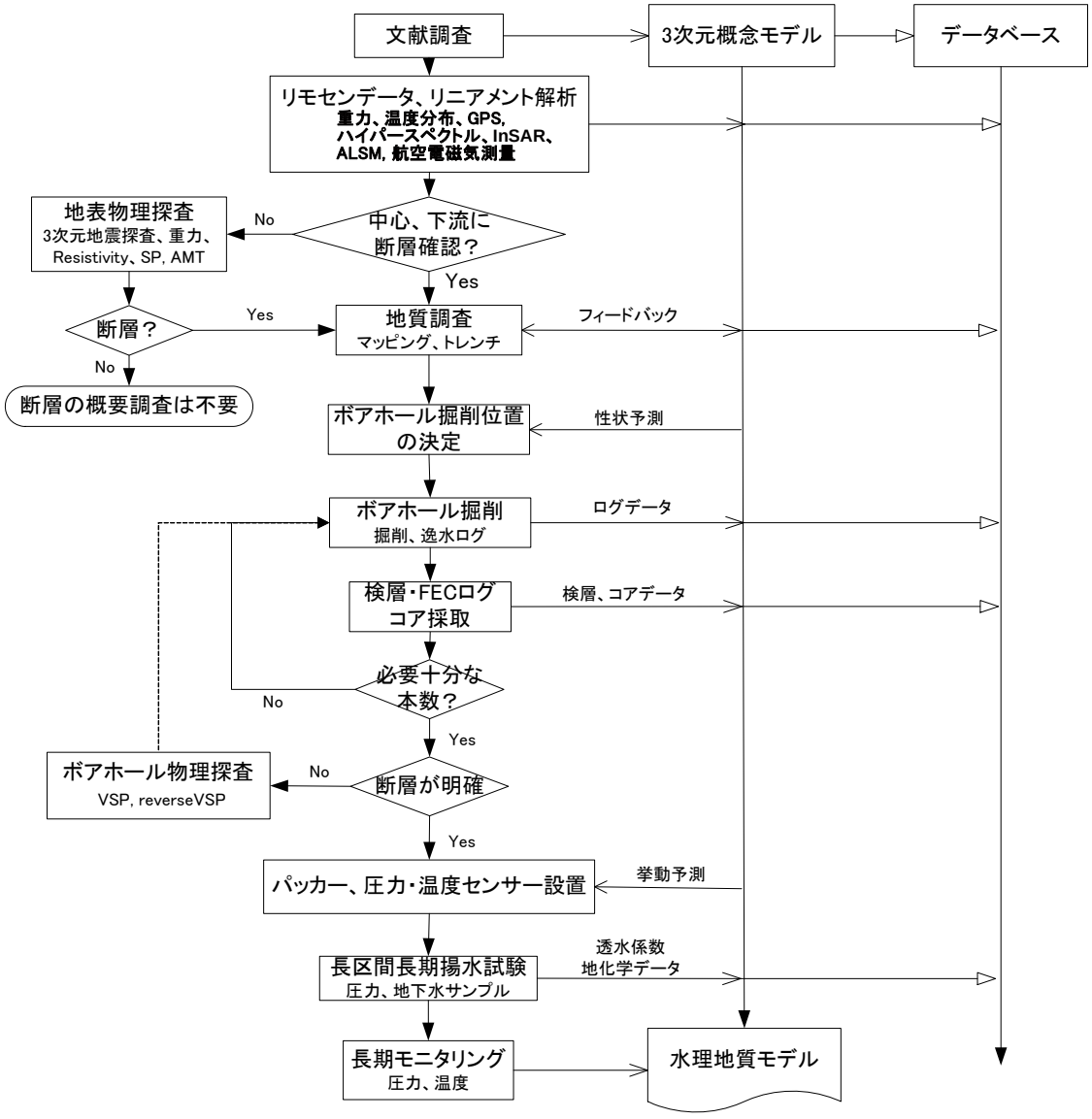

Figure 5-1　　断層調査ステップの流れ

5.4 References

JNC, 高レベル放射性廃棄物の地層処分技術に関する知識基盤の構築、－平成 17 年取りまとめ－、JNC TN1400 2005-020、2006.

Karasaki, K, J. Apps, C. Dounghty, H. Gwatney, C.T. Onishi, R. Trautz, and C.F. Tsang, Feature Detection, Characterization and Confirmation Methodology, NUMO-LBNL Collaborative Project Report, March 2007.

Acknowledgements

Funding for this work was provided by the Nuclear waste Management Organization of Japan, through U.S. DOE Contract No. DE-AC02-05CH11231.

Appendix 1

NUMO－LBNL Collaborative Project

Development of Hydrologic Characterization Technology of Fault Zones

－Work Plan－

August 2007

1. Background and Objectives

In 2006 ANRE (Agency for Natural Resources and Energy) jointly with JAEA (Japan Atomic Energy Agency) identified outstanding technological issues and needs regarding the research and development for geologic disposal of HLW subsequent to the publication of the Second Progress Report by JNC (Japan Nuclear Cycle Development Institute) in 1999. Research organizations in Japan as well as NUMO have been conducting investigations on these issues and needs. In the area of ground water hydrology, four R&D needs were identified and are currently being investigated: Improvement of groundwater flow characterization technology, development of testing and characterization technology in coastal areas, development of testing equipment and technology, and field application of testing and characterization technology. NUMO has been incorporating the results of the outcome of these R&Ds as they become available and deemed appropriate and is in the process of systematizing the testing and characterization technology to form a solid technical foundation for selecting the sites for detailed investigation.

Meanwhile, NUMO has recently conducted a collaborative study with DOE/LBNL, "Optimization of Site Investigation Program" as part of an effort to evaluate testing and characterization technology from the performance assessment perspective. The study has identified the hydrologic properties of fault zones as one of the most important parameters that need to be evaluated during the preliminary investigation stage. Based on the experiences learned at the Mizunami and Horonobe URLs as well as at numerous mines, dams and tunnels, and given the geologic environment of the Japanese Islands, faults are likely to exist almost ubiquitously, which need to be assessed both at the preliminary and the detailed investigation stage (the length scale of the faults of interest would range from several kilometers in the former down to several hundred meters in the latter investigation stage). However, none of the four R&D activities mentioned above sufficiently addresses the development of systematized hydrologic characterization technology specifically tailored for fault zones. At present, it is necessary to use perhaps overly conservative values for the hydrologic parameters of fault zones for the design and performance assessment of a repository. Therefore, development of a more efficient and reliable fault zone characterization technology is highly desirable.

The geologic properties of faults and the relationship among their geometry, type, fault parameters and internal structures are being investigated mostly in overseas. Hydrologic investigation of faults of various sizes are also being conducted at foreign as well as at domestic characterization sites. However, the relationship between geologic and hydrologic properties of faults is not yet studied sufficiently.

The objectives of the present study is to organize the information available in overseas to ultimately establish an efficient and systematized methodology for hydrologic investigation and characterization of faults at the scale of interest during the preliminary investigation stage for more practical design and performance assessment. The present study will be conducted as a collaborative study between NUMO and USDOE/LBNL. It should be possible to apply/transfer the results of the study obtained at a site in the West Coast of the United States, whose tectonic environment is just as active as that in Japan, to the Japanese repository program when they will be needed, which will be also beneficial to the US program.

2. Activities

This is a project of approximately three-year duration from FY2007 through 2009. In 2007 investigations will focus on a literature survey and feasibility study of the methodology. In 2008 and 2009, fieldwork will be conducted to verify the approach and to systematize the methodology. Below describes the first year activity. Specifics of the second and the third year activities will be developed in FY2007.

FY2007

1. Literature Survey

Conduct literature survey and expert solicitation from overseas and at home, to investigate past and current hydrologic characterization activities of fault zones at various scales of interest from the following countries and disciplines.

Countries: USA, Canada, Sweden, Finland, Great Britain, France, Switzerland, Japan, etc.

Dsciplines: Geologic disposal, mineral exploration, civil engineering, earthquake disaster prevention, environmental restoration, etc.

A. Type classification

Classify faults with known hydrologic properties by type based on the geologic properties and summarize the respective hydrologic properties. At the same time, the differences and similarities between the geologic and hydrologic properties of these faults and those in Japan will be highlighted.

B. Field investigation and characterization technology

Collect and organize information regarding actual examples of a sequence of field investigation, modeling and analysis of fault zone hydrology including the technology used. Contrast the differences and similarities with those in Japan. Identify the applicability and the limitations of them to be used at the preliminary investigation stage.

2. Investigation of characterization technology

A. Development of investigation and characterization flow and planning

Examine the most optimum investigation, modeling and analysis methodology for a given fault type classified in Task-1 at the scale of the preliminary investigation stage. Conduct modeling analysis of the most advantageous borehole configurations and testing approach when multiple fault types coexist. Summarize the findings and construct a systematized flow of testing and characterization procedure. In addition, plan and design a field investigation to verify the approach including the siting of a filed demonstration site.

B. Review of results

Conduct critical review of the results obtained in Task1 and deliberate on the verification plan by soliciting participations of experts from domestic universities and research organizations.

FY2008~FY2009

1. Field Investigation

Conduct field investigations at the site according to the plan laid out in the previous year. Analyze available information and conduct surface geologic investigation and geophysical surveys to locate the position of the fault and develop comprehensive understanding of the surrounding geology. Predict the hydrologic properties of the fault zone, followed by the planning of detailed borehole investigations. Conduct field tests, modeling and analysis to develop understanding of the hydrologic properties of the fault.

2. Summary Report

Evaluate the effectiveness of the testing and characterization approach based on the results obtained from the field investigations, and summarize the systematized approach. Make recommendations for testing and characterization methodology to be employed at the detailed investigation stage. Conduct comprehensive evaluation of the results and discuss issues for the next phase by soliciting participations of experts in hydrology from domestic universities and research organizations.

3. Responsibilities

   Activities in each task will be conducted by LBNL. Planning and evaluation of results will be jointly conducted by NUMO and LBNL.

4. Schedule and deliverables.

   The three-year schedule is shown in Table 1. A progress report summarizing the results of FY2007 activities will be submitted to NUMO by the end of February 2008. FY2008 and FY2009 deliverables will be defined in separate planning documents.

Table 1

	FY2007	FY2008	FY2009
Literature Survey	→		
Efficient testing and characterization technology	Workshop △→		
Field investigation	Geologic and geophysical survey →	Workshop △ Borehole testing →	
Reporting			Workshop △→